IS-T 1700

Fundamental studies of the plasma extraction and ion beam formation processes in inductively coupled plasma mass spectrometry

by

Niu, Hongsen

PHD Thesis submitted to Iowa State University

Ames Laboratory, U.S. DOE

Iowa State University

Ames, Iowa 50011

Date Transmitted: February 10, 1995

PREPARED FOR THE U.S. DEPARTMENT OF ENERGY

UNDER CONTRACT NO. W-7405-Eng-82.

DISCLAIMER

DISCLAIMER

Portions of this document may be illegible in electronic image products. Images are produced from the best available original document.

Fundamental studies of the plasma extraction and ion beam formation processes in inductively coupled plasma mass spectrometry

Hongsen Niu

Major Professor: R. S. Houk
Iowa State University

The fundamental and practical aspects are described for extracting ions from atmospheric pressure plasma sources into an analytical mass spectrometer. Methodologies and basic concepts of inductively coupled plasma mass spectrometry (ICP-MS) are emphasized in the discussion, including ion source, sampling interface, supersonic expansion, skimming process, ion optics and beam focusing, and vacuum considerations. Some new developments and innovative designs are introduced.

The plasma extraction process in ICP-MS was investigated by Langmuir measurements in the region between the skimmer and first ion lens. Electron temperature (T_e) is in the range 2000 - 11000 K and changes with probe position

---

[1]This work was performed at the Ames Laboratory under contract No. W-7405-ENG-82 with the U. S. Department of Energy. The United States government has assigned the DOE report no. IS-T 1713 to this dissertation.

inside an aerosol gas flow. Electron density (n_e) is in the range 10^8 - 10^{10} cm^{-3} near the skimmer tip and drops abruptly to 10^6 - 10^8 cm^{-3} downstream further behind the skimmer. Electron density in the beam leaving the skimmer also depends on water loading and on the presence and mass of matrix elements.

Axially resolved distributions of electron number density and electron temperature were obtained to characterize the ion beam at a variety of plasma operating conditions. The electron density dropped by a factor of 10^3 along the centerline between the sampler and skimmer cones in the first stage and continued to drop by factors of 10^4-10^5 downstream of skimmer to the entrance of ion lens. The electron density in the beam expansion behind sampler cone exhibited a $1/z^2$ intensity fall-off (z is the axial position). An second beam expansion originated from the skimmer entrance, and the beam flow underwent with another $1/z^2$ fall-off behind the skimmer. Skimmer interactions play an important role in plasma extraction in the ICP-MS instrument.

The measured floating voltages (V_f) are in the range of +2 to +5 volts. V_f generally decreases downstream of sampler and through the skimmer. Negative values of Vf were measured at downstream of the skimmer. RF amplitude shows a net positive potential in supersonic expansion. The plasma "rectification effect" and the "calorelectric effect" on the plasma potential measurements were discussed. The drop in V_f near the skimmer may be caused by a disturbance in front of the skimmer.

TABLE OF CONTENTS

GENERAL INTRODUCTION

Inductively coupled plasma mass spectrometry (ICP-MS) has emerged as a major technique in the area of elemental analysis since its introduction in 1980. The technique historically stemmed from the development of the ICP as an emission source in atomic spectroscopy (AES) in the late 1960s (1,2). About 10 years later, the first analytical mass spectrometer with an ICP ion source was developed in the Ames Laboratory by Houk *et al* (3), following the work of Gray using a d.c. capillary arc as a ion source for mass spectrometry (4). Since then, ICP-MS has been growing rapidly and become a widely used technique in the analytical community.

ICP-MS Instrumentation and Development

The scope of ICP-MS application has been extended to the fields of biomedical research, geological survey, food nutrition, pharmaceutical quality control, clinical and forensic toxicology, environmental sciences, *etc.* (5-24). Beside its capability for elemental and isotopic analysis, ICP-MS has been used for elemental speciation studies in combination with chromatographic methods for separation (25-27).

The ICP is an excellent ion source for elemental mass spectrometry. The interface for plasma extraction into the mass analyzer is derived from molecular beam techniques developed many years ago. For plasma extraction, the sampler cone is

inserted into the plasma and samples the ions in the axial central flow with a orifice ~ 1 mm diameter. A second cone is located behind the sampler to re-sample the plasma beam into the second vacuum stage. Ion lenses behind the skimmer in the second vacuum stage extract and focus ion beam into an mass analyzer.

A quadrupole most commonly serves as the mass analyzer in ICP-MS. It is commonly used for most analytical instruments because of its low cost, simplicity and tolerance of a wide range of kinetic energies. The quadrupole mass filter is an array of four metal rods biased at appropriate RF and DC voltages. Only ions of a selected mass to charge ratio (m/z) pass and are then collected by a detector. An off-axial detector is mostly used and the ions are reflected into it by a electrical reflector to reduce the high background caused by photon collection. A Channeltron electron multiplier is generally used in the pulse counting mode. The data acquisition operation may use as single-ion monitoring, multiple-ion monitoring, and spectrum scanning. Other mass analyzers may be also combined with ICP such as magnetic sector and time-of-flight.

The success and the popularity of the ICP-MS rely on its following unique features: 1) low detection limit (1-100pg/ml); 2) simple spectra; 3) multielement capability; 4) large linear range and elemental coverage; 5) isotopic ratio measurement. ICP-MS detection limits are 100 - 1000 times better than those obtained by ICP atomic emission (ICP-AES). The analysis speed can be much faster than atomic absorption spectroscopy (AAS) with multielement capability. However, the

technique is not without its problems and the new developments are continuing.

The interface in ICP-MS has been the heart in development of the ICP-MS instrument. Plasma extraction and ion beam formation in the interface play an important role for further improvement of the technique.

The major commercial ICP-MS devices have evolved continuously and a number of new instruments has been introduced in the marketplace. Currently, Sciex and VG Elemental are the two major manufacturers for ICP-MS. In the Sciex ICP-MS, the cryogenic pump in the earlier design was replaced by turbo molecular pumps in Elan 5000 ICP-MS. The unique design in Sciex ICP-MS is the well known center-taped coil introduced by Douglas (28), in an attempt to reduce the secondary discharge at the interface of the instrument.

VG produced an alternative product "PQ Eclipse" ICP-MS besides of its PlasmaQuad system by modifying the instrument with only two vacuum systems. They also introduced a high resolution ICP-MS device that use a magnetic sector mass analyzer with a resolution approaching 10 000 (29). Most isobaric interferences may be overcome but at high cost relative to that of quadrupole mass spectrometers.

Several other manufacturers produce ICP-MS instruments in the market place and each has some different approaches in interface design even through the basic components are same. Finngan MAT is marketing a product named "Sola ICP-MS" that was initially designed by Turner (30, 31). One unique feature of this instrument is its ion optical design. A high acceleration voltage is applied to improve ion

transmission and mass discrimination, and a dual collector system is used for operating at a large dynamic range. Thermal Jarrell Ash, the first U. S. based ICP-MS manufacturer, introduced their "POEMS" at the 1992 Pittsburgh Conference. This design combines ICP optical emission and ICP mass spectrometry in the same instrument and the mass spectrometer uses an offset ion lens system based on the Ames Laboratory design (32) to reduce the levels of background signal and polyatomic ions. In 1993, Varian announced their new ICP-MS instrument so called "UltraMass". The unique feature of this instrument is a different coil geometry called "Turner Coil" (33), which is similar to the center-tapped coil design in principle, with an effort to reduce secondary discharge. Another unique feature of the instrument is a large turbo pump used in the second stage. Another ICP-MS instrument with an unique ion lens design is Yokogawa PMS 2000 (34). The offset ion lenses were used and substantial better detection limit and sensitivity were reported. In 1994 Pittsburgh conference, Hewlett-Packard Yokogawa (35) introduced the first benchtop instrument called HP 4500 ICP-MS. The unique features of HP 4500 ICP-MS include the "Shieldtorch", the offset ion lens, and, most surprisingly, its compact design. Other ICP-MS manufacturers with ICP-MS are Seiko, Hitachi and JEOL in Japan, and Spectro Analytical Instruments of Germany. At this time, more than 1000 instruments have been installed worldwide.

Despite the great success of the instrument, limitations do exist. The shortcomings with the ICP-MS include matrix effects (36-42), mass-bias (38,43),

isobaric spectral interference (44-48), long-term drift (49,50). Besides, inefficient ion extraction and transmission have also been recognized although the ICP-MS can achieve excellent detection limits (1-50 pptr). A large fraction of ions are lost in the beam transport process when the number of ions sampled from the ion source is compared with those collected by detector.

Most of the shortcomings have been postulated to originate from the sampling processes at the interface. However, the mechanisms and the origins in the instrument are still not fully understood. For developing the instruments of the next generation, more fundamental studies are needed to further understand the extraction processes

Dissertation Objectives and Organization

It is the overall purpose of this dissertation to provide a basic understanding of the construction and the performance of the ICP-MS interface. Fundamental principles and design considerations will be described for extracting ions from atmospheric pressure plasma sources into the analytical mass spectrometer. Some important experimental discoveries about ion beam behaviors and instrument functioning are discussed. New mechanisms and possible future improvements are also suggested.

Ion transmission and instrument performance are characterized through the region of the sampler and skimmer downstream to the ion optical lenses. The plasma extraction process was studied by Langmuir probe in a home-made ICP-MS system. Langmuir probe methods are versatile and effective in plasma diagnostics [51-60].

The ion beam is characterized by spatially resolved measurements of electron density, electron temperature and floating potential measurements.

This dissertation is composed of four papers. Each paper in the dissertation stands alone as a complete scientific manuscript with accompanying tables, figures and literature cited. Additional literature citations for this general introduction are given after the general summary and future research.

The first paper of this dissertation is formatted for a general review publication, an invited paper for *Spectrochimica Acta Reviews*. The paper describes the methodology and basic concepts for extracting ions from atmospheric pressure plasmas for mass spectrometry. The fundamental and practical aspects for the instrument designs are discussed. Innovations of interface design, and new ion lens construction or arrangement are introduced.

The second paper is also formatted for the journal *Spectrochimica Acta.* It was published in the Special Boumans Festschrift Issue (*Spectrochimica Acta*, 46B, No. 6/7. pp. 805-817). The paper presents the results of the first beam property measurements behind the skimmer in an ICP-MS system. Beam properties were measured by Langmuir probe along the axial centerline of the beam flow. The feasibility of the electrostatic probe methods and the validity of the measurement results were evaluated for ICP-MS system. Electron density (n_e) is in the range 10^8 - 10^{10} cm^{-3} near the skimmer tip and drops abruptly to 10^6 - 10^8 cm^{-3} downstream further behind the skimmer. Electron density in the beam leaving the skimmer also

depends on water loading and on the presence and mass of matrix elements.

In the third paper, the spatial resolved profiles of extracted ion beam were measured through the skimmer orifice into the first vacuum stage of an ICP-MS instrument. By this way, the local plasma beam properties in both first and second vacuum stages could be depicted along the beam transport centerline. Some detailed information is provided about skimmer interferences around the skimming entrance.

The fourth paper is the second part of a serial paper, the first of which is the Paper III in this dissertation. The paper discusses some electrical effects on the plasma beam flow during the extraction processes. Experimental results of plasma potential measurements are presented. The measured floating voltages are generally in the range of +2 to +5 volts. The RF voltages show a net positive potential in supersonic expansion that in agreement with a floating voltage measurement in the interface of ICP-MS.

PAPER I

FUNDAMENTAL AND PRACTICAL ASPECTS OF EXTRACTING IONS FROM ATMOSPHERIC PRESSURE PLASMAS FOR ANALYTICAL MASS SPECTROMETRY

INTRODUCTION

The last decade has witnessed the rapid growth of plasma source mass spectrometry in the analytical community. The combination of the inductively coupled plasma and mass spectrometry (ICP-MS) is a superior technique for trace elemental and isotopic analysis.

In an atmospheric pressure ion source mass spectrometer, processes by which ions are extracted into the vacuum system for mass analysis has proved to be most critical in developing the analytical instrument. The mass analyzers and detectors have matured in other applications such as organic mass spectrometry. The extraction of a plasma, such as an ICP, at atmospheric pressure provides many benefits, including analytical ruggedness, low background, and straightforward and rapid sample introduction. In the present ICP-MS instruments, the extraction process behaves well enough for analytical purposes, even if all aspects of extraction are not fully understood.

The ICP-MS technique historically stemmed from the development of the ICP as an emission source in atomic spectroscopy (AES) in the late 1960s. Reed designed a plasma torch which could sustain a spheroidal plasma using tangential gas flow in the field of physics (1). Annular ICPs for analytical purposes were developed in 1964 by Greenfield (2) and in 1965 by Fassel (3). In 1978, the first analytical mass spectrometer with an ICP ion source was developed in Ames Laboratory and a paper

was published in 1980 by Houk *et al.* (4). Even though the development of ICP-MS was more derived from atomic spectroscopy rather than from mass spectrometry, the earlier experience in extracting other plasmas and neutral beams with mass spectrometry are important in the instrument design.

The systems used for ion extraction in ICP-MS are based on a long history of extracting ions from flames and other plasmas at atmospheric pressure (5-11). The concept for neutral beam extraction and then ionization by electron bombardment for mass spectrometry even originated about 40 years ago (12,13). Most of those early ion extractions with mass spectrometer were conducted for studying combustion processes and chemical reactions. The conventional combustion plasmas were not used as a means for analytical mass spectrometry, until Knewstubb and Hayhurst advised to use the concept of an "electrical flame" as an ion source for solution analysis. This special flame was reported with a high temperature near 5000 K contrast to about 3000 K in the other flames. A response in the analytical field was made by Alkemade (15), who suggested that the technique of Hayhurst should be coupled to an AA flame. At this time, the alterative plasma sources, which can offer a higher ionization temperature, started to grow in the analytical field and substitute the flame source for the elemental mass spectrometry.

The high temperature plasma sources considered for mass spectrometry at atmospheric pressure, besides the ICP, mainly include direct current (DCP) plasma and microwave-induced plasma (MIP). By the time that ICP as an excellent ion

source for mass spectroscopy was recognized in the field, the efforts in MIP and DCP also turned to developing ICP-MS system. As a matter of fact, the initiation of the ICP-MS was inspired from the work done at Applied Research Laboratories by Gray and his colleagues (16,17), who had demonstrated the feasibility of using a capillary d.c. arc plasma as an ion source for a mass spectrometer. The coupling of the d. c. plasma with a mass spectrometer was based the ion extraction device in flame sampling mass spectrometry. The MIP, another possible ion source for mass spectrometry, was investigated by Douglas *et al* in Canada (18,19). Even though extracting ions with mass spectrometer from either the MIP and the capillary arc plasma was not as successful as with the ICP, their experiences in plasma extraction also contributed greatly to the development of ICP-MS.

The introduction of ICP-MS started a new era in elemental mass spectrometry. In the early stage of the ICP-MS instrument development, the pioneering work was performed primarily in the three research groups: the Ames Laboratory at Iowa state University (4,20), the University of Surrey and VG instruments in Britain (21-26), and Sciex in Canada (27,28). By 1983, commercial instruments of ICP-MS were introduced by Sciex, Inc (29) and VG Instruments (30). Since then, ICP-MS has been growing rapidly and become a widely used technique in the analytical community. This can be indicated by about 10 ICP-MS manufacturers appeared in the marketplace and more than 1000 instruments installed through the world.

The essential parts of an ICP-MS instrument are shown in Figure 1. The

success and the popularity of the ICP-MS mainly rely on its following unique features: low detection limit; simple spectra; multielement capability; large linear range and elemental coverage, and isotopic ratio measurement.

This article describes methodologies and basic concepts for extracting ions from plasma sources. The description is focused on plasma extraction and ion beam formation in ICP-MS. Some of new developments and innovative designs are introduced. MIPs are included where appropriate and where different from the ICP. The extraction systems and the design criteria for other plasmas at atmospheric pressure can be very similar. Glow discharge (GD), an important low pressure ion source, will not be covered extensively. This chapter is not an attempt to have a complete review of ICP-MS, whose detection capabilities and the analytical applications have been reviewed extensively elsewhere (34-42).

ICP AS AN ION SOURCE

The characteristics of the ion source are important for any mass spectrometer. A full discussion of the ICP configuration and properties is beyond the scope of this article, the reader is referred to the Refs. 4, 43, 44 for more detail. The descriptions below will concentrate on those aspects that are particularly pertinent to the ICP as ion source and to extraction processes for analytical mass spectrometry described below.

General Features of ICP Ion Source

ICP is an excellent ion source for elemental mass spectrometry. An ICP in a horizontal configuration generally used for mass spectrometer sampling is shown in Figure 2. The ICP is generated and sustained in a plasma torch with RF power applied to the load coil. Argon gas is supplied to the plasma generally in three separated flows through the torch. The tangential introduction of outer gas ($\sim$15 L min^{-1}) into the torch forms a vortex-like patten in the region enclosed by the load coil.

As compared with other atmospheric pressure plasma sources, the ICP make it a more suitable ion source for coupling with a mass spectrometer. The vortex flow create a low pressure zone in the center of the plasma, which provides a unique opportunity for sample introduction. Samples can be nebulized and carried by argon gas flow through the inner tube into the center of the plasma. The analytes then travel

through the plasma central channel and are vaporized, atomized and ionized. The most important characteristic of an ICP, however, is its high ionization temperature and ionization efficiency.

Gas in the central channel of an ICP is heated mainly by radiation and conduction from the annulus. The gas kinetic temperature in the induction region of the plasma may be as high as 10,000 K and 5000 K in the central channel. The ICP is electrically neutral and contains equal numbers of positive and electrons. Neutral Ar atoms are by far the most abundant with the density about 10^{18} cm^{-3} and the ionization fraction $\sim$ 0.1%.

The plasma center flow forms three distinct zones: initial radiation zone, normal analytical zone and the plasma tail. The initial radiation zone contains mostly molecular species and atoms. The singly charged analyte ions, are mostly abundant in the normal analytical zone and it is from here ions are sampled into the mass spectrometer. As the ions flow further through the axial channel into the plasma tail, recombined oxides and air entertainment will increase.

For ion extraction into mass spectrometer, it is desirable to understand the ion distribution in the plasma radially and along the central channel. The spatially resolved profiles of the ion intensity can be studied simply by moving the ion sampling interface of an ICP-MS across the plasma. An example as shown in Figure 3, as Fe solution was nebulized and introduced into the plasma center (45). It can be clearly seen that the analyte ions are concentrated in the plasma central channel

surrounded by Ar^+. The central channel is about 2 mm wide, which corresponds to the visualized dark center flow in the plasma.

The plasma shape and the optimal sampling position can be changed by varying the aerosol gas flow, solvent loading and RF forward power applied to the load coil. As forward power increases, the plasma shape shifts and the maximum ion intensity moves upstream; while as solvent loading increases the plasma shrinks and the position of maximum ion density shift upstream. It is understandable that increasing nebulizer gas flow rate will move the initial radiation zone closer to the sampling cone of the MS.

In practice, the optimal sampling position is determined by experimental adjustment. The ion sampling cone is usually very close to the torch mouth. From the profile measurements, it seems the position should be as close to the load coil as the torch and the plasma flow permit. As a matter of fact, it is determined by two processes, that is, diffusion and ionization. A longer the residence time favors more efficient ionization. However, the residence time cannot be too long. The plasma position with the high ionization efficiency may not give maximum ion signal due to the ion diffusion from the central flow.

The gas flow is the one of the fundamental aspects that affect of the properties of the plasma. It determines the residence time of the injected species flowing through the plasma. Analytes typically will stay in ICP for several millisecond before flying through the sampler into the mass spectrometer.

Gas velocity distribution in the ICP has been studied by theoretical and experimental investigations (46-48). Barnes and Genna (46) measured the radial velocity profiles for a plasma with 14 L/min outer gas flow as shown in Figure 4. A high-velocity central flow region was reported approximately 1.5 mm from the central axial inside the torch. The flow velocity rapidly decreased with increasing height up to 12 mm above the coil. The gas flow toward the ICP-MS sampler can be ~ 20 m/s based on this measurement if the sampling position is 10 mm from the load coil. Cicerone and Farnsworth (49) reported that gas velocity in the central channel gradually increases with increase in axial height up to 25 mm above the coil. With increasing RF power the gas velocity was found to increase in the center channel of an ICP.

For mass spectrometry sampling considerations, the flow velocity at ~ 10 or 20 m/s above sampling cone may not contribute to the gas dynamic or electrical dynamic effects inside the interface of ICP-MS. Comparing the supersonic velocity (10^3 m/s) as the plasma extracting into the first vacuum stage, the gas flow from the torch should not significantly contribute to the ion kinetic energy.

Ionization Conditions and Mechanisms

The quality of the ICP as an ion source was demonstrated long before it coupled with mass spectrometry. In ICP emission spectroscopy, monatomic, singly charge positive ions generally give the most prominent emission lines (50). Neutral

gas atoms, usually argon, are the dominant species in the plasma at a density of approximately 10^{18} cm^{-3}.

As shown in Table 1, most elements have first ionization energies below 10 eV while there are none whose second ionization energies fall below 10 eV. It is known that most elements are highly ionized with larger than 90% efficiency. The efficiency of ionization for the plasma gas can be estimated from the Saha equation (42,52-55) for the ionization constant K_{M+}

$$M \rightleftharpoons M^+ + e^- \quad (1)$$

$$K_{M+} = (n_{M+} + n_e)/n_M = n_e\, \alpha/(1-\alpha) \quad (2)$$

$$\log K_{M+} = \log Z_{M+}/Z_M + 1.5\ (\log T) - 5040\ E_{ion}/T + 15.684 \quad (3)$$

where α is the ionization fraction; n_e, n_{M+} and n_M (cm^{-3}) are the number density of electrons, ions and atoms, respectively; Z_{M+} and Z_M are the ion and atom partition functions; T_{ion} (K) is the ionization temperature and E_{ion} is the first ionization energy (eV). At an ionization temperature of 7500 K, the equilibrium number density of Ar ions is approximately 1.2×10^{15} cm^{-3}. Calculated values for degree of ionization (%) of M^+ for the elements of the periodic table are shown in Fig. 5 (55).

Formation of singly charged ions (M^+) is very efficient, and Ar^+ is the major ion present in the ICP. Only a few elements such as barium, lanthanum, and the rare earths form appreciable quantities of doubly charged species. The ratio M^{+2}/M^+ is

typically less than 2%; most elements have M^{+2}/M^{+} ratio several orders of magnitude lower. Few cases of interferences from doubly charged ions (M^{2+}) occur, and these can be resolved by determining a correction (51).

Many mechanisms have been proposed for ionization in the plasma including Penning ionization (56,57), charge exchange (58,59,60,61), and electron impact (62,63). All undoubtedly occur to some extent, but the question remains whether one or two are dominant. Other mechanisms such as radiation trapping (64,65,66) and ambipolar diffusion (67,68) may contribute to the atomic excitation in ICP emission spectroscopy and may not cause directly ionization. The three major reactions can be simply depicted as below:

Penning Ionization: $Ar^m + M \rightarrow Ar + M^+ + e^-$ (4)

Charge Transfer Ionization: $Ar^+ + M \rightarrow Ar + M^+$ (5)

Electron Impact Ionization: $M + e \rightarrow M^+ + 2e^-$ (6)

The Penning ionization reaction was first postulated as a major mechanism in ICP emission spectroscopy. In this reaction, argon-metastable atoms (Ar^m) are first formed in ICP and then react with analyte atoms (M) to form analyte ions (M^+). The number density of Ar^m can be predicted from the Saha and Boltzmann equations at about 5×10^{12} cm^{-3}. The measured number density of Ar^m was reported to be 2×10^{11} cm^{-3} (218-220), which is not overpopulated compared to the calculated value from the

experimental T_{exc} and n_e. The results indicates the Penning mechanism is not an important source of M^+ ions.

In the charge transfer reaction, the analyte atom (M) is ionized by transferring the charge of Ar^+ to analyte ion. The ionization potential of M must be lower than that of Ar, 15.67 ev. The charge transfer reaction is more efficient if the excited electronic levels of the analyte ion are close to the first ionization energy of Ar. The number density of Ar^+ ($\sim 10^{15}$) is much larger than that of Ar^m, so charge transfer cab not be significant in an ICP.

The ICP is known as an universal, general ion source. It is remarkable in that it excites maximum emission from hard lines at same time and place. Therefore, general, non-selective mechanism for ionization must be dominant. Such a general ionization mechanism must be electron ionization (EI). The Penning and charge transfer processes may supplement ionization by EI to some extent.

Polyatomic Ions

Although ICP-MS is a highly successful method for trace and ultra-trace elemental analysis, it still suffers problems of spectral interferences. For a large number of elements, the singly charged elemental analyte ion (M^+) is by no means the only analyte species that is observed. Polyatomic molecular ions cause isobaric overlap that complicates the detection of analyte.

In general, oxide formation from major and matrix elements is the most

serious problem. There is considerable debate as to the origin of polyatomic ions. The extent of the polyatomic interferences may depend on sample type, sample nebulization, plasma generation, and instrument operating conditions. There have been statements in literature claiming that oxide ions are made during extraction process. Evaluations can be made by calculating the approximate amount of such species in the ICP.

The ICP is normally considered to be efficient atomization source. Suppose T_{gas} is approximately 5000 K, as determined by the Doppler widths of emission lines and Rayleigh scattering (134), the extent of dissociation of oxide species (MO^+) can be estimated from following equations (127)

$$MO^+ \rightleftarrows M^+ + O \tag{7}$$

$$K_d = n_{M+}n_O/n_{MO+} \tag{8}$$

$$\log K_d = 20.274 + 1.5 \log M_{M+}M_O/M_{MO} + \log Z_{M+}Z_O/Z_{MO+} + 1.5(\log T) - 5040\, E_d/T \tag{9}$$

where n is the number density (cm^{-3}) and the subscript indicates the species. K_d is the dissociation constant; Z is the electronic partition function, T is temperature in K; k Boltzmann's constant, E_d and T are the dissociation energy and dissociation temperature of MO^+, respectively.

One can simply guess the partition function values, estimate the extent of

dissociation in ICP, and then use Saha Equation to calculate relative ionization yield for each species. Douglas estimated (69) atomic oxygen concentration is approximately 10^{15} to 10^{16} cm^{-3} and a MO^+/M^+ ratio of about 0.01 to 0.1. The theoretical calculations are also valid for other molecule ions, although much more complicated to know partition functions.

It can be observed that tough oxide ions would seem to remain in plasma and are not fully dissociated. This agrees with studies of Douglas and Longerich (69,70). The weakly bound adduct ions like ArO^+, Ar_2^+, and ArM^+ probably are not present in ICP. These are most likely formed during extraction. This question will be addressed below when considering collisions during extraction.

Negative Ions

Elemental studies using ICP-MS with positive ion detection can give high analytical performance for most of the elements in the periodic table. However, some elements such as halogens remain difficult to detect. The negative-ion mode is quite common in organic mass spectrometry to measure halogenated compounds.

Several works have investigated negative-ion mode ICP-MS for determination of the halogens (71,72,73). The advantage of this approach for ICP-MS is that the spectrum is absent of the background interferences from positive ions such as Ar^+.

Ionization of an element such as F can be expressed by the equilibrium

$$F^- \Leftrightarrow F^o + e^- \qquad (10)$$

The energy required is the electron affinity of F. It is analogous to the ionization energy, E_{ion}, of F^- ion. This value is 3.5 eV for F, which is the highest value for any element. Yet Na (IE = 5 ev) is quite efficiently ionized in ICP, so F^- should be "ionized" to F even more efficiently. Other elements will show still less tendency to remain as stable X^- in ICP. This explains the basic reason for the usual poor sensitivity for negative ions from the ICP.

Fulford and Quan (73) estimated that approximately 10^4 fewer negative ions (Cl^-) than positive ions (Cl^+) in the ICP. However, they found that the sensitivity for the negative ions of the halogens is comparable to those in the sensitivity for the corresponding positive ions. The results may suggest that negative ions do not originate directly from the plasma but rather from electron capture or reaction downstream of the beam expansion.

In the negative-ion mode, a major handicap arises from the presence of a high background level across the whole mass range studied (71,72). The high noise level, by comparison with the positive-ion mode, is attributed to the electrons that reach the detector. In the positive-ion detection, electrons must overcome the energy barriers to find their way to detector. No electron will have enough kinetic energy to pass over -3 kV at the entrance of the detector.

Noise Characteristics

The plasma is a relatively noisy ion source. The noise signals can directly influence the precision, detection limits, and dynamic range of ICP-MS measurements. In general, precision in ICP-MS is poorer that in ICP-AES. Fundamental studies of the source noise characteristics can provide physical insight and possible ways for further instrument improvement. The signal-to-noise ratio is often measured to evaluate the analytical performance; however, a more fundamental understanding of the noise characteristics requires a knowledge of the noise power spectrum (NPS).

Houk *et al* (74) investigated the noise power spectrum of $^{85}Rb^{+}$ and $^{93}Nb^{+}$ in an ICP-MS and found that the plasma is the source of discrete frequency noise in the mass spectrometric signal. The discrete noise frequencies can be affected by changes in plasma gas dynamics due to interaction between the plasma and the mass spectrometer sampling interface. The major source of signal instability in the inductively coupled plasma mass spectrometer was found to be 1/f noise. Figure 6 compares the noise power spectra of the ion signals from emission and mass spectrometer.

Furuta *et al* (75) identified mostly white noise in the ICP-MS background signal and indicated that the low frequency noise (0-10 Hz) was primarily the result of pulsations introduced by the peristaltic pump. Audio-frequency noise (200-350 Hz) was similar to that noted in ICP-MS measurements.

The sample introduction process is typically the main source of flicker noise in ICP-MS. Luan *et al* (76) described noise characteristics of the aerosols generated by ICP nebulizers. Discrete frequency noise in the aerosol generated by a Meinhard nebulizer or a direct injection nebulizer (DIN) is primarily caused by pulsation in the liquid flow from the pump. The noise can be eliminated by use of a pulse-free pump, such as a gas displacement pump or a dual piston HPLC pump. A Scott-type spray chamber provides lower white noise than a conical, straight-pass spray chamber. A large amount of 1/f noise was observed for an ultrasonic nebulizer. This 1/f noise can not be attenuated by adding carrier gas flow in the chamber as in pneumatic nebulizers.

The ICP is sometimes considered to be a quiescent steady-state source. Actually, it is a dynamic system when observed with a time resolution on the millisecond scale. ICP emission intensity fluctuations occurring on a tens of microsecond time scale have been investigated by Olesik *et al.* (77, 78, 79), Cicerone and Farnsworth (49), and Horlick *et al.* (80).

Hobbs and Olesik (81) studied the signal fluctuations on a microsecond scale in ICP-MS. Large signal fluctuations due to individual aerosol droplets or vaporizing particles were observed by monitoring atom and ion emission intensities in front of the sampling cone. They found that the signal fluctuations in some cases could be larger than 1 order of magnitude on $\sim$ 20 microsecond time scale. Analyte signals are depressed near incompletely desolvated droplets and enhanced near vaporizing

analyte particles. The nature of ICP-MS signal fluctuations at a fixed sampling position is critically dependent on the aerosol gas flow rate. The results indicated that the poorer precision typically observed in ICP-MS in comparison to ICP-AES could be at least in part due to such fluctuations in the sampling process.

The plasma itself also fluctuates on a ms time scale, whether droplets/particles present or not. The fluctuations persist in ICP-MS signal and show up as noise. The high-speed motion photographic studies in Ames Laboratory (82) show that the noise peaks are caused by swell and contraction of the outer gas when air is entrained. Such peak frequencies in the emission measurements can be eliminated by using a long extension of the outer tube of the torch.

The plasma fluctuations in ICP-MS can also be visualized effectively by using high-speed motion photography (83,84,85). Houk *et al* (83) used fulmost a framing rate of 3000 frames s^{-1} while the plasma was sampled for MS. It was found that the axial channel expanded and contracted periodically at frequencies of 260-300 Hz, depending on operating conditions. The frequency of the observed fluctuations decreased as the sampling distance increased. Emission from vapor clouds surrounding the aerosol droplets or particles was observed flowing along the ICP central channel and are readily drawn into the sampling orifice. Transit of these large particles through the ICP could also contribute to flicker noise in the signal observed by the MS.

More recently, Gray *et al.* (85) investigated the plasma instability by

photographic observation together with noise power spectra. That the audiofrequency peak and its harmonic can be removed by using a bonnet over the torch extended the outer wall to beyond the aperture.

PLASMA EXTRACTION PROCESS

Ion Sampling from Plasma Source

Ions generated at atmospheric pressure in an ICP are sampled through a small orifice into a vacuum system for mass analysis. The sampling interface and the plasma source generally used in ICP-MS are shown schematically in Figure 7.

In the early days of ICP-MS, a single cone with a small (50-70 μm) orifice was used. The arrangement was similar to that used in other atmospheric pressure ion sources (86,87,88,89,90). However, condensed solids readily plugged the pinhole-sized orifice when real samples were analyzed, and levels of metal oxide ions were high (4,20,21,22). As soon as the diameter exceeded 120 μm a discharge formed near the orifice.

The extraction interface used in modern ICP-MS is very similar to those used in chemical physics for generating low temperature molecular beams (91,92) or for sampling ions from flames or other plasmas (8,9,14). In a typical ICP-MS instrument, the circular orifice in the tip of the cooled sampler cone is about 1 mm diameter. These problems in the early ICP-MS designs were solved or partially solved by using the fairly large sampling orifice and an additional cone (called a skimmer) to form a differential pumping system.

The plasma flow from the central channel of the ICP enters the orifice from a cross-sectional area of approximately 8 times the orifice diameter. The gas flow is

evacuated by a mechanical pump that maintains a pressure on the order of 1 torr. A supersonic jet thus is formed after the sampler in the first vacuum stage. Some fundamental aspects of sampling and supersonic beam formation will discussed below.

Supersonic Jet Formation

Supersonic nozzle beam sources for dynamic sampling of ions and molecules have been in use since the pioneering work of Kantrowitz and Grey (93) in 1951. The sampling system used in ICP-MS is based on the work of Campargue (92,223,224), who systematically studied the supersonic jet for molecular gas expansion at a larger source pressure. A schematic view of the supersonic gas expansion into the vacuum chamber in ICP-MS is given in Figure 8.

The flow field of the expansion is shielded from the background gas by shock waves, the so called Mach disk and the barrel shock. The barrel shock and Mach disk are caused by collisions between fast atoms from the jet and the background gas. The undisturbed inner region inside the barrel shock wave is called the "zone of silence". The visual observation of the Mach disk and the barrel shock in an ICP-MS instrument has been reported by Gray (94).

The thickness of shock waves is of the order of several mean free paths for gas molecules in supersonic expansion conditions. The barrel shock and Mach disk may be no longer evident visually at low enough pressure (95). The structure of free jets has been studied theoretically and experimentally for conventional molecular

beam expansions (96,97,98).

Gas Dynamic Flow and Beam Properties

Studies of the aerodynamics of free jets produced from plasma ion sources have proved that the ion beam flow can be described by the same theory used for the conventional molecular beam expansion (99-101). Douglas and French present a complete discussion of the gas dynamic properties for the ICP-MS instrument (102). The pertinent features of the free supersonic expansion in ICP-MS are discussed below assuming the ion beam process follow the gas dynamic features only. The other interfering forces such as electrical interactions will be discussed separately later.

Once the sampled plasma passes through the sampling orifice, the gas expands adiabatically into the low pressure region (a few torr) to form a supersonic beam. Through the expansion process, the thermal energy of the gas molecules or atoms are converted to directed motion. The flow velocity can exceed the local speed of sound. The isentropic relation between the gas flow speed ($\bar{u}$) and the local speed of sound (a_o) can be expressed by the Mach number (M)

$$M = \bar{u}/a_o \qquad (11)$$

The ratio of $\bar{u}$ to a_o reaches 1 ($M = 1$) at a distance of 0.5 orifice diameter downstream of the sampler. The Mach number increases from $M < 1$ to $M = 1$ at the

throat and the gas expands into supersonic flow with M > 1. The flux of gas flow F (atoms/sec) through the sampler orifice M = 1 can be calculated from (103)

$$G_{Flux} = 0.562\ A^{*}\ n_o\ a_o \tag{12}$$

$$a_o = (\gamma k T_o/m)^{1/2} \tag{13}$$

where A^{*} is the cross-section area of the sampler orifice and n_o is gas number density. In the typical ICP-MS with an Ar plasma, $a_o = 1.3 \times 10^5$ cm s^{-1}, $A^{*} = \pi(D_o/2)^2$, $D_o = 0.1$ cm, $\gamma = C_p/C_v = 5/3$ for Ar, k is Boltzmann constant, $m = 6.67 \times 10^{-23}$ g/atom for Ar gas. Assuming $n_o = 1.5 \times 10^{18}$ cm^{-3}, $T_o = 5000$ K, the flux of gas flow is $\sim 8.6 \times 10^{20}$ atoms s^{-1}.

The centerline Mach number at a distance X may be described by (104,105)

$$M = A\left(\frac{x - x_0}{D}\right)^{\gamma-1} - \tfrac{1}{2}\left(\frac{\gamma + 1}{\gamma - 1}\right)\left[A\left(\frac{x - x_0}{D}\right)^{\gamma-1}\right]^{-1} \tag{14}$$

where A (flow density ratio) and X_o (distance measured in orifice radii) are constant, A= 3.26, and $X_o/D = 0.075$.

As the gas expands in the jet, the density and temperature decrease along the streamline. By using the one-dimensional gas dynamic relations, expressions for the density field

$$n_o/n = [1 + M^2 (\gamma\text{-}1)/2]^{1/\gamma\text{-}1} \quad (15)$$

and temperature,

$$T_o/T = 1 + M^2 (\gamma\text{-}1)/2 \quad (16)$$

may be obtained, assuming isentropic flow.

In addition, the velocity at any axial distance may be calculated. At a Mach number of about 5, which corresponds to an X/D of 2.5, the gas flow velocity will be constant at nearly the terminal velocity

$$u = \frac{2\gamma}{(\gamma\text{-}1)} (kT_o/m)^{1/2} \quad (17)$$

For Ar plasma

$$u = (5kT_o/m)^{1/2} \quad (18)$$

where T_o the source gas kinetic temperature, and m the mass of the plasma gas. Thus, the bulk gas velocity in the free expansion will be determined by the source temperature. In the typical ICP-MS, assuming T_o = 5000 K at the sampling position, $u = (5kT_o/m)^{1/2} = 2.3 \times 10^5$ cm s^{-1}.

Within the supersonic jet, the density decreases along each streamline in proportion to the inverse square of distance from the source. The number density at a

position, n (x), can be calculated from (104)

$$n(x) = 0.161\ n_o\ (x/D_o)^{-2} \qquad (19)$$

The density of the expansion gas decreases rapidly with increasing distance from the sampler orifice. The free-jet expansion is surrounded by a barrel shock and terminate in a perpendicular shock wave known as the Mach disk. In the case of ideal expansion, the flow velocity in the expansion region or the zone of silence will be almost constant and the enthalpy of the source gas will be converted into directed flow. The Mach disk location X_m, i. e., the axial distance from the sampler orifice to the onset of the Mach disk, is related to the pressure ratio by (103)

$$X_m = 0.67\ D_o\ (P_o/P_1)^{1/2} \qquad (20)$$

where D_o is the orifice or nozzle diameter; P_o is the pressure of plasma source and P_1 the background pressure of the first vacuum chamber. The relationship has been confirmed experimentally for $15 < P_o/P_1 < 15{,}000$ (105).

X_m is fully determined by the pumping speed available in the area near the nozzle. For example, if $D_o = 1$ mm and $P_1 = 1$ torr, X_m can be estimated as 15 mm. The expansion will shrink (i.e. X_m decrease) if a smaller pump or narrower pumping line is used.

The location of the Mach disc is important in determining the skimming position in order to obtain the maximum intensity in ICP-MS. Douglas (69) compared the measured and calculated gas flow through the skimmer of an ICP-interface at three different pumping speeds, and found the measured flow was in general agreement with the calculation. Kawaguchi (131) describes optical observations of a supersonic jet formed downstream from the sampling orifice using a quartz vacuum chamber with an ICP ion source. The experimental data for determining the location of Mach disc fit Eq. 19 very well. The observations indicate that the spatial locations of the Mach disc, the barrel shock and the zone of silence are similar to those expected from a supersonic molecular beam with neutral gases.

The density decreases along the streamline in proportion to the inverse square of distance downstream of the sampler. If charged species behave the same as the neutral gas, the above description is also suitable for ions and electrons. Thus,

$$n_x = \frac{1}{X^2} \qquad (21)$$

where n_x is the number density of electrons or ions at a axial position X downstream of sampler. A straight line should be obtained by plotting n_x vs. the $1/X^2$ if the flow follows the gas kinetic description.

Even through the gas dynamic force may dominate in the first extraction stage

in an ICP-MS instrument, the free jet expansion may be perturbed in several ways and the beam movement may depart from the ideal beam description. Those interference effects can directly influence the analytical performance of the ICP-MS as discussed below.

Effects of Boundary Layer Formation

As the plasma flows around the metal sampling cone, a thick boundary layer outside the sampler will be formed because the sampler is cooler than surrounding gas and the gas is cooled by thermal contact the cone. This is similar to the wave around the nose cone of a space vehicle re-entering the atmosphere.

The boundary layers affect neutral and charged species alike, and lead to changes in the velocity, temperature and composition of the bulk plasma before they pass into the mass analyzer. Figure 9 is a schematic diagram showing the boundary layer formation around the sampler tip.

Chemical reactions such as oxide formation occur readily in the cool layer, as can be seen by the red color near the metal surface when a concentrated solution of yttrium is introduced into the plasma. Physical interactions such as recombination, reflection and collision will also happen on the interface wall. When the pinhole-sized sampler orifice was used ($<100\ \mu m$) in the early instrument design, it was mainly the boundary layer that was sampled into the vacuum system for mass spectrometric analysis (4,16,17). It is undesirable that the oxide species formed in the boundary

layer surrounding the orifice are extracted into the mass spectrometer.

It is usually accepted (106,107) that if the orifice diameter exceeds a value of 100 λ (λ is gas mean free path) in front of the entrance, the gas flow will break through the boundary layer. Thus, the size of the sampling orifice should be large enough compared to the mean free path of the gas extracted at sampler so that the behavior of the expansion can fall into the continuum flow regime of gas dynamics. A minimum orifice diameter of 100 μm at 5000 K is needed to provide uninterrupted flow from the plasma into the vacuum system.

Mean free path along the axial position (x) inside the interface of an ICP-MS instrument can be calculated from

$$\lambda = (\sigma\, n_x)^{-1} = (\sqrt{2}\, \pi\, D^2\, n_x)^{-1} \qquad (22)$$

where D = atomic diameter of Ar = 3.8×10^{-8} cm and σ = cross-sectional area of neutral atoms. Taking the number density $n_x = 1.5 \times 10^{18}$, the mean free path is approximately 1×10^{-3} mm at the sampling entrance.

In a modern ICP-MS instrument, the sampling orifice (diam. $\sim$ 1 mm) is large enough for the plasma to flow through without interference by the boundary layer around the edge of the sampler tip. The gases sampled form the plasma source are therefore not cooled much by interaction with the sampling cone. However, even though the boundary layer may not be in front of the entrance, it contains cooled

plasma species all around the edge and some may be entrained by collision with plasma gases.

Effects of Electrical Sheath Formation

The sampling cone is an electrical conductor. As the sampler is inserted into the plasma, an electrostatic double layer will build up next to the surface of the cone. The zone, known as the space charge, sheath co-exists with the boundary layer. The sheath is no longer electrically neutral, and charge carriers from the plasma can be neutralized as encountered with the sheath on the surface. Growth of an extended space-charge sheath may modify the beam properties by electrical interactions and the beam may not represent the bulk plasma anymore. Figure 9 shows the charged double layer together with the gas boundary layer around the sampler surface.

The plasma is mainly neutral argon. It contains about 0.1% ions and electrons. Since the original material used to create plasma is neutral and we do not deliberately add or take away charges, the plasma as a whole should be electrically quasineutral. Ion density is balanced by equal electron density. If both electrons and positive ions go to the metal cone, electrons are much more mobile, and a sheath will form around cone with primarily positive ions.

The gas dynamic theory of a free jet expansion describes the movement of neutral species. If there is no electrical interaction at the sampling orifice, the ion beam will simply follow the behavior of the neutrals and the beam will remain quasi-

neutral. In this case no charge separation occurs as the plasma proceeds through the sampler. Experimental studies of the supersonic beam properties with other RF plasmas have demonstrated that the plasma could retain bulk characteristics after sampling through the orifice into a low-pressure chamber (97,99,107-110).

In modern ICP-MS instrument, it is generally believe that the bulk properties of the plasma remain unchanged as the plasma flows through the sampling orifice (102). The thickness of the electrical sheath can be estimated from Debye length λ_D calculation,

$$\lambda_D = \frac{\left[\epsilon_o k T_e\right]^{1/2}}{\left[e^2 n_e\right]}$$

$$\lambda_D \text{ (cm)} = 6.9 \, (T_e/n_e)^{1/2} \qquad (23)$$

where ϵ_0 = permittivity of free space, k = Boltzmann constant, e = electron charge, T_e (K) is the electron temperature and n_e (cm^{-3}) the electron number density at the position of sampling entrance. The value of λ_D is about 10^{-4} mm at the entrance of the sampler. The thickness of the sheath should be of the order of a few Debye lengths. Because $\lambda_D << D_o$, the plasma should expand through the sampler orifice basically as a quasineutral plasma.

Secondary Discharge and Ion Kinetic Energy

The plasma can arc strongly to the sampler. This discharge was called as "pinch" effect in the early work (112), it is now usually referred to as a secondary discharge. Douglas and French (113) found that the discharge is not a true electro-gas dynamic effect but rather appears to be simply an electric arcing between the ICP and the sampling cone. A severe discharge can cause numerous problems, including orifice erosion, high background emission, multiply charged ion formation, high ion energy, and high kinetic energy spread.

The secondary discharge is caused by a high radio frequency voltage induced capacitively in the plasma. The plasma is maintained by RF energy and the potential applied on load coil can couple to the plasma capacitively. Plasma, as good conductor, is connected to the grounded sampler through the low impedance of the sheath. The RF current flow to the grounded sampling cone is modified by the different mobilities of ions and electrons in the sheath. Because electrons are more mobile than ions, the plasma assumes a net mean positive DC potential. The phenomenon has proved by numerous experimental studies with Langmuir probe measurements (113-119).

The severity of the secondary discharge depends on load coil geometry and grounding arrangement. There are two basic types of coil arrangements: 1). end-tapped coil, or unbalanced coil; 2). center-tapped coil, or balanced coil. Either coil arrangement can yield good analytical results with proper care.

With the unbalanced coil, RF voltage is applied on one end and the other is grounded. This type has two different arrangements used in ICP analytical instrument, the conventional or normal geometry and the reverse geometry (Fig. 10). The reverse coil is usually used in ICP-MS by grounding the end of the coil nearest to the interface to reduce the electric field close to the sampling cone. The coil geometry shown in Fig. 10a is mostly used in ICP-AES. Because the coil is unbalanced, one can still either see visual discharge or observe telltale symptom of discharge under certain plasma conditions. With this coil arrangement, the discharge may be minimized by such as closer the sampling interface to the end of coil; lower aerosol gas flow; using higher forward power; and adding sample as dry as possible.

With the balanced coil, either the center-trapped (Fig. 10c) or the new design from free-running generator, little or no discharge can be seen under any plasma conditions. Plasma potential and ion kinetic energy depend only slightly on plasma operating conditions. The center-tapped load coil arrangement was introduced by Douglas and French (113) in attempt to reduce the plasma potential. The impedance matching networks used in the end-tapped and center-trapped arrangements are shown in Figure 11. It was found that the plasma RF potential can be greatly reduced with the modified load coil. If the ground is near the center of the coil at C, point B and D will have nearly equal RF amplitude but will have opposite phases. The sum of the effects of the capacitively produced voltage will then cancel.

All species in the gas are accelerated to the same speed as neutral Ar in the

supersonic jet, therefore the ion kinetic energy is dependent on mass. If the plasma potential is small, the ions reach the same speed as the terminal velocity u. The kinetic energy $E(m_i)$ for an element ion of mass m_i is

$$E(m_i) = 1/2\ m_i u^2 \tag{24}$$

$$E(m_i) = (m_i/m_{Ar})\ E_{Ar} \tag{25}$$

where E_{Ar} is the energy of the argon ions and m_{Ar} the mass of argon. A straight line should be obtained by plotting of the ion energy versus mass. Since the residue potentials contribute to the total ion kinetic energy, the ion energy are more accurately described by (69)

$$E(m_i) = (m_i/m_{Ar})\ E_{Ar} + V_p \tag{26}$$

where V_p is approximately the plasma potential inside the interface of ICP-MS.

The ions originate from a region in the ICP ion source is positive with respect to the grounded sampling cone. As ions in the plasma flow through the orifice they are accelerated across this potential difference to higher kinetic energies than they would get just from the expansion alone. The values of offset potential (V_p) vary with the different load oil geometry (94,121,129), aerosol gas flow rate (129), and amount of solvent load (122,141).

Diagnostic Studies of Ion Sampling Process

Essentially, the plasma should be extracted though sampler without major changes in chemical composition, except perhaps for formation of weekly-bound adducts with Ar. The mass spectrometer can be simply used as a diagnostic tool. The mass spectra will be reasonably reflective of probable ionic composition of ICP.

Ion electron recombination is unlikely significant because of short time frame ($\sim 3\mu s$) of collisions during extraction. Ionization temperatures can be determined by ICP-MS measurements (127-129) as a diagnostic parameter. If recombination was significant, it would not be seen that reasonable value of T_{ion} by mass spectrometric measurements. Collisions may still be rich for the first few orifice diameters and essentially less collisions at high Mach number region within the jet. With the gas velocity $u \sim 3 \times 10^5$ cm s^{-1}, it will take about 3 μs for the plasma to flow from the sampler to the skimmer. This corresponds to approximately 250 collisions between neutral Ar atoms and other species as estimated by Douglas and French (102). Thus there will be enough collisions to cause Ar adduct formation such as ArH^+, Ar_2^+, and ArO^+. More of such adducts can be seen than would be expected from the ICP alone. The density of oxygen species in the plasma should be much less than that of neutral Ar, so it would not be expected to have much MO^+ during extraction, unless the cross-section for oxide formation between M^+ and O were very large.

Fluorescence studies (130) indicate that there is little neutral sodium Na inside the zone of silence of the free jet, which shows that little ion-electron recombination

occurs during the initial extraction and supersonic expansion. Gas kinetic temperatures T_{gas} in the Mach disc region are of the order of 2200 K, as determined from linewidth and OH measurements. Collisions in the Mach disc re-heat the sampled gas substantially. These observations substantiate previous theoretical descriptions of the various properties of supersonic expansion from an ICP source.

The electron number density (n_e) and electron temperature (T_e) are two important parameters to describe the properties of the extracted beam. Langmuir probe studies (114,132,133) indicated that T_e in the jet at least as high as that in the ICP. This possibly is the evidence that T_e is enlarged by interaction between plasma and sampler. Figure 12 presents a profile of the measured T_e at 1.0 l/min aerosol gas flow rate in the first stage between the sampler and the skimmer. The magnitude of T_e decreases as the beam proceeding downstream. Generally, T_e increases as the aerosol gas flow rate increases, as power decreases, and as water loading increases. These results are opposite to the trends that would be expected from the ICP itself (134). It is believed that the high T_e value is due to the residual discharge that is not overly strong if plasma conditions are adjusted properly.

The dependence of neutral gas density on the axial position in an ideal supersonic expansion is well-known and the profiles of electron number density measured between the sampler and the skimmer demonstrated a $1/x^2$ fall off along the axial centerline of the plasma flow except at the position very closing to the skimmer cone (Fig. 13a and 13b). It is indicated that the movements of ions or electrons are

very similar to the neutral beam expansions in the supersonic jet. The experimental results support the hypothesis that the charged particles flow though the sampler as a quasineutral plasma without significant separation of positive and negative charges.

Measurements of the ion kinetic energy can also be useful for diagnosis of the ion sampling conditions in ICP-MS. The ion kinetic energy can be measured by applying a positive stopping voltage to the quadrupole mass analyzer and the ion-optic lenses (114,120-124,165), or by means of retarding plates installed in the MS system (126). The studies have demonstrated that the ion kinetic energy does indeed increase with mass and slightly vary with plasma operating conditions. The results from the experimental measurements with a center-tapped load coil (121) and reversed load coil (129) are shown in Figure 14. The intercepts of the plots are all not zero, which indicate residual plasma potential existing in the ion beam. A offset potential of $\sim$ 2 eV (Fig. 14a) is resulted from a system with the center-tapped load coil, and a higher potential over 5 eV from a house-made Ames instrument with a reversed load coil (Fig. 14b). It can be seen that varying the aerosol gas flow slightly changes the ion kinetic energy. By simply increasing the solvent load, Hutton and Eaton (122) reported that the ion kinetic energies can be altered from 3-5 eV to 10-12 eV across the mass range.

SKIMMING PROCESS

Skimmer Operation

Kantrowitz and Grey [93] designed the first skimming system with an axisymmetric converging-diverging nozzle and described theoretical treatments for the ideal skimming with isentropic beam expansion. The success of using skimming technique in ICP-MS were first demonstrated by Douglas (27), and Date and Gray (25) based on the early molecular beam work of Campargue (91). A diagram of the skimmer arrangement is shown in Figure 15.

Proper functioning of the skimmer is the key to success in nozzle beam design. Figure 16 gives the schematic picture of the skimming position relative to the Mach disk in a supersonic jet extracted from an ICP, a) skimming position behind Mach disc; b) skimming position at Mach disc; b) skimming position at ~2/3 of the jet from sampler orifice; d) skimming position too close to the sampler orifice.

In practice, if skimming at a position $X_s > X_m$, the shock wave forms in front of the skimmer and the skimmed ion beam will be dominated by effusion of ions that have been scattered by the shock (135). For $X_s \sim X_m$, the maximum beam intensity will be obtained and background gas will be also entrained. For $X_s < X_m$, the skimmer is inserted inside the jet at a proper position, penetration by background gas will minimized. As skimming position very close to sampler, the supersonic beam is not well developed and it may make ion collection and focusing more difficult.

A number of unanswered questions remained. Most important of these is the question of whether the gas could pass though the skimmer without interference. The interaction of the jet with the skimmer may cause a nonideal beam and some attenuation of beam intensity will occur at high jet density.

Plasma Flow through Skimmer

In the ideal skimming condition, the skimmer should be not affect the upstream flow and should be no shock formed at the tip and downstream. The flux of gas flow through the skimmer is given by

$$G_{Flux} = n(X_s)\, u(X_s)\, A_s \qquad (27)$$

where X_s is the distance from sampler orifice to the skimmer tip, $u(x_s)$ the flow speed at the skimmer, and A_s the area of the skimmer entrance. For a ideal skimming process, $n(x_s)$ and $u(x_s)$ can be calculated from the descriptions of supersonic jet (Equations 16 and 15) provides the skimmer tip is well within the zone of silence.

If neutral density n_o at the sampling entrance is 1.5×10^{18} cm^{-3}, skimming position at 10 mm downstream from the sampler and the skimmer orifice diameter D_s = 1 mm, the neutral density at the tip the skimmer can be calculated (from Eq. 19) to be approximately 2.4×10^{15} cm^{-3}. Taking $u = (5kT_o/m)^{1/2} = 2.3 \times 10^5$ cm s^{-1}, the gas flow through the skimmer should be about 4.3×10^{18} atoms/s.

Douglas (225) compared the measured and the calculated flow through the skimmer of an ICP-MS interface (Fig. 17). The interface had a sampler of 1.14 mm orifice diameter and sampler of 0.88 mm orifice diameter. The dashed line shows the beam flow profile calculated from Equation 23. The measured flow profiles at three different pumping speed clearly show the corresponding Mach disk positions. The results of measured beam flow through the skimmer show a systematic deviation from the theoretical calculation which is greatest at small X_s.

For a given skimmer shape the flow may be characterized by the skimmer Knudsen number (Kn). The interferences can be minimized by operating the skimmer at large Kn (Kn > 1). Knudsen number is basically the ratio of mean free path λ to the size of an object immersed in the flow. For this calculation

$$Kn = \lambda/r_p = 1/(\sqrt{2}\ \pi\sigma^2 n r_p) \qquad (28)$$

σ^2 = collision cross section for Ar atoms[1] = 4.1×10^{-15} cm^2 [1,2]

Because the mean free path and flow characteristics of the expansion change with axial position, Kn also must be calculated separately at each position. The neutral density is assumed to drop proportionately to $1/x^2$, as described above. As stated earlier, the Knudsen number in our system is less than unity ($\sim$0.24). This is close to the calculation of Kn = 0.3 in Elan Sciex ICP-MS reported by Douglas (102). Therefore, it is reasonable to believe that the collisional frequency is still

considerable at skimmer orifice and consequently the beam flow may be interrupted by the presence of the skimmer cone.

Ar atoms (majority specie) in the plasma gas can reflected from the external and inside surface of the skimmer and formed shock wave in the beam process. Such effect will depend on the density of the jet approaching the skimmer. For a very low gas density in the supersonic expansion, $Kn >> 1$, the flow is nearly free molecular and the scattering is negligible. For higher density plasma beam as in the first stage of the ICP-MS instrument, $Kn < 1$, the flux of the plasma gas is believe to be sufficiently high to drive Ar atoms reflected in front of and inside the skimmer and shock wave may be formed around the skimming entrance in a severe case. The density of the neutral Ar atoms is about 2×10^{15} cm^{-3} at the skimmer entrance. With a large number of collisions, the ion movement will become more randomly directed. Therefore ions have a great chance to interact with the skimmer wall and scattered away from the beam centerline or lost by neutralization on the wall.

Niu and Houk (133) measured the electron densities inside the skimmer tip as given in Tables 2 and 3. The measured n_e values are below those expected from the $1/x^2$ fall of n_e in the supersonic jet. For an ideal skimmer, the electron density behind the skimmer would continue to drop with the same dependence as described for beam expansion in a supersonic jet. Instead, the measured values of n_e behind the skimmer are much lower than those expected and the attenuation of the number intensities are more sever in the wet plasma conditions. The ratio of measured n_e to the calculated n_e

decreases as aerosol gas flow increase at the simmer entrance.

Quadrupole-based ICP-MS devices measure roughly one analyte ion for every 10^4 to 10^6 analyte ions through the skimmer. The low n_e values behind the skimmer represent one possible contribution to ion loss and overall inefficiency in ion extraction in ICP-MS.

If the plasma beam flow through the skimmer without perturbation, it should continue to expand isentropically with the number density fall off in the scale of $1/x^2$ from the sampler orifice. The experimental studies by Niu (133) indicated that the skimming process is far from ideal and a second expansion may exist as the beam flow downstream of the skimmer in a home-made ICP-MS instrument. The interferences in the beam processes are believe mainly caused by the gas interactions with the metal surfaces. A shock wave can be formed near the skimmer tip or inside the skimmer and scatter the beam in the centerline of the gas flow.

The electrostatic effects may be no significant in the region until the beam approach to the region of the ion optic lenses. Under the normal operation conditions, the plasma pass through the skimmer should remain quasi neutral. Electrical forces that possibly affect the beam processes at and after the skimmer will be discussed in the following.

Electrical Interaction with Skimmer

As the beam passing through the skimmer, an electric sheath forms around and inside the edge of the skimmer orifice. Electrical interferences can be estimated by evaluation of the electrical sheath, which should be no more than a few Debye lengths thick around the skimmer orifice (136). The value of the Debye length can be calculated from Equation 23 by measuring or estimating T_e and n_e at each axial position along the centerline of the plasma flow.

For aerosol gas flow at 1 L/min, the estimated λ_D is about 10^{-2} - 10^{-3} mm at the metal surface of skimmer tip. For a typical skimmer (orifice diameter about 1 mm), the sheath will be much smaller than the hole diameter. It is therefore reasonable to assume the bulk plasma extracted through skimmer still remains quasineutral.

As beam expands beyond skimmer, electron number density drops along the flow. The higher the number density, the smaller the λ_D value. At a distance far enough behind skimmer and near the ion lens, the beam may be no longer quasineutral. λ_D value may be increased more steeply to about 0.1 - 2 mm. Here the Debye length is significant compared to the dimensions of the ion lenses. Some charge separation will likely occur, even if no potential is applied to ion lenses. In the normal operation of ICP-MS, a negative voltage may be applied on the first ion lens to extract and focus ion beam. The electrical field produced by the negative voltage on ion lenses, may exacerbate the charge separations.

Douglas (169, 170) found that ion transmission through the skimmer can be strongly affected by the relative RF potential between the skimmer and ICP. The potential can be controlled by applying an RF signal of variable phase and amplitude to the skimmer. Arcing at the interface was eliminated and the signal to noise ratio was improved by a factor of approximately 2 by correct RF biasing of the skimmer. In Ames, a floating interface was studied for plasma extraction from an ICP (221). As modest voltages (10 - 50) were applied to the sampler and skimmer cones the ion transmission was improved. The mass discrimination was reduced with this instrument as the sampler floating and skimmer biased by 30 V.

Space Charge Effects in Beam Process

Space-charge effects cause problems in the ion beam processes in ICP-MS. The electrical forces in a ion beam can give rise to three basic phenomena: 1) modifying the potential in the region that it traverses, 2) beam spreading due to space-charge repulsion effects, 3) current limitation.

The maximum ion current limit I_{max} (in μA) through a cylindrical lens due to the space charge effect can be obtained from (137,102)

$$I_{max} = 0.9\ (m/z)^{1/2}\ (D/L)^2\ V^{3/2} \qquad (29)$$

where D and L (D/L=0.5) are the diameter and length of a cylindrical lens,

respectively. V (volt) is ion energy. The equation pertains only to major ions, not to trace analyte species.

Olivares and Houk (31) made the first suggestion that space charge might be important in the ion optics of ICP-MS as they estimate a high ion current flowing downstream of the skimmer to the entrance of ion lens. Gillson *et al.* (139) reported that the total measured ion current collected at ion optics region was only about 6 μA. The difference was considered to be caused by space charge effects within the skimmer and ion optics.

If Ar gas flow through the skimmer at 1 x 10^{19} atoms/s into the ion optics and taking ionization fraction as 0.1%, the ion current can be very high about 1 mA (69), which is large than predicted maximum current. The space charge effects probably are substantial in this region. The computer simulation models have been described with and without considering space charge effects in the ion beam formation (139,140). The results of ion trajectory calculations demonstrate great beam explosions downstream of the skimmer to the region of ion lens due to the electrical effects. Figure 18 shows the trajectories calculated for $^{24}Mg^{+}$ as a function of incident ion current. At higher incident ion current, more ions are defocused onto the inside walls of the skimmer.

In the experimental diagnostic studies, Chambers and Hieftje (116,126, 141,142) investigated the ion sampling process by measuring floating potential, kinetic energy and ion signal intensity at a variety of operating conditions. They stated that

the extracted plasma beam was electron-poor and hence electrostatic forces played a significant role in the transport process. According to the hypotheses, the bulk plasma sampling from ICP is questionable and space charge may dominate the processes both in the first and the second stages of ICP-MS in some extent. The beam behavior may not be described accurately by the gas dynamic consideration along.

It has been also suggested (139) that space charge effects in the ion optics can contribute to non-spectroscopic interelement interferences. More detail will discussed in the next section.

Matrix Effects in Beam Process

Matrix effects in ICP-MS can cause either spectroscopic interferences or nonspectroscopic interferences. The interferences are a result of a high concentration of a concomitant and may arise from different areas in the instrument: 1) sample introduction, 2) plasma ion source, 3) ion sampling and skimming processes, 3) ambipolar diffusion or space charge effects in the ion beam process; 5) mass discrimination in ion optical system.

Although many investigators have investigated the dependence of matrix effect on various parameters (32,139,143-153), the origins have not been fully understood. Matrix effects were reported to be more severe in ICP-MS than in ICP-AES, thus it must be more associated with the ion extraction and beam focusing processes in mass spectrometer. A diagnostic study by Niu *et al.* (132) revealed that the fall-off of

electron density in the beam downstream of the skimmer can be altered by adding concentrated matrix elements. In general, heavy matrix ion tend to suppress analyte ion signals more extensively than light matrix, and low mass analytes are subject to more serious suppression than heavy analyte ions.

Space charge effects have been broadly discussed related to the matrix effect during the ion extraction and beam transmission processes (139,140,32). Yet, the mechanism is still hypothetical. The space charge depend on the electrostatic forces of individual ions and the electrical Coulomb force tends to make the ion beam divergent. The extent of beam deflection depends on ion kinetic energy. As beam expands from supersonic jet, atoms with different mass are accelerated by aerodynamic forces to about the same velocity. Light ions have lower kinetic energies and are deflected more. Light analyte ions are deflected most extensively by heavy matrix ions, so they suffer the greatest matrix effects.

The matrix effects also cause mass discriminations in the present ICP-MS. Approaches to minimizing such problems have been reported by adjusting the voltages applied on ion optical lenses (139,145,149,156,157). In applications, the interferences can be compensated by internal standard (154), standard additions and isotope dilution (155,156). Alternatively, Ross and Hieftje (158) reported a way to mitigate matrix effects by adjusting either the plasma condition (solvent load, or central-gas flow) to alter the expansion in the first vacuum stage or to optimize the first-stage pressure. They also investigated (159) the modified ion-optic lens configuration to eliminate the

matrix effects. It was reported that the simplification of the ion lens system in ICP-MS can overcome mass dependent interferences. The optimal configuration was found to be one which had no photon stop and no second-stage optics. However elimination of the second stage optics only would cause substantial ion transmission loss.

Crain *et al.* (149) studied the influence of skimmer orifice dimension. It was found that smaller skimmer induce more extensive signal suppression effects for light element in presence of heavy matrix elements.

It is understandable that a high accelerating voltage can suppress space charge and matrix effects. Boorn *et al.* from Sciex (160) reported a modified ion optical arrangement for alleviyating some of the matrix effect by providing a higher extraction potential downstream of the skimmer. The ICP-MS system developed by Turner (161) uses a high accelerating voltage ($\sim$ 2000 V) on the cone behind the skimmer. The matrix effect due to space charge may be overcome as ions are accelerated to a high kinetic energy in the ion extraction and beam formation processes.

ION OPTICS AND BEAM FOCUSSING

Ion Optics and Lens Design

After the beam passes the skimmer, ions are transferred to the mass analyzer via an ion lens system. The transmission efficiency of a mass analyzer can be strongly dependent on the spatial characteristics of the ion beam produced by the lens. A number of general references can be found in the literature on ion optics and beam focusing (138,162-164). The design of ion lens has been greatly facilitated in recent years by computer program such as SIMION (166), in particular a revised version for use on a personal computer (167). The ion lenses used in ICP-MS instruments can be represented by Sciex and VG designs as shown in Figure 19.

Electrostatic lenses are generally used to produce a focused beam of ions in mass spectrometer. The number of possible electrode combinations is infinitely large and there is a variety of feasible sets of element geometries and dimensions that all lead to different lenses. Even for a simple two-cylinder arrangement, the properties of the system depend on a large number of parameters, such as electrode voltage ratios, cylinder dimensions, and diameter to length ratio, electrode thicknesses and spacings between them.

The lens need to be fabricated accurately. Stainless steel is commonly used for the electrode material. The design of electrostatic lenses is usually done by trial and error. To predict focusing properties, the trajectory calculation can be helpful by

using computer program. However, it has to be reminded that the programs such as SIMION may only give a rough picture and sometimes may have a substantial deviation from the real situation. In recent years, SIMION with space charge consideration have been developed (139,140).

Figure 20 gives a schematic diagram illustrating the paths of positive ions in a two-cylinder ion lens. The electrodes are held at potential V1 and V2. Deep inside each cylinder, the potential are very close to those of the electrodes, but in the center of the system the potential changes quite rapidly. The electrical field between the lenses forms the pattern of equipotential surface, which will act like a optic lens to provide focusing property for positive ions or electrons. Ions move through an electric field just as light rays do through a medium with a continuously variable index of refraction. For focusing ion beams, the electrode potential are negative. Ion 1, which travels on centra, will act upon symmetrically and pass straight through the lens. Ion 2, which travels off axis of the lens, will be deflected closer to the central flow. As ions move further downstream through the second lens, the ion may cross the axis and diverge again. More electrodes may be used to provide additional focusing action to transmit ions after skimmer to mass analyzer.

Einzel lens is commonly used in mass spectrometry to focus ion beam as shown in Figure 21 (as the arrangement in Sciex ICP-MS). Generally, an einzel lens system refer to a three-element lens operated symmetrically, with V3 = V1 and with V2 taking any appropriate value. The system does not change the ion kinetic energy

while providing the focusing action. In the Sciex ICP-MS, a typical einzel lens setting is that V1 = V3 = -12 V and V2 = -130 V (140). The ion trajectories through the ion optics have reported by Vaughan and Horlick (171).

The trajectory of an ion in an ideal lens is independent of its m/z ratio provided that ion of different mass start with the same initial kinetic energy and position. The ion motion is governed by the Laplace equation. The focal properties of an electrical ion lens system should not differ for ions with different m/z, and a single ion lens voltage set may be used to transmit ions of all m/z values with uniform efficiency.

Like optical lenses, ion lenses can be characterized by focal points, principal planes, etc. Unlike optical lenses, the ion transmission and focal properties of ion lens can be simply adjusted by changing voltages applied to the ion lenses. However, it is much more difficult to design specific ion lens for guiding ion beam and to correct the aberrations. In optical system, the focusing properties of lens can be more easily detected or visualized. In addition, ion beam focusing may suffer more interferences such as space charge effects. The mass discrimination in ICP-MS instrument, until recently have been poorly understood (34). It is obvious that the ion lens configuration can have a substantial influence on mass-dependent matrix effects in ICP-MS.

New Ion lenses developed for ICP-MS

Turner lens system A three aperture sampling system is used in the TS SOLA ICP-MS instrument (Fig. 22). The system was designed by Turner (161). The innovative approach is using a accelerator cone which is some 10 mm behind the skimmer cone. This arrangement is identical to that commonly used in duoplasmatron ion sources (168) and has been described by Hayhurst and Telford (90). Quite high voltage (-2 kV) applied on the accelerator cone. The first lens used in Ames was somewhat like this. The main function of this electrode is to provide a strongly accelerating and convergent electrostatic field to minimize the space charge spreading of the substantial ion beam emerging from the plasma sampling interface. A secondary function of the accelerator cone is to act as a differential pumping aperture between the second and third pumping stages of the vacuum system. Figure 22 also shows the ion beam trajectories through the accelerator cone. An accelerating potential of 2000 volts is used on the acceleration cone, and behind this a simple deflection system with a single variable einzel lens focussing potential is used to transfer the ion beam onto the entrance aperture of the analyzing mass spectrometer. It is possible to focus ions of a wide energy spread into the quadrupole, and hence minimize the mass discrimination in this section of the instrument.

Yokogawa lens system A unique ion optical system employs an offsetting lens arrangement to eliminate photon noise, resulting in random background level. Both the PMS 2000 and the new design of HP 4500 of Yokogawa use the offsetting

system as shown in Figure 23). It was claimed that the ion counts obtainable with the lens are very high (~ 10^8) counts s^{-1} ppm^{-1}) with a typical background below 50 counts s^{-1} (< 2 cps in new design).

Ames lens system The Ames laboratory new ion optical system (172) is shown in Figure 24. The ion lens deflects ions off center and then back on center into the differential pumping orifice. No photon stop is needed in the in the center of the beam. Calculation of ion trajectories with SIMION show that only those ions that leave the skimmer on the center are transmitted, whereas most other lenses used in ICP-MS transmit only ions that leave the skimmer off axis. Together with the new ion lens, a relatively large sampling orifice (1.31 mm) improved signals and minimized plugging from deposited solids. The photon emission from the ICP is blocked effectively by the offsetting ion lens. The new ICP-MS with the ion optics system yield very low levels of many troublesome polyatomic ions such as ArO^+, ArN^+, Ar^{2+}, ClO^+, and $ArCl^+$. Grounding the first electrode of the ion lens can reduce the severity of matrix effect to about 20% loss in signal for Co^+, Y^+ in present 10 mM Sr, Tm or Pb. This, this latter lens setting minimizes matrix effects with only about 30% reduction in sensitivity for analyte elements.

INTERFACE DESIGNS AND PRACTICAL CONSIDERATIONS

Sampler and Skimmer Designs

The development of the ion sampling interface have been the heart in the success of ICP-MS. The sampling and skimming cones are crucial parts of the interface. The basic principles have been described in the above sections for plasma beam extraction. Here some considerations for designs and practice are discussed. New approaches to sampler and skimmer construction are introduced.

The basic requirements for sampler construction are: 1) providing bulk sampling by using a sufficiently large orifice (0.7 - 1.2 mm diam. is common); 2) orifice tapered toward the ion source to provide appropriate flow pattern and to avoid the boundary layer extraction; 3) the material used to construct cones must have a sufficient high thermal conductivity to withstand the high temperature of an ICP.

Sampling cones are usually mounted on a water-cooled front flange of the first vacuum chamber. Cones are also designed to have a screw base for convenient replacement. A variety of metal materials can be used to construct sampling cones such as copper, nickel, aluminum, platinum. Nickel is most commonly used due to the durability and cost. In some special cases, sampler with different materials may have to be used depending on the types of sample introduced such as high acid, salts or oxygen concentration. The sampler can be easily worn out by surface pitting and cracking, or by plugging with deposited solids. The improper sampling condition can

be noticed by monitoring the first stage vacuum pressure and spectral interference from ions from the sampler material. As the solid deposition become severe, the effective diameter of the orifice will be reduced, consequently the vacuum pressure in the first stage will gradually drop, and the analytical signal will decrease. On the other hand, if the pressure increases to a value beyond the normal condition, the sampler or the skimmer tip is probably melted and need to be replaced.

Figures 25 and 26 show the photographs of the sampler and skimmer in VG and Sciex ICP-MS instruments. In Ames ICP-MS instruments, the cones of sampler and skimmer are relatively bigger (Figure 1) than the commercial ones. The sampler (Figure 27) is rounded in contour near the orifice in contrast to the more sharply pointed orifice in VG and Sciex designs.

The skimmer is inserted in the supersonic jet for re-sampling ion beams. It is rare for the skimmer to be blocked, however, the tip may be melted very easily especially when the Mach disc immersing on the tip of the skimmer. In normal operation, the skimmer usually get very hot because of the shock wave surround the jet. When the first stage pressure is too high, the expansion shrinks and the Mach disk may move in front of the skimmer tip.

The skimmers are mostly constructed from stainless steal or nickel materials. Great care must be taken in design to avoid disturbance of gas flow. Generally, ion transmission is maximum if the external angle of the skimmer is about 60°. The internal angle should be large to allow easy escape of the scattered atoms into the

chamber pump. The edge of the skimmer orifice must be sharp to prevent formation of a shock wave. A large external angle or imperfections of the skimmer orifice will result in disturbance of the beam process.

Sampler and skimmer construction has been continuously improved by instrument manufacturers and few can be found in publication. Followings are some new approaches to ion lens design for ICP-MS:

Lichte sampler The sampler was made by coating a platinum sampler with ThO_2 (201). The advantage of this sampler is that it gets very hot. It can last longer because of the protective oxide coating can be regenerated readily.

Rounded skimmer of Doherty It is claimed that the rounded skimmer can improve stability. Because the skimmer heats up anyway in ICP-MS, and even small change in profile of tip due to erosion or deposition can change signal drastically, it is perhaps best to accept inevitable and use rounded-off skimmer.

Two-angle skimmer from VG The skimmer has a sharp, short tip on the shallow base (Fig. 25b). It is claimed the design yields substantially higher analyte signal. This perhaps will allow extraction field of first lens closer to skimmer tip.

Polish inside of sampler and skimmer The technique was developed by Hutton in an attempt to reduce polyatomic ions (222). This indicates that some polyatomic ions may be generated as beam interaction with the metal surfaces of the sampler or the skimmer cones.

Solid Deposition and Interface Erosion

Solid deposition and sampler erosion on the extraction interface are the problems unique to ICP-MS. Deposition on the sampler and skimmer may cause orifice blockage and thus cause long-term drift in mass calibration.

Douglas and Kerr (173) investigated the rate of deposition of solid resulting from the analysis of solution with 0.1-1% dissolved solid. They concluded that deposition decreased with both increasing power and decreasing aerosol flow-rates. In addition, it was observed that a pseudo-steady-state could be reached after a period of time. Williams and Gray (174) showed that different plasma operating conditions led to different rates of solids deposition and that individual analyte signals decay at different rates when cone blockage occurs, making correction with internal standards difficult. It was also found that the rates of solids deposition and erosion reached a steady state.

Solids also deposit on the ion optical lenses leading to electrical charging and a change in the optical system optimization. The effect of the deposition depends on the specific interface designs, plasma operation, rate of nebulization, as well as elements and concentrations. A deposition rate of approximately 10^{-8} g s^{-1} was reported (173). If a insulating layer coated on the surface of lens elements, the ion optical system will function differently in beam focusing. Even slow deposition rate can cause instrument drift and poor long term stability.

Ion optics for ICP-MS must be tolerant of deposition of salts from the plasma

source. Especially, for an ion optical design if a small change in voltage of an ion lens causes a large change in ion signal, the optical design will be very sensitive to the salt deposition and will suffer from long team drift.

Changing the sampler and skimmer geometries have little effect on the deposition rate. An effective way to protect the ion lens is made by Sciex. In Sciex ICP-MS, a small stop at the base of the skimmer is installed to "shadow" the entrance to the Bessel Box to prevent salt deposition on ion optical lenses (Fig.12a). It was claimed that the long term stability of the instrument was greatly improved, particularly for the real sample analyses.

Vacuum System in ICP-MS

The operation of mass spectrometer requires a vacuum environment because low pressure is essential to sustain ions or electrons in the gas phase and preserve detecting power in mass analyzer. The vacuum equipment and designs are therefore are important for extracting plasma from atmospheric pressure into mass spectrometer. The discussion in this section is restricted to the vacuum system for ICP quadrupole instrument. The general description of the vacuum system can be found in the literature for interested readers (175-179).

Several types of vacuum system designs can be used in the mass spectrometry. The simple one could be the single-stage vacuum system as shown in Fig. 28a. Ions are extracted from ion source through ion optics to mass analyzer. This system need a

high speed vacuum pump and the sampling orifice has to be small (typically ~ 20 - 100 μm). Fig. 28b is a two-stage vacuum system with a differential pumping plate in front of the mass analyzer. This may represent the earlier experiences in developing ICP-MS with a boundary layer sampling (4,21,22).

All present ICP-MS instruments use differential pumping vacuum system with skimming process. In the early design of Sciex Elan ICP-MS, a two stage system was used because the large pumping capacity of a cryogenic pump installed in the second stage after the skimmer. Fig. 28c shows a three-stage system with ion lenses and mass analyzer. The purpose of the multiple-stage vacuum is the use of a large orifice and extraction of a large number of ions. By using a skimming cone, a better shaped beam will be presented to the mass analyzer. The flow of ions and neutral gases into the mass analyzer is limited by the speed of pump of the second stage.

The pumping speed, S_p, can be defined as volume of gas removed in unit time, t (s), at a pressure, P (torr). Pumps are available with speed from a few l/s to thousands of l/s. If two chamber are separated by an orifice of area A (cm^2) and the diameter of the orifice is such that Kn > 1 for air at 22 °C, the conductance of a orifice will be C(l/s) = 12 A. The conductance of a circular tube in the molecular flow conditions can be expressed as $C = 12D^3/L$, where D is the diameter and L the length of the tube. For a vacuum system with the net pumping speed S_2 (pressure at P_2) and gas inlet from a orifice of conductance C_1 (pressure at P1), the throughput will be balanced by the equation of $P_1C_1 = P_2S_2$.

In ICP-MS, a mechanical pump is generally used on the first vacuum stage for maintaining a pressure ~ 1 torr. If 10^{21} atoms/s extracted into the first chamber and usually 1% pass through the skimmer, the bulk of the extracted gas need to be removed here. Generally, a pumping speed of 10 l/s will work well. Varying the pumping speed of the first stage will not affect the gas flow in the zone of silence very much even though it does change the relative position of Mach disc or shock waves. Sometimes, the relatively small gain achieved may not justify the large expenses and difficulties of the installation of large high vacuum pumps.

In the second stage, ion optics are arranged after the skimmer. The pressure is about 10^{-3} - 10^{-4} torr. Gas flow through the skimmer (D_s = 1 mm) can be estimated by calculated the conductance (C_{skim}) to be ~ 0.12 l/s at molecular low condition. Supposing P_1 = 1 torr and $P_2 = 2 \times 10^{-4}$ torr, the pumping speed S_2 = 600 l/s can be estimated based on $P_1 C_{skim} = P_2 S_2$. Therefore, a large pumping speed is needed. The turbo pumps and diffusion pumps are generally used to meet the vacuum requirement. The pumping speed and pressure in the second stage may determine the sensitivity in a great extent. Usually, a compromise on pumping will compromise sensitivity.

The third stage pressure is about 10^{-5} - 10^{-6} torr. Gas flow from the second stage through a differential aperture. If the geometry of the entrance taken as a short tube with diameter D_{DP} = 0.25 cm and length L_{DP} = 0.1 mm, the conductance C_{DP} can be estimated to be about 2 l/s. From $P_2 C_{DP} = P_3 S_3$ and taking $P_3 = 2 \times 10_{-6}$, the

pumping capacity can be calculated to be about 200 l/s for the third stage. Therefore, a small turbo pump are adequate here, even though the large pumping speed may provide better performance.

Interfaces for Alterative Mass Spectrometry

1. Magnetic Sector Mass Analyzer

The quadrupole mass analyzer is typically operated at unit mass resolution. It is sufficient to resolve the mass numbers of isotopes across the mass range but it can not resolve most of polyatomic ions at same mass as the analyte ion. Table 4 presents some examples of mass resolution required to separate polyatomic and analyte ions. Many polyatomic ion interferences could be overcome with an ICP coupled with a double focusing magnetic sector mass spectrometer.

Bradshaw *et al.* (181) described a high resolution ICP-MS design. A resolution of 10,000 is readily achievable with this instrument. The interface region is similar to that used in VG quadrupole ICP-MS. A schematic diagram is shown in Fig. 29. The significant difference is that the whole interface system is electrically isolated and very high voltage ($\sim$ 4 kV) applied to the sampler and skimmer cones. The magnetic sector mass analyzer requires an initial ion energy that is significantly higher than that of the quadrupole to minimize aberrations. Typical accelerating voltage is about 4 kV. A capacitor (1000 pF, 10kV) is used to link the interface and the torchbox and also the pump has to be isolated from ground. In order to efficiently

transmit ions through the instrument it is necessary to change the shape of the ion beam from a circular cross section to a rectangular cross section. The kinetic energy attained through the interface will be determined by the potential on the sampler plus acceleration imparted by the supersonic jet.

For positive ions, beam acceleration can be achieved by either float interface positive at a potential or float flight tube at a negative potential. In principle, these should be identical. Otsuka *et al.* (226) described an ICP-MS using a high resolution double focusing mass spectrometry. A interface was developed with a high voltage (5 kV) applied on the flight tube to obtain high ion transmission efficiency (Fig. 30). In the VG high resolution ICP-MS, the high positive potential are applied to the float sampler and skimmer. It is interesting that ions still pass through sampler while sampler held a high positive voltage. This is another indication that charge neutrality holds during early phases of extraction, or ions would never go through such a high positive potential on sampler. It seems like the apparent DC potential in plasma simply floats relative to that on the sampler, so one can put high potential on latter and still get ions through.

With a resolution power of 10 000, most of the polyatomic ions can be well resolved in ICP-MS spectrum. Some isobaric interferences still cannot be resolved, for example, $^{87}Rb^{+}$ and $^{87}Sr^{+}$ which need a resolution of greater than 300 000. As expected in any magnetic sector mass spectrometer, the increase of resolution will be at the cost of ion transmission.

2. Time-of-Flight Mass Spectrometry

TOFMS can provide high throughput and relatively high resolution comparing with quadrupole mass analyzer. Simultaneous multi-element capability can be achieved with typical mass resolution of > 1000. Most TOF mass spectrometries make use of so called pulsed ion source. Continuous ion sources like the ICPs are need spatially modulated to create the desired ion packets for TOF mass analysis. However, short signal pulses of typically 10 ns duration with a high repetition frequency require powerful data processing.

Two groups have started to investigate the techniques for combining the ICP with TOFMS (182, 183). An interface design is shown in Fig. 25 for coupling TOF-MS with an ICP ion source (183). The ion beam is extracted through the sampler and skimmer as same as in a quadrupole ICP-MS. However, as beam flows into the third stage the beam will be deflected by a right angle pulsing device for time-of-flight mass analysis.

SPECIAL ASPECTS OF EXTRACTING IONS FROM OTHER PLASMAS

Mixed-gas Ar Plasmas

While Ar has been used almost exclusively in ICP-MS, mixed gas ICPs may provide alternative techniques to improve the performance of ICP-MS. Gases that have been used include N_2 (184-193), O_2 (187), air (187), Xe (195), H_2 (191,196), and He (197,151). The mostly used mixed-gas plasma is the Ar-N_2 ICP. It has being routinely used to minimize the levels of oxides and polyatomic species in ICP-MS application. It can be divided into two different types 1) nitrogen in outer gas flow or Ar-N2 mixed gas flow; 2) nitrogen added into aerosol gas flow.

Effect of N2 in outer gas flow With the addition of small amount (5-10%) of N_2 to the outer gas flow, analyte signal can be increased somewhat and maximized at higher nebulizer gas flow rates (187). The plasma size shrinks as foreign gases such as N_2 are added to the out flow. This has been partly attributed to the thermal pinch effect that is brought about by the dissociation of molecular gases. Thus, to maximize the signal, one has to either increase aerosol flow to move the ionization zone toward sampler or decrease the sampling position to enable the ionization zone more closer to sampling orifice.

Effect of N2 in central gas flow While the plasma getting smaller with N2 introduced in the outer gas flow, the centra channel will become more "dark" as N2 is added into the carrier gas flow. Therefore, the gas flow rate must be reduced

to get the maximum signal. The operating conditions for mixed gas ICP will not drastically changed by chemical modification of the aerosol gas flow through the injector. However, the concentrations of nitrogen-containing polyatomic ions are increased, and the overall background level is increased in ICP-MS applications (185,184).

Other mixed gas in central flow With Xe addition to the centra gas flow, inferences from polyatomic ions can be reduced substantially. The count rates from various polyatomic ions are reduced more extensively than the count rates for analyte ions and thence detection limit also can be improved. In the Ar-Xe ICP-MS, Xe^+ is the major background, however, polyatomic ions containing Xe, such as XeH^+, XeO^+, $XeAr^+$, $NaXe_2^+$ can not be observed. Alternative gas ICPs are not only used to reduce oxides or polyatomic ion interferences but they also been used to improve the sensitivity for some elements that are not ionized efficiently in an Ar ICP.

Helium Plasmas

He ICP have been investigated as an alternative ion source for analytical mass spectrometry (198-200). The ionization energy of He is 24.6 ev, instead of 15.8 eV of Ar, thus it is possible to provide an environment for higher ionization elements such as nonmetals. He is monoisotopic and occurs at a low mass, therefore the Ar related mass interferences experienced in the Ar ICP (e.g. three isotopes of Ar: $^{36}Ar^+$, $^{38}Ar^+$, $^{40}Ar^+$, and polyatomic ions such as $^{40}Ar^{16}O^+$, $^{40}Ar^{40}Ar^+$, $^{40}Ar^{35}Cl^+$) can be eliminated.

Montaser *et al.* (200) described the first successful coupling of an atmospheric pressure He ICP to a commercial ICP-MS. The spectral background of the helium ICP showed no interferences above m/z 40. He-Ar mixed gas has also been used in ICP-MS to improve sensitivity for helogens or other high ionization potential elements (194,197). To sustain a He ICP and interface to mass analyzer, some modifications of the load coil, plasma torch and impedance network are necessary. A longer plasma confinement tube (60-90 mm length) has to be used to obtain the maximum ion signal. For aqueous sample introduction, shorter tubes will not give enough resident time for analyte to efficiently interact with plasma gas. Even though, the detection limits of metal analyte are still generally not as good as in Ar ICP-MS. This is mainly because that He plasmas have lower electron number densities and gas temperatures that the Ar ICP (227,228).

As expected, the sampling orifice for extracting plasma form a He ICP has to be smaller than the normally used in Ar ICP-MS because the high pressure will be resulted by a large flux of He flow. Otherwise, additional pumping speed will be required. This can be done by simply adding another pump and pumping line to the interface or using pumps with large pumping capacity.

Since the gas kinetic temperature T_o in a He plasma is lower ($\sim$ 2000 K) than in an Ar ICP (227), the number density n_o in Equation 12 is larger ($\sim$ 3.8×10^{18} cm^{-3}) and the speed of sound is higher ($2.6 \times 10_5$ cm/s, from Equation 13). If use of the same interface as used in Ar ICP-MS, the He gas flow through the sampler would be

about 4.3 x 10^{21} atoms/s (approximate 10 L/min), in contrast to the Ar gas flow at ~ 8.4 x 10^{20} atoms/s in the Ar ICP-MS.

An intense discharge between a He ICP and the sampling cone have to be solved. Attempts to reduce this discharge by varying sampling orifice, central gas flow, first stage pressure and RF power have been shown unsuccessful. The center-tapped load coil has been efficiently used to reduce the interface discharge in Ar ICP. Unfortunately, only a very weak He ICP could be generated with a center-tapped load coil. Another approach to reduce the secondary discharge is to use samples made from nonconductive materials. It was found that an anodized aluminum sampler can significantly reduce the intensity of the secondary discharge. This is due to a oxide layer formation on the surface. It has been pointed out (198) that future investigations of the He ICP-MS should focus on optimizing the plasma extraction interface and developing a more robust He plasma that can be sustained at the interface for an extended period.

Microwave-induced Plasmas

Similarly to the ICP, the coupling of microwave-induced plasma source (MIP) with mass spectrometry started in the early 1980s (19). General reviews of MIP sources can be found in the literature (202-204). One of the main development has been the use of MIP as a detector for gas chromatography (205-207). Microwave plasmas have been investigated for mass spectrometry with support gas with Ar

(18,19,208), nitrogen (209-211), and helium (142,212,213).

The development of atmospheric pressure MIPs started with an improvement in cavity design by Beenakker (214). In the original design for coupling of the MIP to a mass spectrometer (19), a Beennakker cavity was constructed and an excitation temperature of 5400-5900 K was measured. Air entrainment caused substantial NO^+ formation in the plasma. Similar to the situation in ICP sources, the introduction of a shield gas can significantly reduce NO in the plasma. Satzger *et al.* (212) modified the interface by applying a quartz bonnet to enclose the transition region between the open end of the discharge tube and the sampling cone to elevated temperature and a slight overpressure at the position.

Chambers *et al.* (142) investigated the fundamental process of ICP-MS by replacing the ICP with a helium microwave-induced plasma. The Ar ICP-MS interface was modified to sample He-MIP plasma. Air entrainment can be minimized by using large plasma gas flow rate relative to the gas extracted through the sampling orifice. A high He plasma flow was used at about 21.1 L/min in order to reduce air penetration. As a 0.4-mm orifice used, extracted He gas was calculated to be 1.7 l/min, which is close to that in the Ar ICP with a 1-mm orifice diameter.

In MIP-MS, matrix interferences are much more severe than in ICP-MS. The operating power required for the MIP (30-400W) is much less than that of ICP. Because it requires low operation power and support gas, MIPs will continue to drew attentions in developing plasma sources alternative to ICPs.

Moderate Pressure Plasmas

A low pressure Ar plasma was explored to interfacing to a commercial ICP-MS (215). The interface, as shown in Fig. 27, was modified by replacing the sampling cone with a 0.75 in ultra-Torr fitting on a aluminum base. A water cooled ICP torch was used and gas sample introduced from gas chromatography. The major concerning may be the background interferences can be minimized with the use of a low-pressure plasma (216), however, the background spectrum has shown containing many of the polyatomic ions for atmospheric plasma in this work. Improvement is needed in torch design, especially the vacuum seals. The detection limit can not be expected to improve over the ICPs at atmospheric pressure because of less collisions and low temperature of low pressure source.

CONCLUSION

Inductively coupled plasma mass spectrometry is still relatively young even though it has become one of the most powerful techniques in elemental analysis. The success of an ICP-MS instrument design is critically dependent on the ion extraction at the mass-spectrometer interface. The present instrumentation already commercially provides impressive detection limit, fast sample analysis, a broad dynamic range and multielement and isotope detection capabilities.

Yet the fundamental aspects of the ion extraction and beam formation inside the vacuum chamber have not been fully understood. Several shortcomings suffered in the present ICP-MS instruments have been postulated to be originated from the sampling processes at interface such as: matrix effect, mass-dependent effect, metal-oxide formation, long-term drift. Besides, inefficient ion extraction and transmission have been recognized in the instruments as comparing the number of ions sampled from the ion source with that collected by detector. The basic understand of the mechanism and origins of the problems are especially valuable for instrument improvement.

Scientific innovations and engineering advances will lead to continued improvements for atmospheric pressure plasma mass spectrometry. Interface designs and ion optics arrangements in ICP-MS obviously will be the critical parts for the new generation of ICP-MS instrument. High resolution ICP-MS is already available to

solve most of the overlap problems, however at a high capital cost. Lower the instrument cost and operation cost of ICP-MS will be favorable in the future marketplace. Glow-discharge mass spectrometry will be an effective method for solid sample analysis even though the plasma operated in low pressure. In next the decade, ICP-MS will undoubtedly continue to grow as a major technique for elemental and isotopic analysis, while other new or modified plasma ion sources will be explored as alternative sources in the analytical mass spectrometry.

REFERENCES

1. T. B. Reed, *J. Appl. Phys.* 32, 821-824 (1961).
2. V. A. Fassel, R. N. Kniseley, *Anal. Chem.* **46**, 1110A, 1155A (1974); V. A. Fassel, *Science* **202**, 183 (1978).
3. S. Greenfield, I. L. Jones, C. T. Berry, and D. I. Spash; British Patent 1 109 602, *Chem. Abstr.* (1968)
4. R. S. Houk, V. A. Fassel, G. D. Flesch, H. J. Svec, A. L. Gray and C.E. Taylor, *Anal. Chem* **52**, 2283 (1980).
5. P. F. Knewstubb, K. F. Smith and T. M. Sugden, *Nature*. **178**, 693 (1956).
6. J. Deckers and A. V. Tiggelen, *Combust. Flame* **1**, 281 (1957).
7. P. F. Knewstubb, T. M. Sugden, *Nature*. **181**, 474 (1958).
8. T. M. Sugden and J. N. Green, *9th Symp.(Int.) Combust.* Academic Press, New York (1963).
9. A. N. Hayhurst and D. B. Kittelson, *Proc. R. Soc.* **338**, 155 (1974).
10. S. Foner and R. L. Hudson, *J. Chem. Phys.* **21**, 8 (1953).
11. T. M. Sugden, *Mass spectrometry* Ed. R. I. Reed, Academic Press, New York, 347-358 (1965).
12. G. C. Eltenton, *J. Chem. Phys.* **10**, 403 (1942).
13. G. C. Eltenton, *J. Chem. Phys.* **15**, 455 (1947).
14. A. N. Hayhurst, *IEE Trans. Plasma Sci.* **PS2**, 115-121 (1971).

15. C. Alkemade, *Proc. Soc. Anal. Chem.* **10** 130-143 (1973).

16. A. L. Gray, *Anal. Chem.* **47**, 600, (1975).

17. A. L. Gray, *Analyst* **100**, 289 (1975).

18. D. J. Douglas, E. S. K. Quan and R. G. Smith, *Spectrochim. Acta* **38B**, 39-48 (1983).

19. D. J. Douglas and J. B. French, *Anal. Chem.* **53**, 37-41, (1981).

20. R. S. Houk, V. A. Fassel and H. Svec, *J. Dyn. Mass Spectrom.* **6**, 234-251, (1981).

21. A. R. Date and A. L. Gray, *Analyst* **106**, 1255-1267 (1981).

22. A. L. Gray and A. R. Date, *Dyn. Mass Spectrom* **6**, 252-266 (1981).

23. A. R. Date and A. L. Gray, *Analyst* **108**, 159-165, (1983).

24. A. L. Gray and A. R. Date, *Int. J. Mass Spectrom. Ion Phys.*, **46**, 7-10, (1983).

25. A. L. Gray and A. R. Date, *Int. J. Mass Spectrom. Ion Phys.* **48**, 357-360, (1983).

26. A. R. Date and A. L. Gray, *Spectrochim. Acta* **38B**, 29-37, (1983).

27. D. J. Douglas, E. S. K. Quan and R. G.Smith, *Spectrochim. Acta* 38B, 39-48. (1983).

28. D. J. Douglas, A. Boon and N. Neve Quan, *Proc. Symp. Multielment Anal.* H. F. Ebel, Ed., Verlag Chemie, Weinheim, German, (1984).

29. Elan ICP-MS system, Sciex, 55 Glen Cameron Rd., Thornhill, Ontario, L3T

1P2, Canada.

30. Plasma Quad ICP-MS system, V. G. isotopes Ltd., Ion Path, Road Three, Winsford, Cheshire, CW 73BX, England.

31. J. A. Olivares and R. S. Houk, *Anal. Chem.* **57** 2674 (1985).

32. S. H. Tan and G. J. Horlick, *Anal Atom. Spectrom.* **2**, 745-763 (1987).

33. B. S. Ross and G. M. Hieftje, *Spectrochim. Acta.* **46B**, 1263-1273 (1991).

34. G. M. Hieftje and L. A. Norman, *Int. J. Mass Spectrom. Ion Phys.* **118/119,** 519-573 (1992).

35. G. M. Hieftje and G. H. Vickers, *Anal. chim. Acta* **216**, 1-24 (1989).

36. K. E. Jarvis, A. L. Gray and R. S. Houk, *Handbook of Inductively Coupled Plasma Mass Spectrometry*, Blackie, London (1992).

37. A. Montaser and D . W. Golightly, (Eds.), *Inductively Coupled Plasma in Analytical Atomic Spectrometry*, 2nd Edition, VCH, New York, Ch. 12, 13, 14 (1992).

38. G. Holland and A. N. Eaton, (Eds.), *Application of Plasma Source Mass Spectrometry,* Royal Soc. Chem., Cambridge (1991).

39. K. E. Jarvis, A. L. Gray, J. G. Williams and I. Jarvis (Eds.), *Plasma Source Mass Spectrometry*, Royal Soc. Chem., Cambridge (1990).

40. A. R. Date and A. L. Gray (Eds.), *Applications of Inductively Coupled Plasma Mass Spectrometry,* Blackie, London (1989).

41. A. L. Gray, *Adv. Mass. Spectrom.* **11B**, 1674 (1989).

42. R. S. Houk, *Anal. Chem.* **58** 97A (1986).

43. R. M. Barnes, *CRC Crit. Rev. Anal. Chem.* **7** 203-296 (1978).

44. A. Montaser and D . W. Golightly, (Eds.), *Inductively Coupled Plasma in Analytical Atomic Spectrometry*, 2nd Edition, VCH, New York, Ch. 8 (1992).

45. N. Jakubowski, I. Feldmann and D. Stuewer, *J. Anal. At. Spectrom.*, **8**, 969 (1993).

46. R. M. Barnes and J. L. Genna, *Spectrochim. Acta* **36B**, 299-323 (1981).

47. R. M. Barnes and G. R. Schleicher, *Spectrochim. Acta* **36B**, 81-101 (1981).

48. M. I. Boulos, *Pure Appl. Chem.* **57**, 1321-1352 (1985).

49. M. T. Cicerone and P. B. Farnsworth, *Spectrochim. Acta* **4B**, 897-907 (1989)

50. R. K. Winge, V. A. Fassel, V. J. Peterson, M. A. Floyd, *Inductively coupled plasma emission Spectrometry: An Atlas of Spectral Information.* Elsevier: New York, N. Y., (1985).

51. A. R. Date and Y. Y. Cheung, *Analyst*, **112**, 1531-1540 (1987).

52. P. W. J. M. Boumans, *Theory of Spectrochemical Excitation*, Hilger and Watts: London, U. K., 1966; Chapter 7 (1966).

53. J. L. Radaziemski, J. M. Mack, *Physica (Utrecht)* **102B**, 35-40 (1980).

54. L. de Galan, and R. Smith, J. D. Winefordner, *Spectrochim. Acta* **23B**, 521-525 (1968).

55. R. S. Houk and J. J. Thompson, *Mass Spectrom. Reviews* **7**, H. L. Gross (ed.) 425-461 (1988).

56. I. M. Mermet, *C. R. Acad. Sci* **B 281**, 273-275 (1975)

57. P. W. J. M. Boumans and F. J. de Boer, *Spectrochim. Acta* **32B**, 365-395 (1977)

58. P. B. Farnsworth and N. Omenetto, *Spectrochim. Acta* **48B**, 6/7, 809-816 (1993).

59. A. Goldwasser, and J. M. Mermet, *Spectrochim. Acta* **41B**, 7, 725-739 (1986)

59. J. A. M. Van Der Mullen, I. J. M. KM. Raaijmakers, A. C. A. P. van Lammeren, D. C. Schram, B. van Deer Sijde and H. J. W. Schenkelaars, *Spectrochim. Acta* **42B**, 9, pp. 1039-1051 (1987)

60. V. M. Goldfarb, *Developments in Atomic Plasma Spectrochemical Analysis,* Ed. R. M. Barnes, p.725, Heyden, London (1981).

61. D. C. Schram, I. J. M. M. Raaymakers, H. J. Schenkelaars and P. M. J. M. Boumans, *Spectrochim. Acta* **38B**, 1545 (1983).

62. J. F. Alder, R. M. Bombelka and G. F. Kirkbright, *Spectrochim. Acta* **35B**, 163 (1980).

63. G. M. Hieftje, G. D. Rayson and J. W. Olesik, *Spectrochim. Acta.* **40B**, 1007 (1985).

64. M. W. Blades and G. M. Hieftje, *Spectrochim. Acta.* **37B**, 191 (1982).

65. M. W. Blades, *Spectrochim. Acta.* **37B**, 869 (1982).

66. J. W. Mills and G. M. Hieftje, *Spectrochim. Acta.* **39B**, 859 (1984).

67. F. Aeschbach, *Spectrochim. Acta.* **37B**, 987 (1982).

68. H. U. Eckert, *Developments in Atomic Plasma Spectrochemical Analysis*, Ed. R. M. Barnes, p.35, Heyden, London (1981).

69. D. J. Douglas, "Fundamental Aspects of Inductively Coupled Plasma Mass Spectrometry", *Inductively Coupled Plasma in Analytical Atomic Spectrometry*, A. Montaser and D . W. Golightly, Eds., 2nd Edition, VCH, New York, Ch. 13, (1992).

70. E. Poussel and Jean-Michel Mermet, *J. Anal. At. Spectrom.*, **9**, 61 (1994).

71. G. H. Vickers, D. A. Wilson and G. M. Hieftje, *Anal. chem.*, **60**, 1808 (1988).

72. M. Chtaib and J. P. Schmit, *J. Anal. At. Spectrom.*, **3**, 969 (1988).

73. J. E. Fulford and E. S. K. Quan, *Appl. Spectr.* **42**, 3, 425-428 (1988).

74. J. S. Crain, R. S. Houk, and D. E. Eckels, *Anal. chem.*, **61**, 6, 611, (1989).

75. N. Furuta, C. A. Monnig, P. Yang, and G. M. Hieftje, *Spectrochim. Acta.* **44B**, 649 (1989).

76. S. Luan, H. Pang, S. Shum, and R. S. Houk, *J. Anal. At. Spectrom.*, **7**, 799 (1992).

77. J. W. Olesik, L. J. Smith, E. J. Williamsen, *Anal. chem.*, **61**, 2002 (1989).

78. J. W. Olesik, L. J. Smith, E. J. Williamson, *Spectrochim. Acta.* **46B**, 851 (1991).

79. J. C. Fister, J. W. Olesik, *Spectrochim. Acta.* **46B**, 869 (1991).

80. G. Horlick, F. Qin, *Federation of Analytical Chemistry and Spectroscopy*

Societies Meeting XVII, Cleveland, OH, P 603 (1990).

81. S. Hobbs and J. W. Olesik, *Anal. chem.*, **64**, 274-283 (1992).

82. R. K. Winge, D. E. Eckels, E. L. Dekalb and V. A. Fassel, *J. Anal. At. Spectrom.*, **3**, 849 (1988).

83. R. K. Winge, J. S. Crain and R. S. Houk, *J. Anal. At. Spectrom.*, **6**, 601 (1991).

84. N. Furuta, *J. Anal. At. Spectrom.*, **6**, 199 (1991).

85. A. T. Ince, J. G. Williams and A. L. Gray, *J. Anal. At. Spectrom.*, **8**, 899 (1993).

86. E. C. Huang, T. Wachs, J. J. Conboy, and Jack D. Henion, *Anal. Chem.*, **62**, 713A-724A (1990).

87. E. C. Horning, M. G. Honrning, D. I. Carroll, J. Dzidic, R. N. Stillwell, *Anal. chem.*, **45**, 936-943 (1973).

88. R. V. Serauskas, G. R. Brown, R. Pertel, *Int. J. Mass Spectrom. Ion Phys.* **16**, 69-87 (1975).

89. B. Rowe, *Int. J. Mass Spectrom. Ion Phys.* **16**, 209-223 (1975).

90. A. N. Hayhurst and N. R. Telford, *Combust. Flame.* **28**, 67-80 (1977).

91. H. C. W. Beijerink, R. J. F. van Gerwen, E. R. T. Kerstel, J. K. M Martens, E. J. W. van Vliembergen, M. R. T. Smits and G. M. Kaashoek, *Chem. Phys.* **96**, 153-173 (1985).

92. R. Campargue, "High Intensity Supersonic Molecular Beam Apparatus", 4th

Symposium on Rarified Gas Dynamics, Ed. J. H. de Leeuw, Academic Press, New York, 279-298 (1966).

93. A. Kantrowitz, and J. Grey, *Rev. Sci. Instrum.* **22**, 328 (1951).

94. A. L. Gray, *Anal. At. Spectrom.* **4**, 371-373, (1989).

95. P. L. Owen, C. K. Thornhill, *The flow in an Axially Symmetric Supersonic Jet from a Nearly Sonic Orifice into Vacuum.* Aeronautical Research Council, United Kindom, R & M 2616, 1948.

96. K. Bier and O. F. Hagena, *4th RGD.* **2**, p. 260 (1964).

97. E. S. Love, *NACA TN* 4195, January (1958).

98. E. S. Love, *NACA TN* R-6 (1959).

99. R. B. Fraser, F. Robben, and L. Talbot, *Phys. Fluids,* **14**, 2317-2327 (1971).

100. A. Witte, T. Kubota, and L. Lees, "Experimental investigation of a highly ionized Arc Heated Supersonic Free Jet", *AIAA* Paper 68-135.

101. W. K. McGregor, "Diagnostics of a Free Jet of Arc-heated, Low Density, Supersonic Argon Plasma", *AIAA* Paper 66-163.

102. D. J. Douglas and J. B. French, *Anal. Atom. Spectrom.* **3**, 743-747, (1981).

103. E. W. Becker, and K. Bier, *Z. Naturforsch..* **9A**, 975 (1954).

104. H. Ashkenas and F. S. Sherman, *4th RGD*, Vol2, P.84, (1964).

105. J. B. French, *Molecular Beams for Raried Gasdynamic Research,* Institute for Aerospace Studies, University of Totonto, Canada, AGARDograph 112 (1966).

106. K. Bier and B. Schmidt, *Z. Angew. phys.* **13**, 34 (1961).

107. A. L. Gray, *Adv. Mass. Spectrom.* **11B**, 1674 (1989).

108. C. A. Stearns, F. J. Kohl, G. C. Fryburg and R. A. Miller, *Nat. Bur. Stan. Spec. Publ. No.* 561, 1, 303 (1979).

109. R. H. Kirchoff, E. W. Peterson and L. Talbot, *AIAAJ.* **9**, 1686 (1971).

110. R. H. Kirchoff and L. Talbot, *AIAAJ.* **9**, 1098 (1971).

111. E. W. Peterson and L. Talbot, *AIAAJ.* **8**, 1391 (1970).

112. R. S. Houk, , H. J. Svec, and V. A. Fassel, *Appl. Spectrosc.* **35**, 308-384 (1981).

113. D. J. Douglas and J. B. French, *Spectrochim. Acta.* **41B,** 197-204, (1986).

114. H. B. Lim, R. S. Houk, and J. S. Crain, *Spectrochim. Acta.* 1989, **44B**, 989-998.

115. R. M. Clements and P. R. J. Smy, *Phys. D: Appl. Phys.*, **7**, 551. (1977).

116. A. L. Gray, and R. S. Houk, J. S. Williams, *J. Anal Atom. Spectrom.*, **2**, 283, (1987).

117. R. S. Houk, H. B. Lim, *Anal. Chem.* **58** 3244, (1986).

118. D. M. Chambers; J. Poehlman; P. Yang and G. M. Hieftje, *Spectrochim. Acta.* 1991, **46B**, 741-760.

119. Hongsen Niu, Shen. Luan, X. Chan, H. Pang, and R. S. Houk, *Spectrochim. Acta* (1994).

120. J. A. Olivares and R. S. Houk, *Appl. Spectrosc.* **39**, 1070 (1985).

121. J. E. Fulford and D. J. Douglas, *Appl. Spectr.* **40**, 971 (1986).

122. R. C. Hutton and A. N. Eaton, *J. Anal Atom. Spectrom.*, **2**, 595, (1987).

123. J. S. Crain, R. S. Houk, and F. G. Smith, *Spectrochim. Acta.*, **43B,**, 1355, (1988).

124. A. L. Gray and J. G. Williams, *J. Anal. At. Spectrom.*, **2**, 599 (1987).

125. S. D. Tanner, *J. Anal. At. Spectrom.*, **8**, 891 (1993).

126. D. M. Chambers, B. S. Ross and G. M. Hieftje, *Spectrochim. Acta.*, **46B**, 785-804 (1991).

127. R. S. Houk, H. J. Svec and V. A. Fassel, *Appl. Spectr.*, **35**, 4, 380 (1981).

128. D. A. Wilson, G. H. Vickers and G. M. Hieftje, *J. Anal. At. Spectrom.* **2**, 875 (1987).

129. J. S. Crain, F. G Smith and R. S. Houk, *Spectrochim. Acta.* **45B**, 249 (1990).

130. H. B. Lim, R. S. Houk, M. C. Edelson and K. P. Carney, *J. Anal. At. Spectrom.*, **4**, 365 (1989).

131. Hiroshi Kawaguchi, Kiyoshi Asada, and Atsushi Mizuike, *Mikrochim. Acta*, **III**, 143-152 (1988).

132. H. Niu, K. Hu and R. S. Houk, *Spectrochim. Acta.* 46B, 805-817, (1991).

133. H. Niu and H. S. Houk, *Spectrochim. Acta.* in press, (1994).

134. M. Huang and G. M. Hieftje, *Spectrochim. Acta.* 1991, **44B**, 739 (1989).

135. R. Pertel, *Int. J. Mass Spectrom. Ion Phys.* **16**, 39, (1975).

136. S. D. T. Axford and A. N. Hayhurst, *Int. J. Mass Spectrom. Ion Phys.* **110,**

31, (1991).

137. J. R. Pierce "*Theoty and Design of Electron Beams*" 2nd ed, Van Nostrand, New York, 1954.

138. M. Szilagyi, Electron and Ion Optics, Plenum press, New York (1988).

139. G. R. Gillson, D. J. Douglas, J. E. Fulford, K. W. Halligan, and S. D. Tanner, *Anal. Chem.*, **60**, 1472-1474, (1988).

140. S. D. Tanner, *Spectrochim. Acta.* **47B**, 809 (1992).

141. D. M. Chambers and G. M. Hieftje, *Spectrochim. Acta.* **46B**, 761 (1991).

142. D. M. Chambers and G. M. Hieftje, *Spectrochim. Acta.* **46B**, 1745 (1991).

143. J. A. Olivares and R. S. Houk, *Anal. Chem.* **58** 20 (1986).

144. A. L. Gray, *Spectrochim. Acta.* **41B**, 151 (1986).

145. D. Beauchemin, J. W. McLaren, and S. S Berman, *Spectrochim. Acta.* **42B**, 467 (1987).

146. D. C. Gregoire, *Spectrochim. Acta.* **42B**, 895 (1987).

147. H. Kawaguchi, T. Tanaka, T. Nakamura, M. Morishita and A. Mizuike, *Anal. Sci.* (Japan) **3**, 305 (1987).

148. Y-S. Kim, H. Kawaguchi, T. Tanaka, and A. Mizuike, *Spectrochim. Acta,* **45B,** 333 (1990).

149. J. S. Crain, R. S. Houk and F. G. Smith, *Spectrochim. Acta.* **43B**, 1355-1364 (1988).

150. R. D. Satzger, *Anal. Chem.* **60** 2500 (1988).

151. B. S. Sheppard, Wei-lung Shen, and J. A. Caruso, *J. Am. Soc Mass Spectrom,* **2,** 355-361 (1991).

152. C. Vandecasteele, M. Nagels, H. Vanhoe, R. Dams, *Anal. Chim. Acta,* **211,** 91 (1988).

153. R. C. Hutton and A. N. Eaton, *J. Anal Atom. Spectrom.*, **3**, 547, (1988).

154. J. J Thompson and R. S. Houk, *Appl. Spectr.*, **41**, 801 (1987).

154. J. W. McLaren, D. Beauchemin and S. S. Berman, *Anal. Chem.* **59,** 610 (1987).

155. J. R. Garbarino and H. E. Taylor, *Anal. Chem.* **59,** 1568 (1987).

156. G. H. Vickers, B. S. Rose and G. M. Hieftje, *Appl. Spectr.*, **2**, 1330 (1989).

157. J. Wang, W. L. Shen, B. S. Sheppard, E. S. Evans, F. L Fricke, and Joseph A. Caruso, *J. Anal Atom. Spectrom.*, **5**, 445, (1990).

158. B. S. Ross, and G. M. Hieftje, *J. Am. Soc. Mass Spectrom.* **2**, 785 (1991).

159. B. S. Ross and G. M. Hieftje, *Spectrochim. Acta.* **46B**, 1263-1271 (1991).

160. A. Boorn, G. Gillson, D. Douglas and E. Quan, paper presented at *the 1987 Winter Conference on Plasma and Laser Spectrochemistry*, Lyon, France, Jan. 12 -16 (1987).

161. P. J. Turner, Application of Plasma Source Mass Spectrometry, presented at *2nd International Conference on Plasma Source Mass Spectrometry*, Durham, U. K., (1990).

162. H. Wollnik, *Optical of Charged Particles*, Academic press, Inc. Orlando, FL

(1987).

163. A. Septier, *Focusing of Charged Particles*, Academic press Inc. New York (1967).

164. K. W. Busch and M. A. Busch, *Multielement Detection System for Spectrochemical Analysis*. Wiley, New York, 392-303 (1990).

165. G. H. Vickers, D. A. Wilson and G. M. Hieftje, *Anal. chem.*, **60**, 1808 (1988).

166. D. C. McGilvery, *Ph. D. Dissertation,* LaTrobe University, (1978).

167. D. A. Dahl and J. E. Delmore, Rep. EGG-CS-7233, Idaho National Engineering Laboratory, Idaho Falls, ID 83415.

168. C. J. Lejeune, *Nuclear Instruments and Methods*, **116**, 417-428 (1974).

169. D. J. Douglas, Some current perspectives on ICP-MS, *Can. J. Spectrosc.* **34,** 2, 38, (1989).

170. D. J. Douglas, *Method and Apparatus Having RF Biasing for Sampling a plasma into a Vacuum Chamber,* U.S. patent 4,682,026.

171. M. A. Vaughan, and G. Horlick, *Spectrochim. Acta.* **45B**, 1301 (1990).

172. K. Hu, P. S. Clemons and R. S. Houk, *J. Am. Soc Mass Spectrom,* **4,** 28-37 (1993).

173. D. J. Douglas and L. A. Kerr, *J. Anal Atom. Spectrom.*, **2**, 749, (1988).

174. J. G. Williams and A. L. Gray, *Anal. Proc.* **25**, 385-388 (1988).

175. J. F. O'Hanlon, *A Users's Guide to Vacuum Technology,* 2nd Ed., John Wiley

& Sons (1989).

176. E. Grimsrud, *Vacuum Envelope for High Pressure Mass Spectrometry Application.* Anal. Chem., 50: 382-384, (1987).

177. A. Chambers, R. K. Fitch and B. S. Halliday, *Basic Vacuum Technology*, Adam Hilger, Bristol (1989).

178. A. Roth, *Vacuum Sealing Technique*, Pergamon Press, New York, (1966).

179. G. Lewin, *Fundamentals of Vacuum Science.* McGraw-Hill, New York (1965).

180. S. M. Dushman and J. M. Lafferty, *Scientific Foundation of Vacuum Technique*, 2nd Ed., Wiley, New York (1962).

181. N. Bradshaw, E F. H. Hall and Neil E. Sanderson, *J. Anal Atom. Spectrom.*, **4**, 801, (1989).

182. D. P. Myers, G. Li, P. Yang, P. P. Mahoney, and G. M. Hieftje, presented at *the 1994 Pittsburgh Conference*, No. **381**, Chicago, Illinois (1994).

183. M. Wu, P. B. Farnsworth, M. L. Lee, E. D. Lee, and J. Prince, "Time-of Flight mass spectrometry for use in ICP-MS", presented at *the 1994 Pittsburgh Conference*, Atlanda, Georgia, No. **1342** (1993).

184. R. S. Houk, A. Montaser, and V. A. Fassel, *Appl. Spectr.*, **27**, 425-428 (1983).

185. R. C. Hutton and A. N. Eaton, *J. Anal Atom. Spectrom.*, **4**, 299, (1989).

186. R. C. Hutton and A. N. Eaton, *J. Anal Atom. Spectrom.*, **5**, 425, (1990).

187. J. W. H. Lam and G. Holick, *Spectrochim. Acta.* **45B**, 1313 (1990).

188. J. W. H. Lam and G. Holick, *Spectrochim. Acta.* **45B**, 1327 (1990).

189. J. W. H. Lam and G. Holick, *J. Anal Atom. Spectrom.*, **5**, 419 (1990).

190. D. Beauchemin, J. M. Craig, *Spectrochim. Acta.* **46B**, 603 (1991).

191. H. Louie and S. Y. P. Soo, *J. Anal Atom. Spectrom.*. **7**, 557 (1992).

192. J. M. Craig and D. Beauchemin, *J. Anal Atom. Spectrom.*, **7**, 937 (1992).

193. S. J. Hill, M. J. Ford and Ebdon., *J. Anal Atom. Spectrom.*, **7**, 719 (1992).

194. J. Wang, E. S. Evans, and J. A. Caruso, *J. Anal Atom. Spectrom.*, **7**, 929, (1992).

195. F. G. Smith, D. R. Wiederin, and R. S. Houk, *Anal. Chem.* **63,** 1458-1462 (1991).

196. N. Shibata, N. Fudagawa, M. Kubota, *Anal. Chem.* **63,** 636-640 (1991).

197. B. S. Sheppard, W. L. Shen, and Joseph A. Caruso, *J. Anal Atom. Spectrom*, **5,** 697 (1990).

198. S. Nam, W. R. L. Masamba and A. Montaser, *Anal. Chem.* **65,** 2784 (1993).

199. D. W. Koppenaal, and L. F. Quinton, *J. Anal Atom. Spectrom.*, **3**, 667 (1988).

200. A. Montaser, S. K. Chan and D. W. Koppenaal, *Anal. Chem.* **59,** 1240 (1987).

201. F. E. Lichte, A. L Meier, and J. G. Crock, *Anal. Chem.* **59,** 1150 (1987).

202. P. C. Uden, *Trends Anal. Chem.* **6,** 238 (1987).

203. K. C. Ng and W. L. Shen, *Anal. Chem.* **58,** 2084 (1986).

204. A. T. Zander and G. M. Hieftje, *Appl. Spectr.*, **35**, 357 (1981).

205. J. T. Creed, A. H. Mohamad, T. M. Davidson, G. Ataman and J. A. Caroso, *J. Anal Atom. Spectrom*, **3**, 923 (1988).

206. A. H. Mohamad, J. T. Creed, T. M. Davidson and J. A. Caroso, *Appl. Spectr.*, **27**, 1127 (1989).

207. H. Suyani, J. T. Creed, J. A. Caroso and R. D. Satzger *J. Anal Atom. Spectrom*, **4**, 777 (1989).

208. R. D. Satzger, F. L. Fricke and J. A. Caroso, *J. Anal Atom. Spectrom*, **3**, 319 (1988).

209. D. A. Wilson, G. H. Vickers and G. M. Hieftje, *Anal. Chem.*, **59**, 1664 (1987).

210. W. L. Shen, T. M. Davidson, J. T. Creed, and J. A. Caroso, *Appl. Spectr.*, **44**, 1003 (1990).

211. W. L. Shen, T. M. Davidson, J. T. Creed, and J. A. Caroso, *Appl. Spectr.*, **44**, 1011 (1990).

212. R. D. Satzger, F. L. Fricke, P. G. Brown and J. A. Caroso, *Spectrochim. Acta.* **42B, 705** (1987).

213. P. G. Brown, T. M. Davidson and J. A. Caroso, *J. Anal Atom. Spectrom.*, **3**, 763 (1988).

214. C. I. M. Beenakker, *Spectrochim. Acta.* **31B**, 483 (1976).

215. E. H. Evans and J. A. Caruso, *J. Anal Atom. Spectrom.*, **8**, 427 (1993).

216. B. S. Sheppard and J. A. Caruso, *J. Anal Atom. Spectrom.*, **9**, 145 (1994).

217. J. D. Ingle and S. R. Crouch, *Spectrochemical Analysis*, Chapter 7, p196, Prentice-Hall, NJ (1988).

218. H. Uchida. K. Tanabe, Y. Nojiri, H. Haraguchi, and K. Fuwa, *Spectrochim. Acta.* **35B**, 881-883 (1981).

219. H. Uchida. K. Tanabe, Y. Nojiri, H. Haraguchi, and K. Fuwa, *Spectrochim. Acta.* **36B**, 711-718 (1981).

220. Y. Nojiri, K. Tanabe, H. Uchida. K. Tanabe, H. Haraguchi, and K. Fuwa, *Spectrochim. Acta.* **38B**, 61-74 (1983).

221. K. Hu and R. S. Houk, *J. Am. Soc Mass Spectrom,* **4,** 733-741 (1993).

222. R. C. Hutton, U.S. Patent 4760253, 1988.

223. R. Campargue, *Enyropie*, **30**, 15, (1969).

224. R. Campargue, *Rev. Sci. Instrum.* **35**, 111, (1964).

225. D. J. Douglas, Paper IL 11, presented at the Winter Conference on the Plasma Spectrochemistry, St. Petersburg, FL (1990).

226. K. Otsuka, M. Iwanaga, M. Morita, T. Uehiro, H. Ito, presented at the 39th ASMS Conference on Mass Spectrometry and Allied Topics, p216, (1991).

227. S. Chen and A. Montaser, *Spectrochim. Acta.* **42B**, 591 (1987).

228. I. Ishii, H. Tan, S. Chan and A. Montaser, *Spectrochim. Acta.* **46B**, 901 (1991).

229. N. Jakubowski, B. J. Raeymaekers, J. A. C. Broekaert, adn D. Stuewer, Study of Plasma Potential Effects in a 40 MHz Inductively Coupled Plasma Mass Spectrometry, *Spectrochim. Acta.* **42B**, 591 (1987).

Table 1. Distribution of ionization energies of elements for single and double charged ions. Reproduced from reference 41, with permission.

Ionisation energy (eV)	Elements	
< 7	Li, Na, Al, K, Ca, Sc, Ti, V, Cr, Ga, Rb, Sr, Y, Zr, Nb, In, Cs, Ba, La, Ce, Pr, Nd, Pm, Sm, Eu, Gd, Tb, Dy, Ho, Er, Tm, Yb, Lu, Hf, Tl, Ra, Ac, Th, U	
7–8	Mg, Mn, Fe, Co, Ni. Cu, Ge, Mo, Tc, Ru, Rh, Ag, Sn, Sb, Ta, W, Re, Pb, Bi	
8–9	B, Si, Pd, Cd, Os, Ir, Pt, Po	
9–10	Be, Zn, As, Se, Te, Au	2^+ *ions*
10–11	P, S, I, Hg, Rn	Ba, Ce, Pr, Nd, Ra
11–12	C, Br	Ca, Sr, La, Sm, Eu, Tb, Dy, Ho, Er
12–13	Xe	Sc, Y, Gd, Tm, Yb, Th, U, Ac
13–14	H, O, Cl, Kr	Ti, Zr, Lu
14–15	N	V, Nb, Hf
15–16	Ar	Mg, Mn, Ge, Pb
> 16	He, F, Ne	All other elements

Table 2. Electron number density measured at skimmer tip and the predicted results calculated from ideal supersonic jet expansion with a dry plasma.

Aerosol Gas Flow (L/min)	Number Density (cm^{-3})		
	Measured	Expected	Ratio
0	5.7×10^{12}	9.4×10^{12}	0.61
0.6	2.5×10^{12}	4.1×10^{12}	0.61
1.0	0.55×10^{12}	2.1×10^{12}	0.26
1.3	0.23×10^{12}	1.3×10^{12}	0.18
1.5	0.16×10^{12}	1.1×10^{12}	0.15

Table 3. Electron number density measured at skimmer tip and the predicted results calculated from ideal supersonic jet expansion with a wet plasma.

Aerosol Gas Flow (L/min)	Number Density (cm^{-3})		
	Measured	Expected	Ratio
0	$1.1x10^{13}$	$1.1x10^{13}$	1.0
0.6	$1.9x10^{12}$	$2.9x10^{12}$	0.65
1.0	$8.6x10^{10}$	$6.0x10^{10}$	0.14

Table 4. Mass resolution required to separate some polyatomic and analyte ions

m/z	Ion Pair	Required Resolution
39	$^{39}K^+$, $^{38}ArH^+$	5570
51	$^{51}V^+$, $^{35}CL^{16}O^+$	2580
56	$^{56}Fe^+$, $_{40}Ar^{16}O^+$	2500
58	$^{58}Ni^+$, $^{40}Ar^{16}OH_2^+$	1550
63	$^{63}Cu^+$, $^{2}3Na^{40}Ar_+$	2800
65	$^{64}Zn^+$, $^{32}S^{16}O_2^+$	1950
68	$^{68}Zn^+$, $^{40}Ar^{14}N_2^+$	6070
72	$^{72}Ge^+$, $^{40}Ar^{16}O_2^+$	2390
75	$^{75}As^+$, $^{40}Ar^{35}Cl^+$	7800
80	$^{80}Se^+$, $^{40}Ar_2^+$	9700

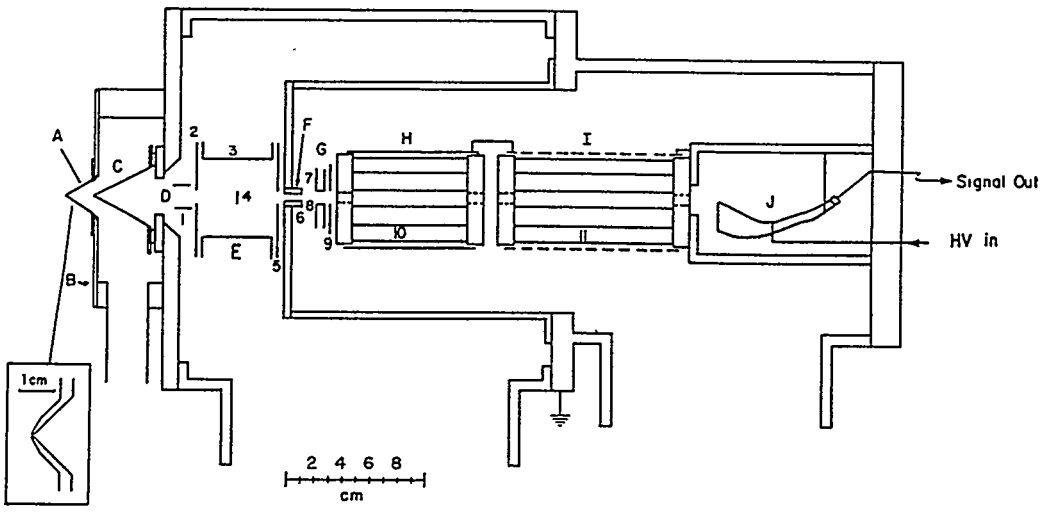

Figure 1. Schematic diagram of an ICP-MS instrument (fabricated in Ames). (A) sampler cone; (B) water-cooled sampling flange; (c) skimmer cone; (D) cylindrical ion lens; (E) Bessel box assembly; (F) differential pumping orifice; (G) ion lens elements; (H) RF only quadrupole and solid RF shield; (I) quadrupole mass filter and wire mesh RF shield; (J) Channetron electron multiplier. The ICP equipment and nebulizer system are not shown.

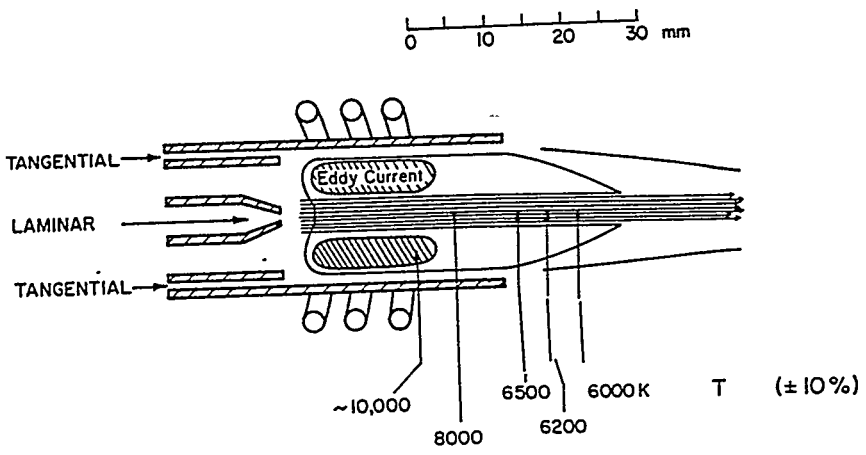

Figure 2. Cross section disgram of ICP, the analyte aerosol travels through the plasma in the axial channel as indicated by the horizontal arrows.

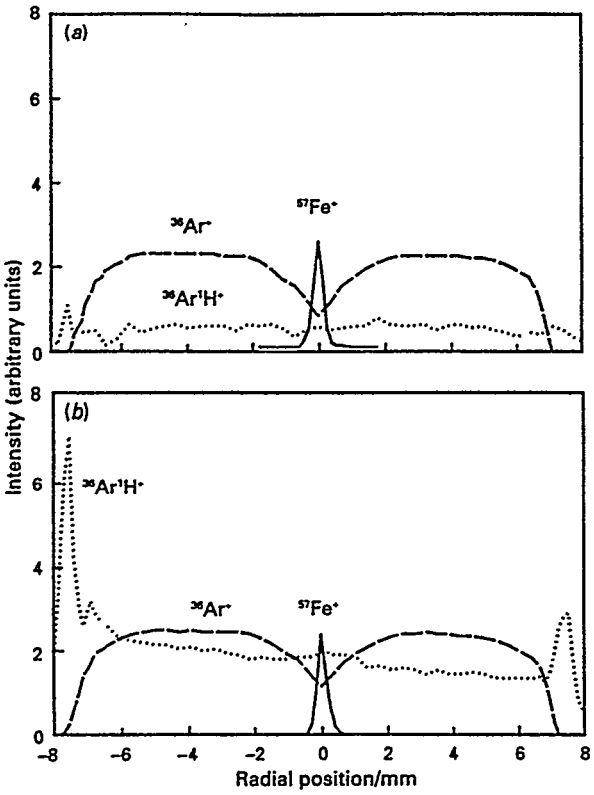

Figure 3. Ion distribution across the plasma at sampling positions, (a) d_s = 8 mm, and (b) d_s = 11 mm. Reproduced from reference 45, with permission.

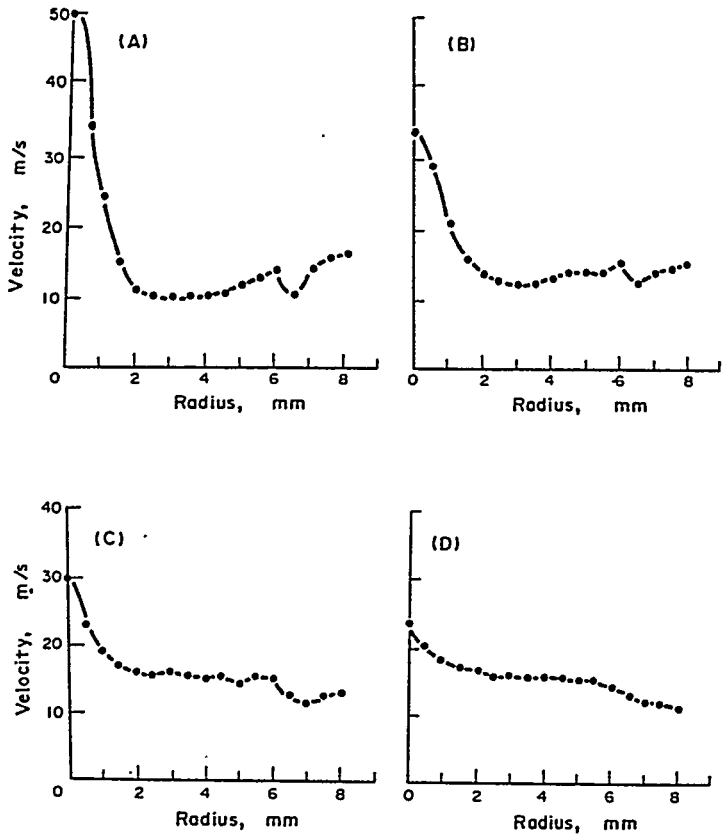

Figure 4. Radial velocity profiles of an ICP with 14 L/min outer gas flow and 1.0 L/min aerosol gas flow. Axial position are (A) -7 mm, (B) 0 mm, (C) 4mm, (D) 6 mm, from the top of the coil. Reproduced from reference 45, with permission.

Table 1. Calculated values for degree of ionization (%) of M_+ and M^{2+} at T_i = 7500 K, $n_e = 1 \times 10^{15}$ cm^3.

H 0.1																	He
Li 100	Be 75											B 58	C 5	N 0.1	O 0.1	F 9×10^{-4}	Ne 6×10^{-8}
Na 100	Mg 98											Al 98	Si 85	P 33	S 14	Cl 0.9	Ar 0.04
K 100	Ca 99(1)	Sc 100	Ti 99	V 99	Cr 98	Mn 95	Fe 96	Co 93	Ni 91	Cu 90	Zn 75	Ga 98	Ge 90	As 52	Se 33	Br 5	Kr 0.6
Rb 100	Sr 96(4)	Y 98	Zr 99	Nb 98	Mo 98	Tc	Ru 96	Rh 94	Pd 93	Ag 93	Cd 65	In 99	Sn 96	Sb 78	Te 66	I 29	Xe 8.5
Cs 100	Ba 91(9)	La 90(10)	Hf 96	Ta 95	W 94	Re 93	Os 78	Ir	Pt 62	Au 51	Hg 38	Tl 100	Pb 97(.01)	Bi 92	Po	At	Rn
Fr	Ra	Ac	Unq	Unp	Unh	Uns	Uno										

Ce 96(2)	Pr 90(10)	Nd 99*	Pm	Sm 97(3)	Eu 100*	Gd 93(7)	Tb 99*	Dy 100*	Ho	Er 99*	Tm 91(9)	Yb 92(8)	Lu
Th 100*	Pa	U 100*	Np	Pu	Am	Cm	Bk	Cf	Es	Fm	Md	No	Lr

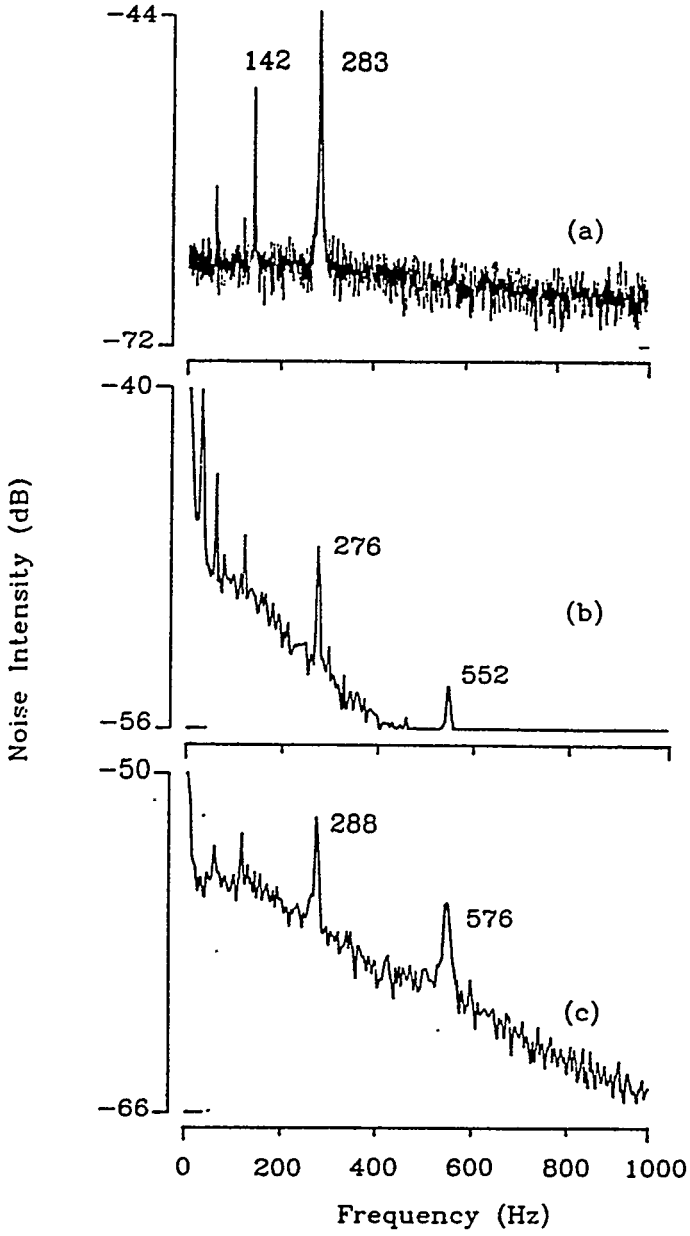

Figure 6. Comparison between frequency spectra from (a) ICP emission noise, (b) ICP emission upstream of the ICP-MS sampler, (c) ICP mass spectrometer noise. ICP outer gas flow 15.5 L/min. Reproduced from reference 74, with permission.

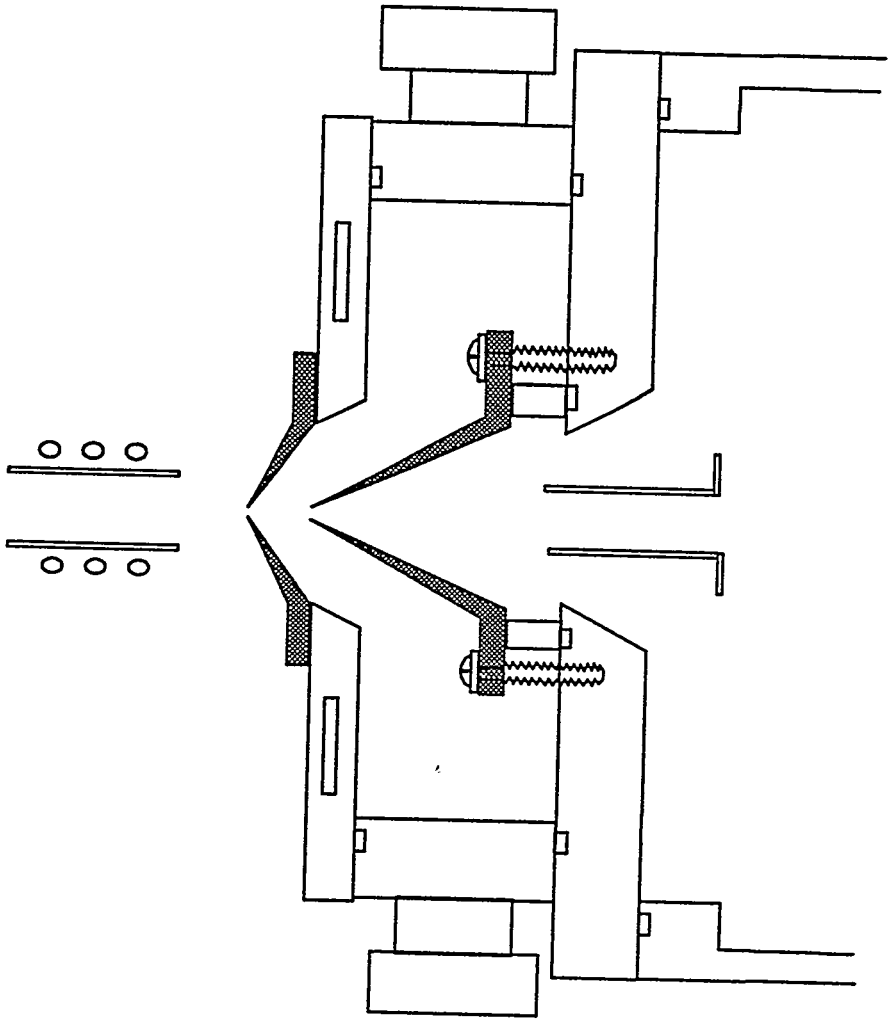

Figure 7. Schematic diagram of a typical extraction interface of ICP-MS.

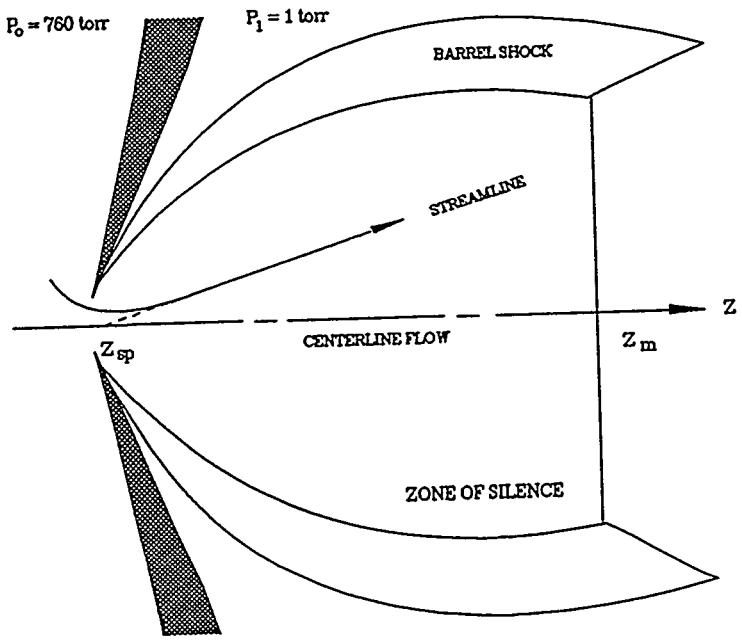

Figure 8. Schematic view of a supersonic expansion into the first vacuum chamber without presence of skimmer, arrows indicate the direction of flow stream.

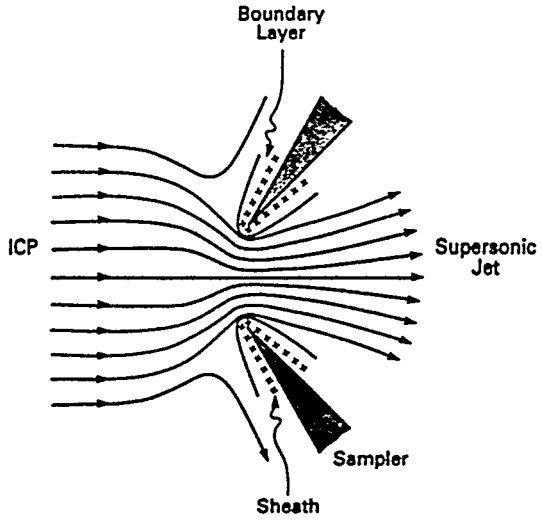

Figure 9. Boundary Layer and electrical sheath around the sample tip. The thickness of the boundary layer has been exaggerated here. Reproduced from reference 36, with permission.

a.

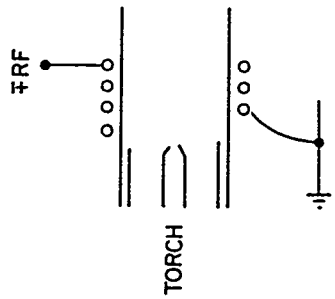

b.

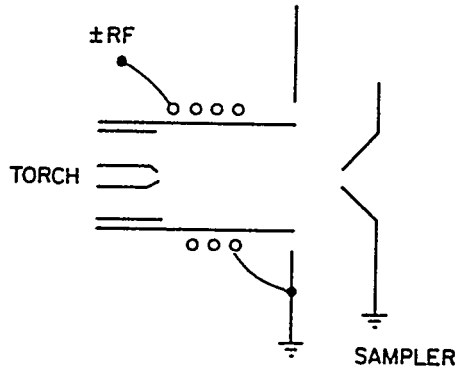

c.

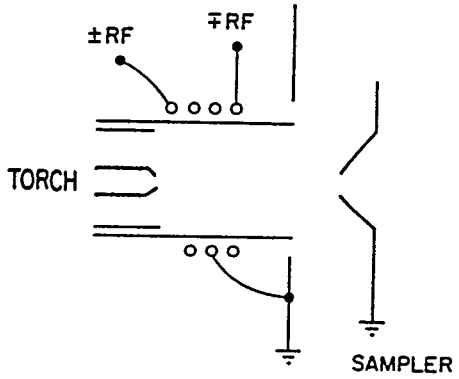

Figure 10. Load coil at the different ground situations, a) Conventional; b) Reversed; b) Center-tapped coil.

a.

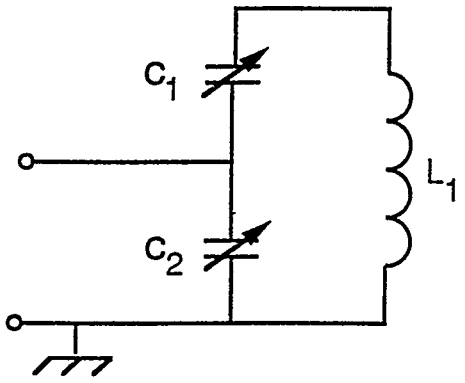

Figure 11. Impedance matching networks for ICP-MS instruments: a) unbalanced coil of end grounding; b) balanced coil of center grounding; c) Balanced load coil by coupled capacitively to ground at both ends with the RF voltage applied to the center of the coil. The Variable capacitors are used for tuning and impedance matching, and the inductance L is the load coil. Reproduced from references 37 and 229, with permission.

b.

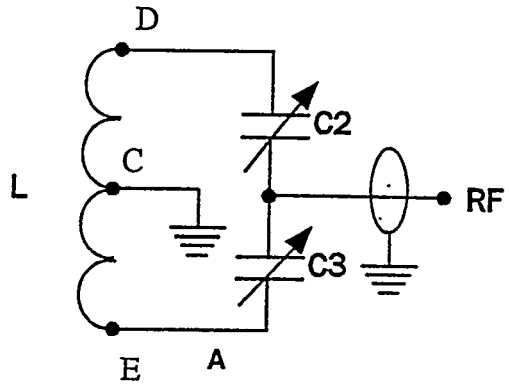

C.

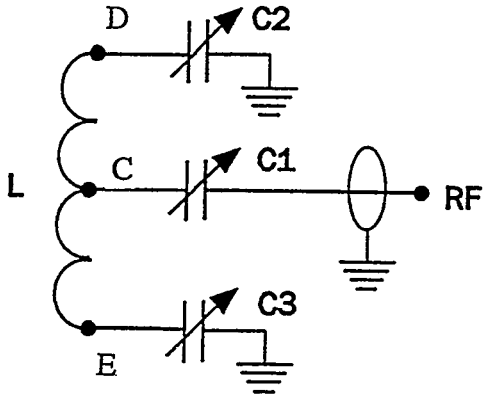

Figure 11. (continued)

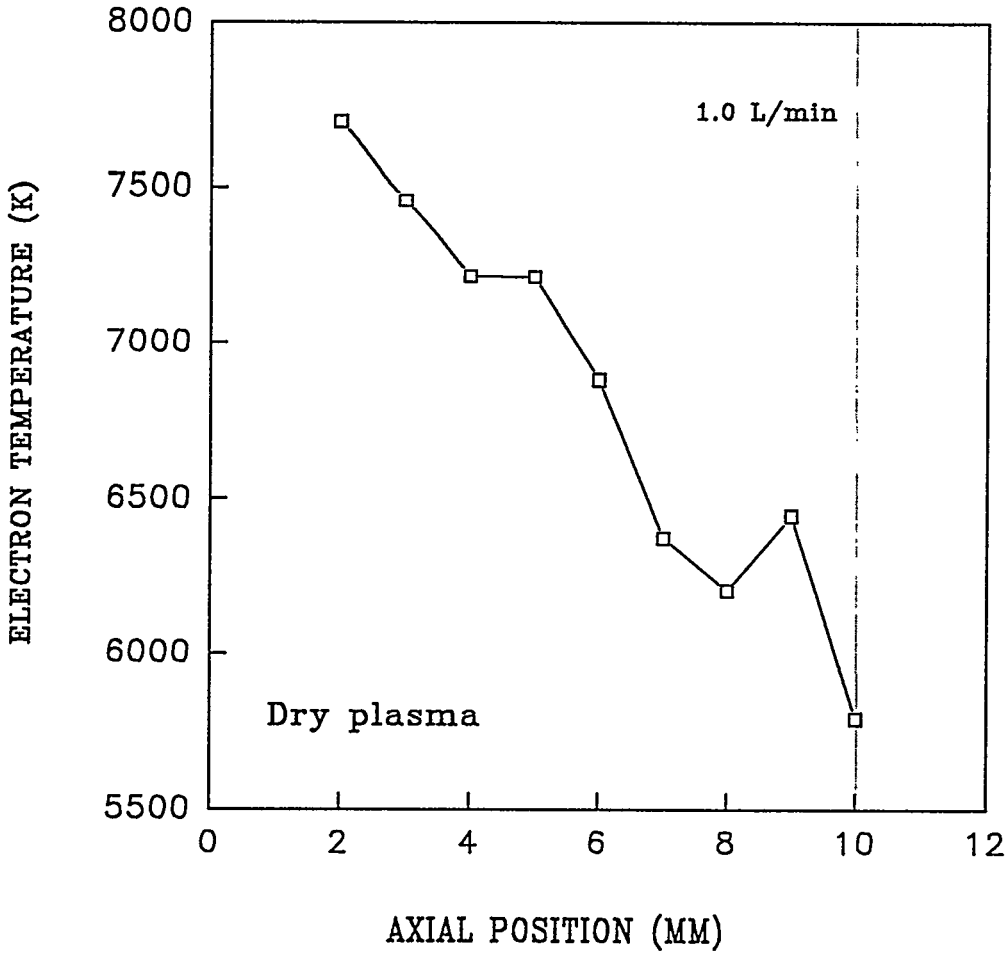

Figure 12. Profiles of electron temperature measured at the axial positions between the sampler and the skimmer in an ICP-MS instrument for dry plasma. The skimmer tip is at 10 mm from the sampler. The aerosol gas flow rate is 1.0 L/min.

a.

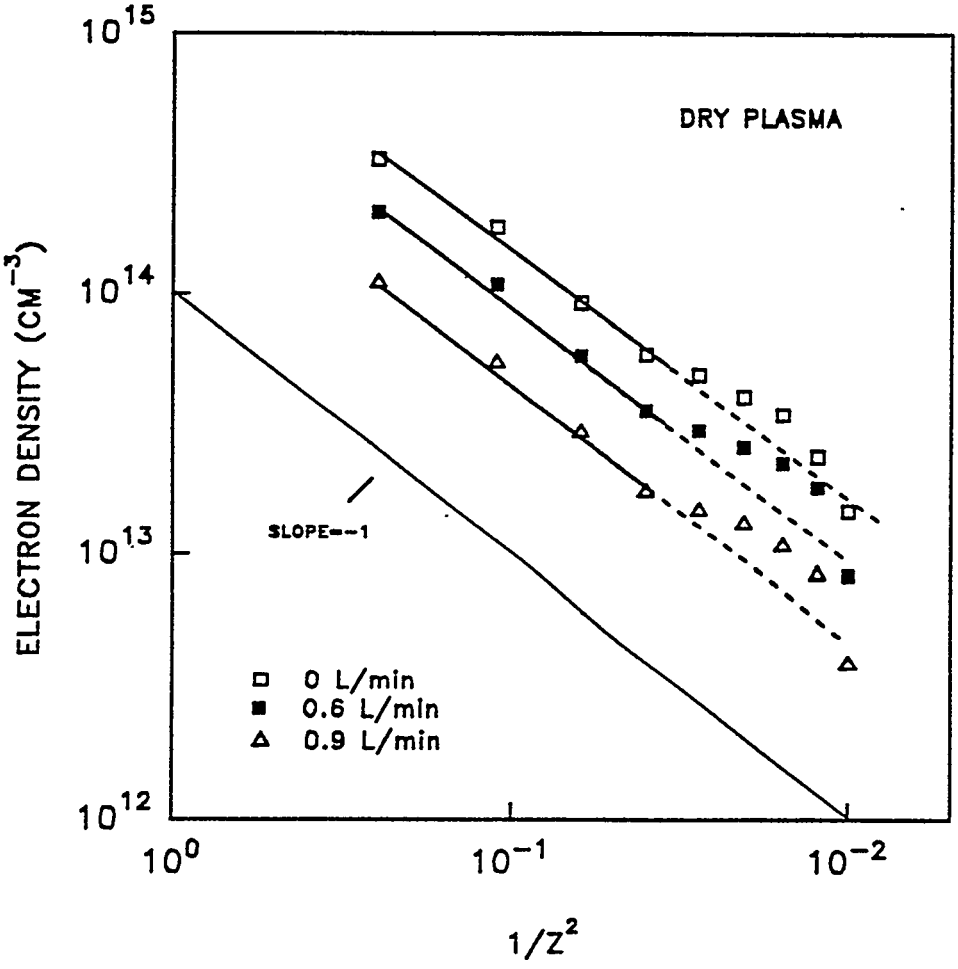

Figure 13. Profiles of electron number density measured at axial positions between the sampler and the skimmer in an ICP-MS instrument, with a) dry plasma, and b) wet plasma condition. Slope = -1 indicates $n_e \sim 1/x^2$. The leftmost point is 2 mm behind the sampler and the righmost point is at the skimmer tip.

b.

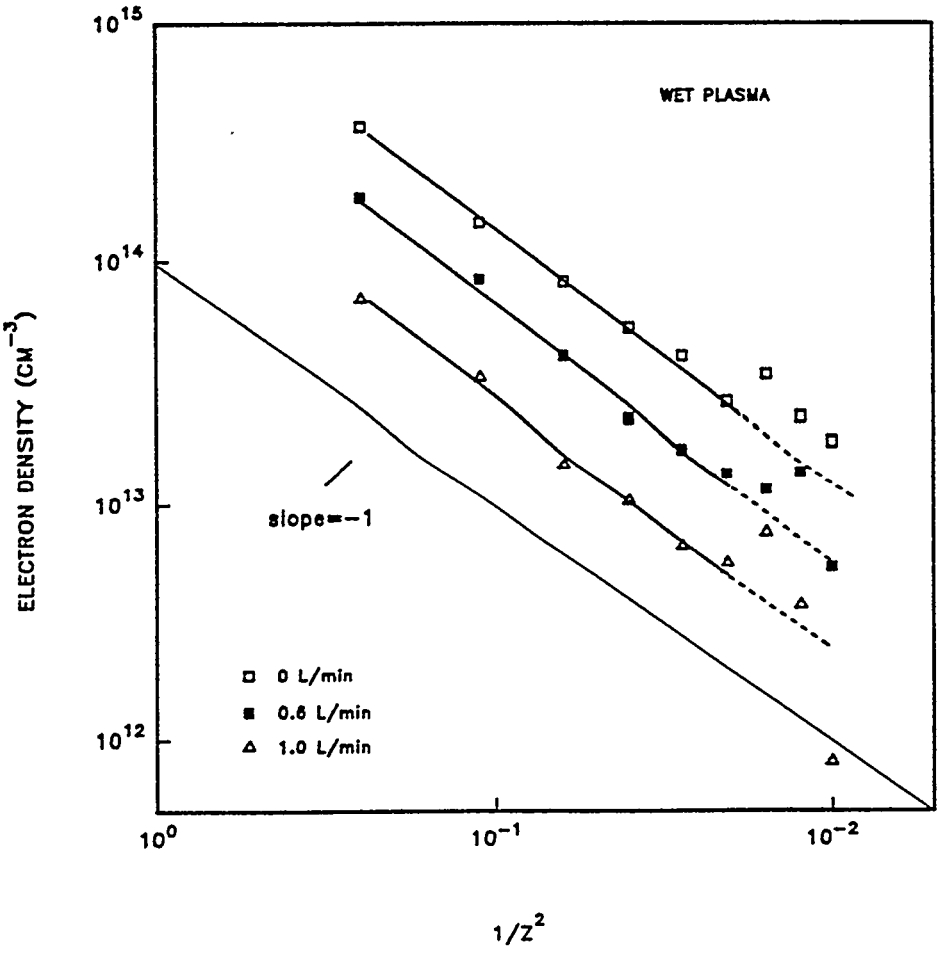

Figure 13. (continued)

a.

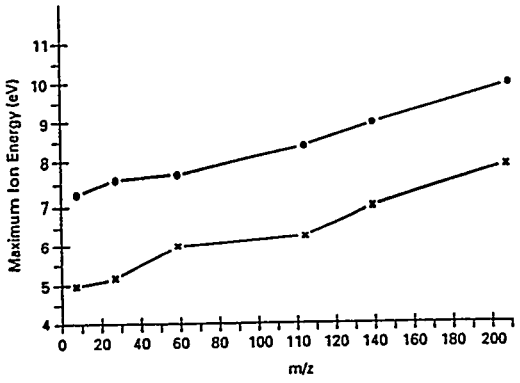

b.

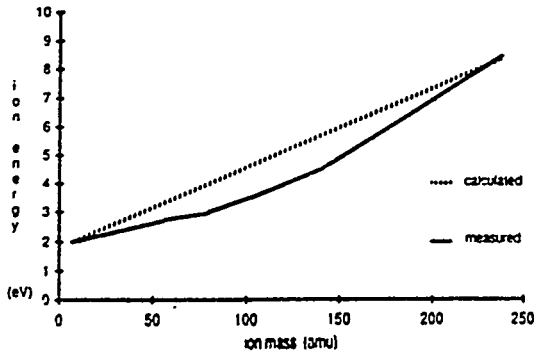

Figure 14. Ion kinetic energies as a function of m/z, a) with a reversed load coil in Ames instrument, and b) with center-tapped load coil in Sciex instrument. Reproduced from references 129 and 121, with permission.

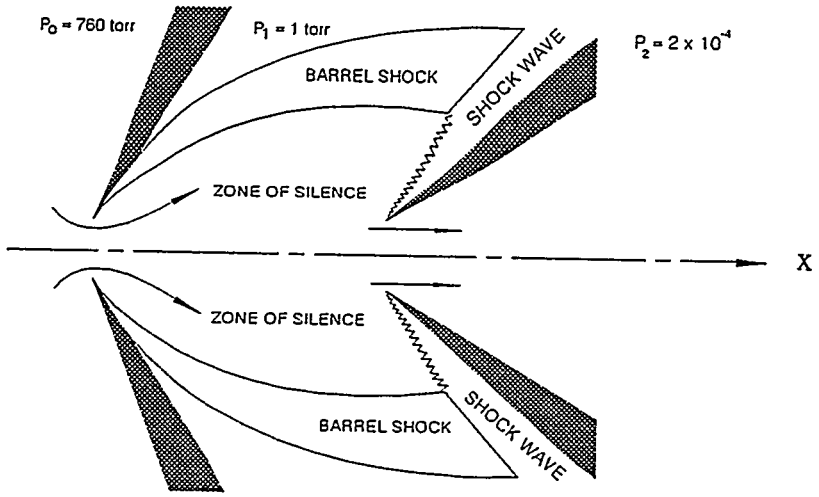

Figure 15. Schematic diagram of supersonic flow and skimming process for ICP-MS.

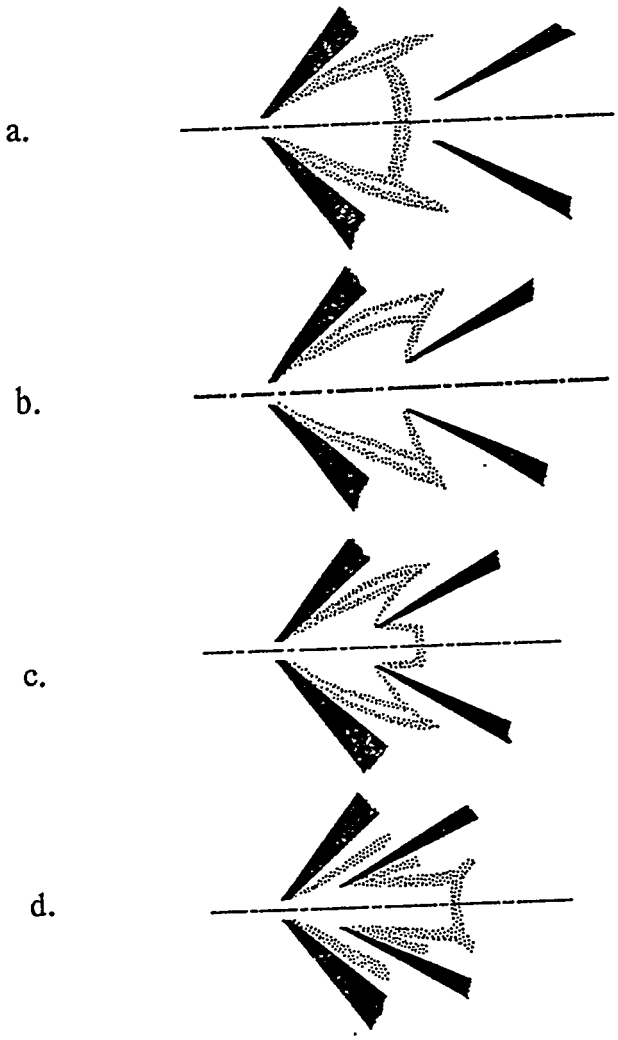

Figure 16. Schematic picture of beam formation at different skimming positions relative to the Mach disk for ICP-MS, a) skimming position behind Mach disc; b) skimming position at Mach disc b) skimming position at ~2/3 of the jet from sampler orifice b) skimming position too close to the sampler orifice. Reproduced from references 135, with permission.

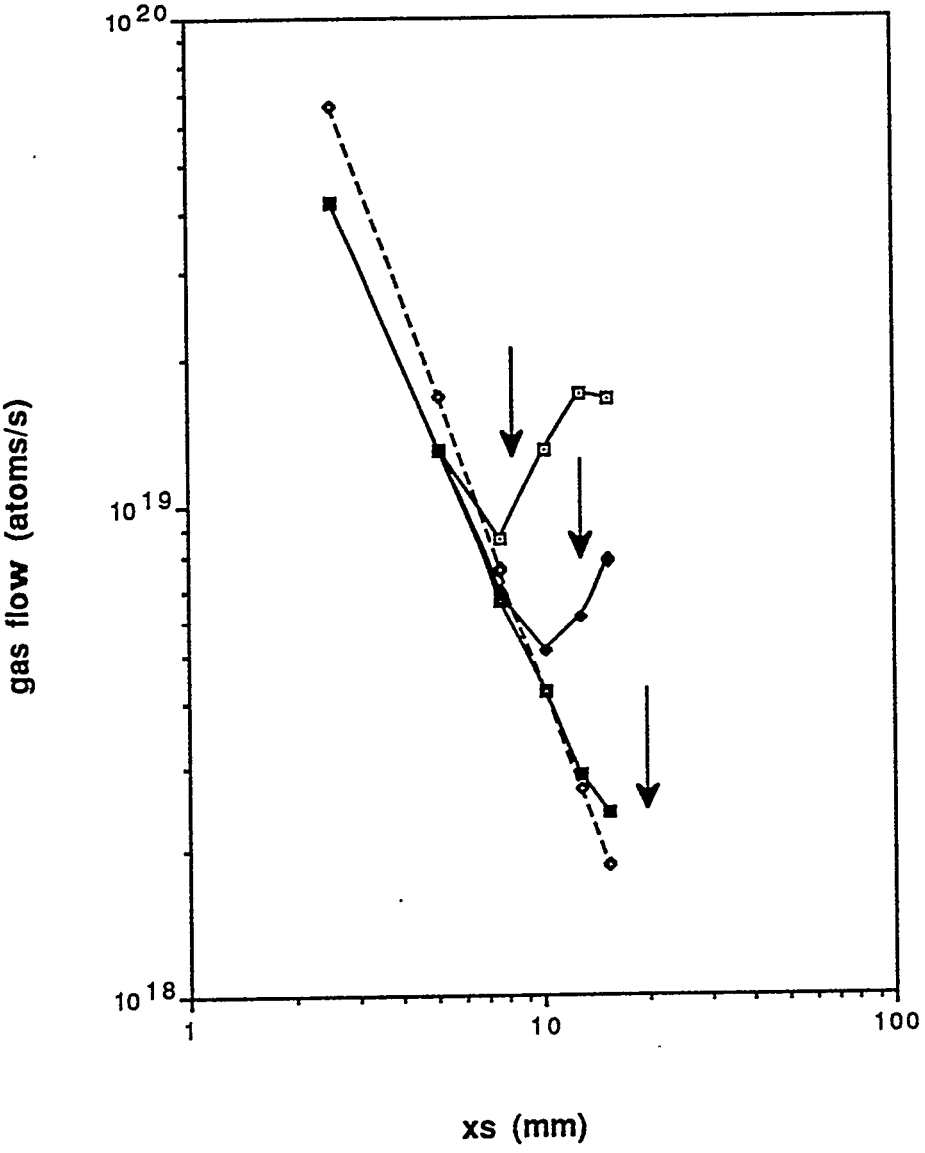

Figure 17. Measured gas flow through the skimmer for different skimming position X_s. Three different pumping speeds are used, (□) 6 L/s; (♦) 13 L/s; and (▪) 30 L/s. The dashed line was calculated from Equation 19. The arrows indicate the Mach disk positions. Reproduced with permission.

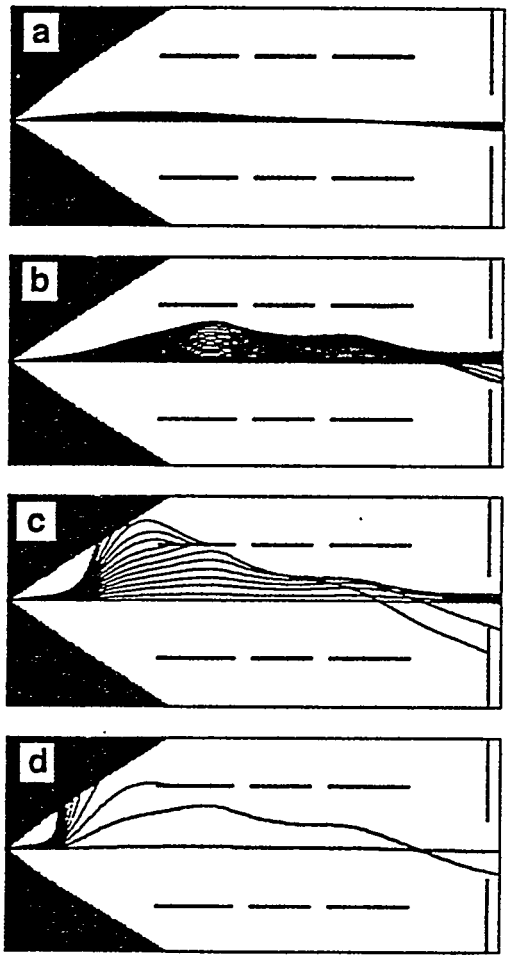

Figure 18. Calculated ion trajectories for $^{24}Mg^{+}$ in the absence of space charge a), and with the space charge at different incident ion current through the skimmer: 0.75 μA b); 1.75 μA c); and 5.0 μA d).

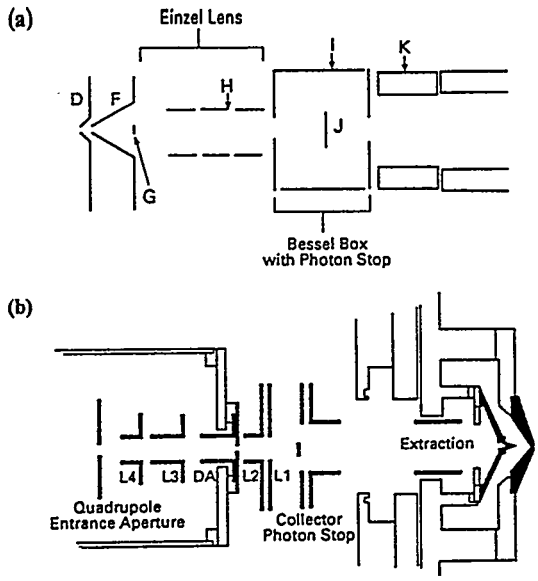

Figure 19. Ion lenses used in ICP-MS commercial instruments, a) Sciex Elan system; b) VG PlasmaQuad system. Bessel box and two photon stops are used in Elan ICP-MS. The first lens in Plasma Quad is used for extraction ions from the plasma beam.

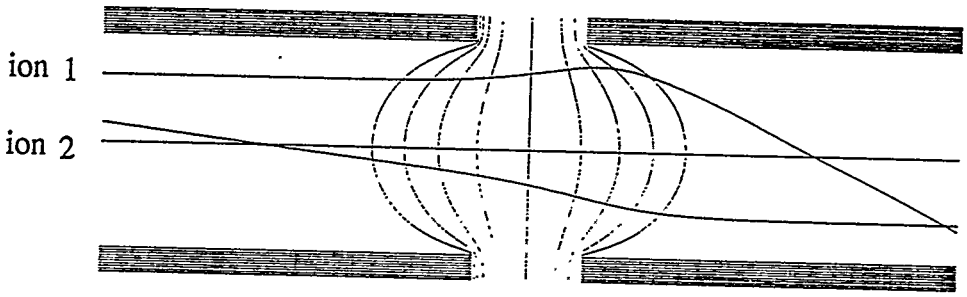

Figure 20. The action of a two-cylinder lens system. The equapotential surface and the paths of charged particles are shown in the electrical lenses.

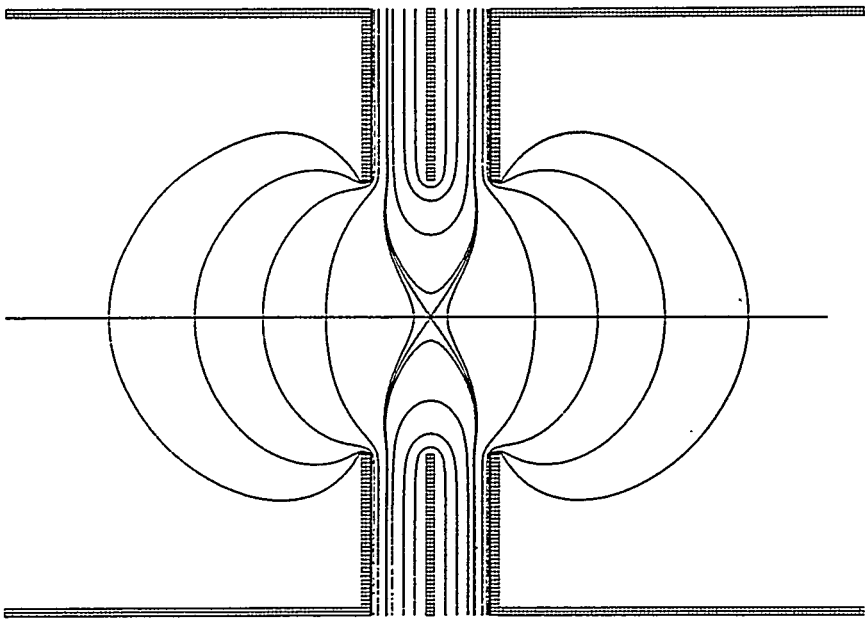

Figure 21. Equipotentials in an einzel lens.

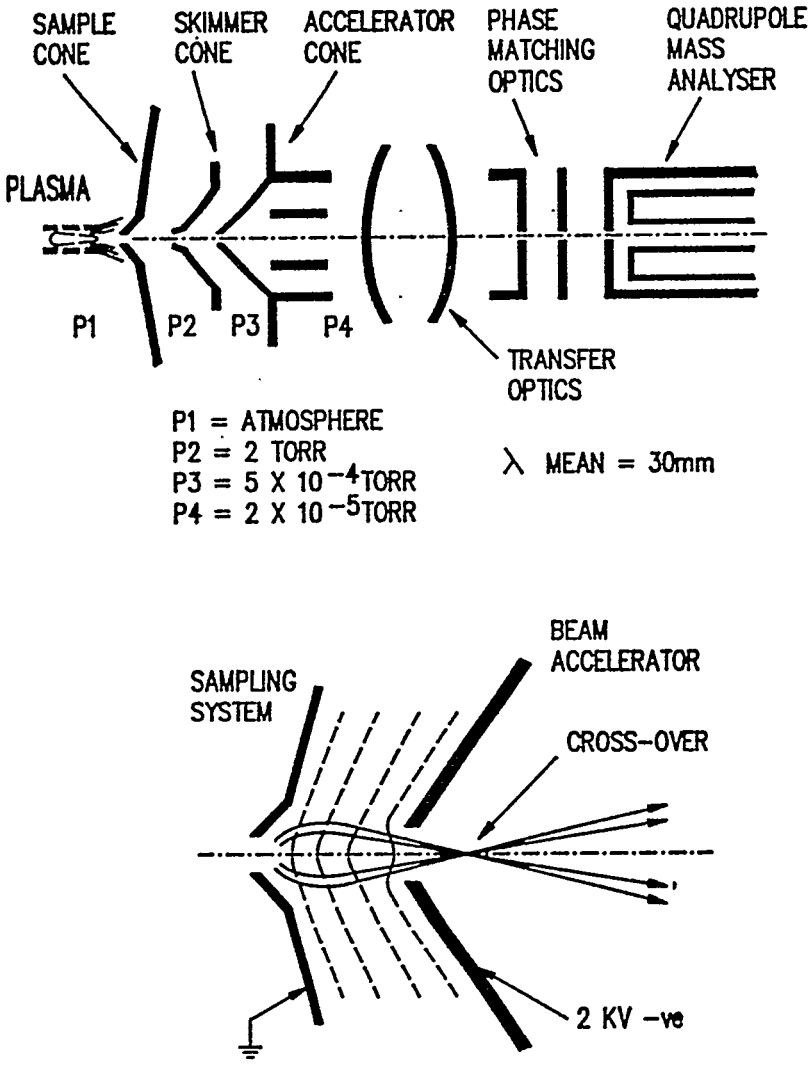

Figure 22. Ion optical system designed by Turner. An accelerating potential of 2000 volts is used on the acceleration cone, and behind this a simple deflection system with a single variable einzel lens focussing potential is used to transfer the ion beam onto the entrance aperture of the analyzing mass spectrometer. Reproduced with permission.

a.

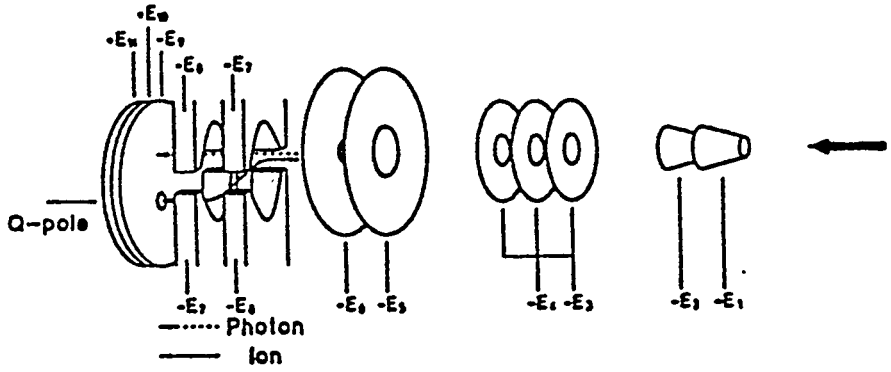

b.

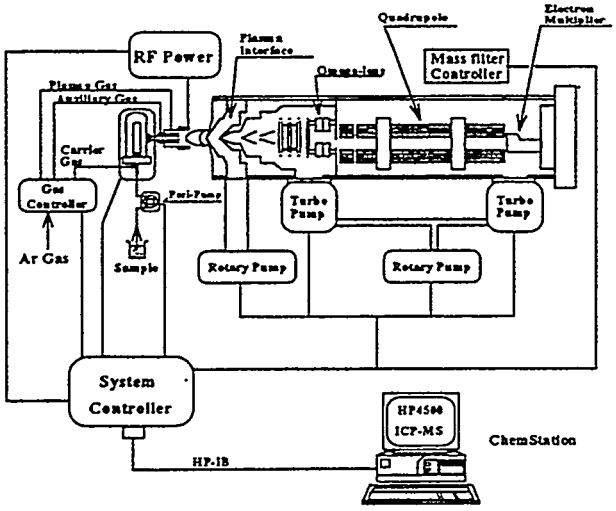

Figure 16. The PMS 2000 (a) and HP 4500 (b) of Yokogawa with offsetting lens arrangements. Reproduced with permission.

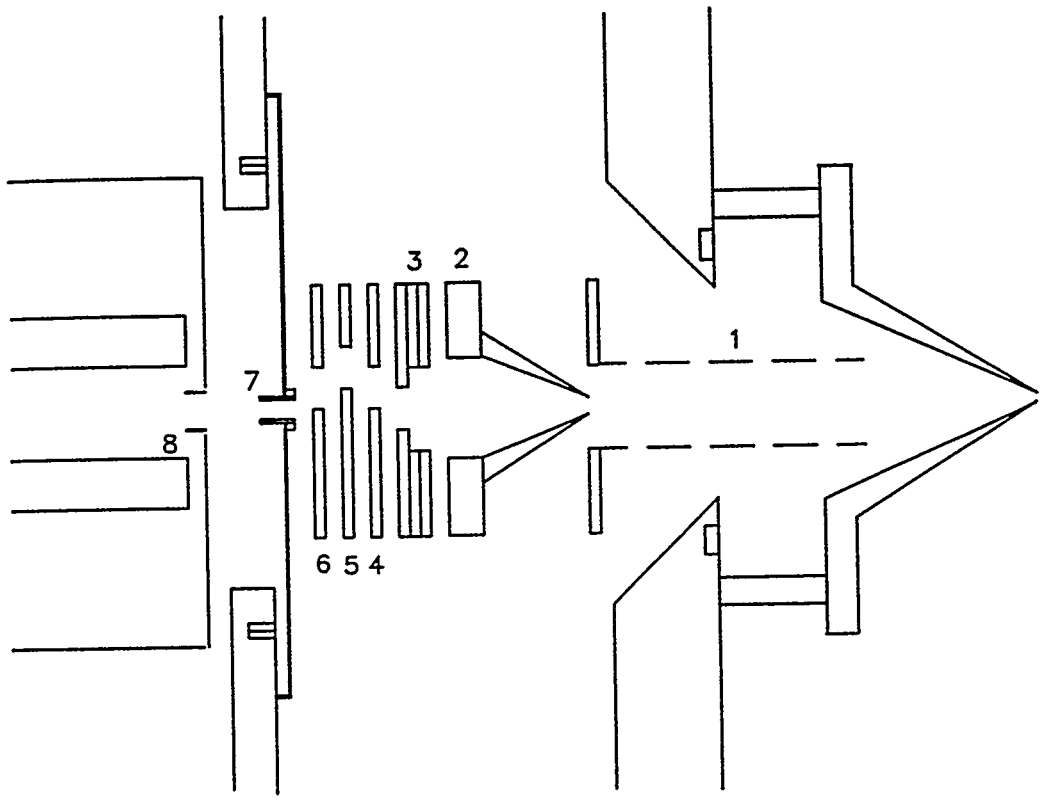

Figure 24. The Ames laboratory new ion optical system. The ion lens deflects ion off center and then back on center into the differential pumping orifice. Reproduced from reference 172, with permission.

a.

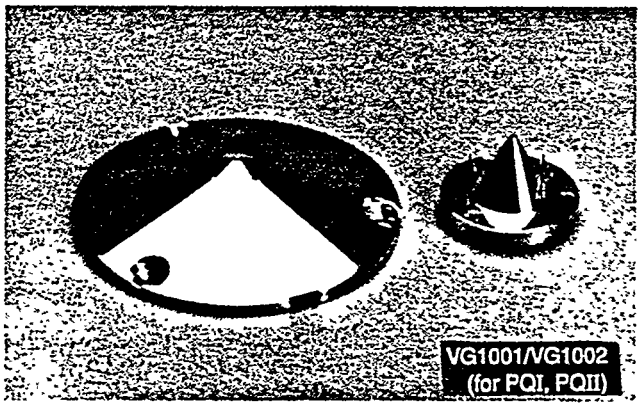

b.

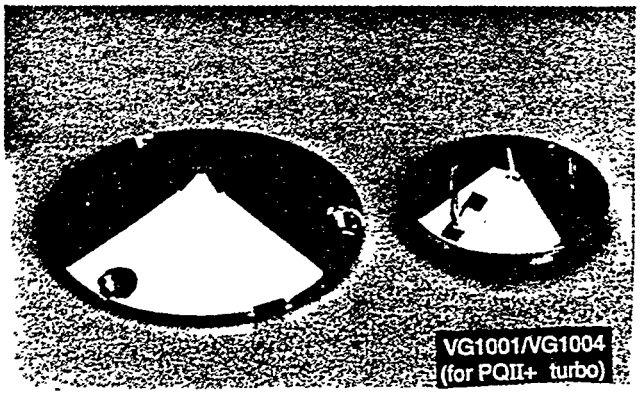

Figure 25. VG ICP-MS sampler and skimmer designs, for a) VG 1001/VG1102 (for PGI,4PQII), and b) VG1001/VG1004 (for PQII+ turbo) with a two angle skimmer design. Reproduced with permission.

a.

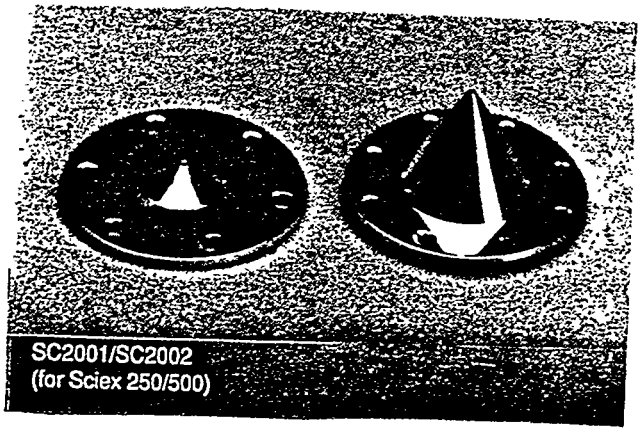

b.

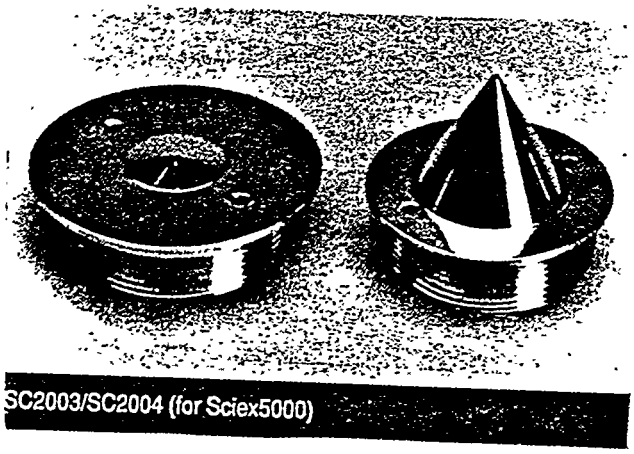

Figure 26. Sciex ICP-MS sampler and skimmer designs, for a) Sciex 250/500, and b) Sciex 5000. Reproduced with permission.

Figure 27. Photograph of sampling cone used in Ames ICP-MS instruments.

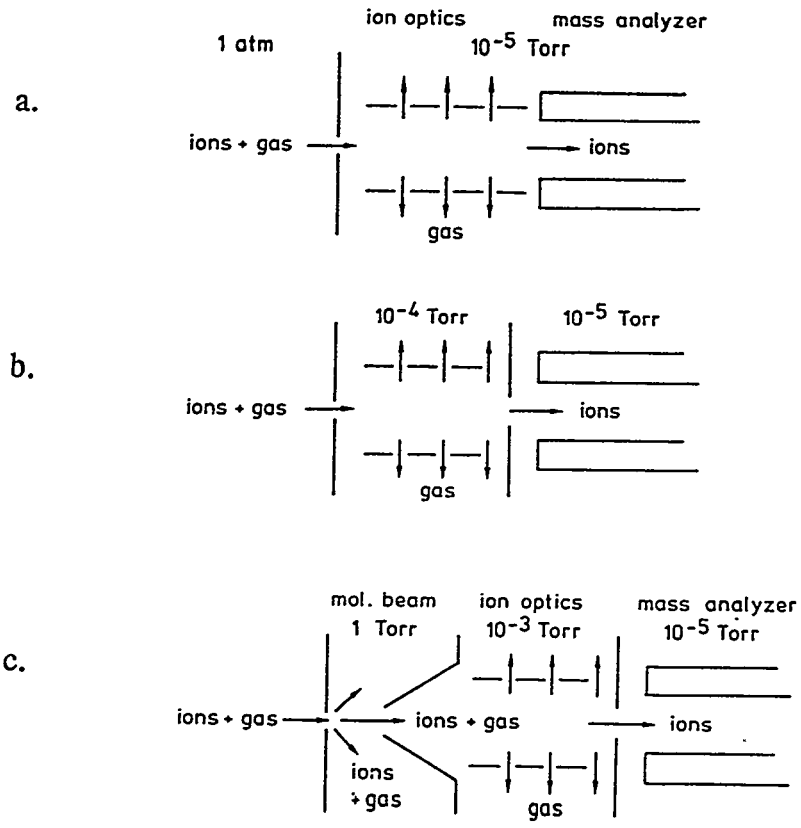

Figure 28. Vacuum systems for atmospheric pressure plasma ion sources, a) single-stage vacuum system. b) a two-stage system with ion lenses and mass analyzer; c) a three-stage system with sampler, skimmer and differential pumping plate.

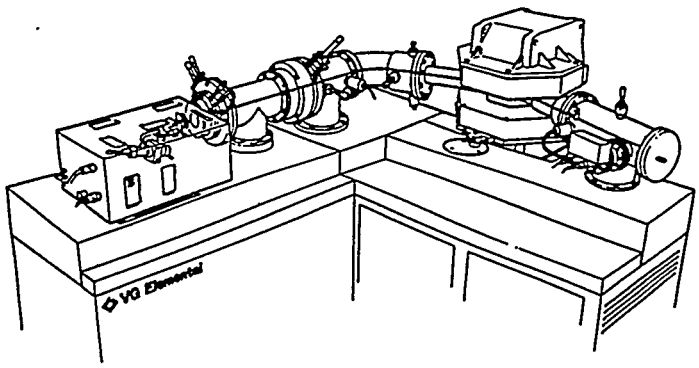

Figure 29. High resolution ICP-MS instrument from VG. Reproduced with permission from VG.

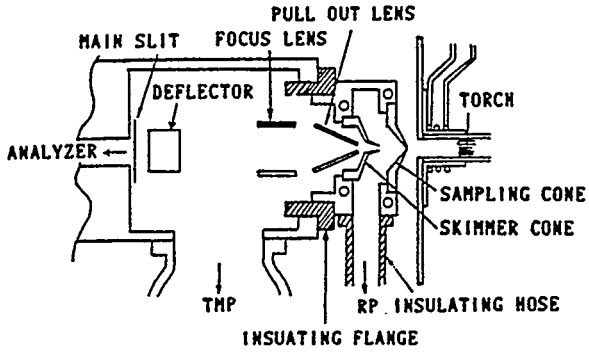

Figure 30. A schematic diagram of the ICP interface for the high resolution mass spectrometer. Reproduced from reference 216, with permission.

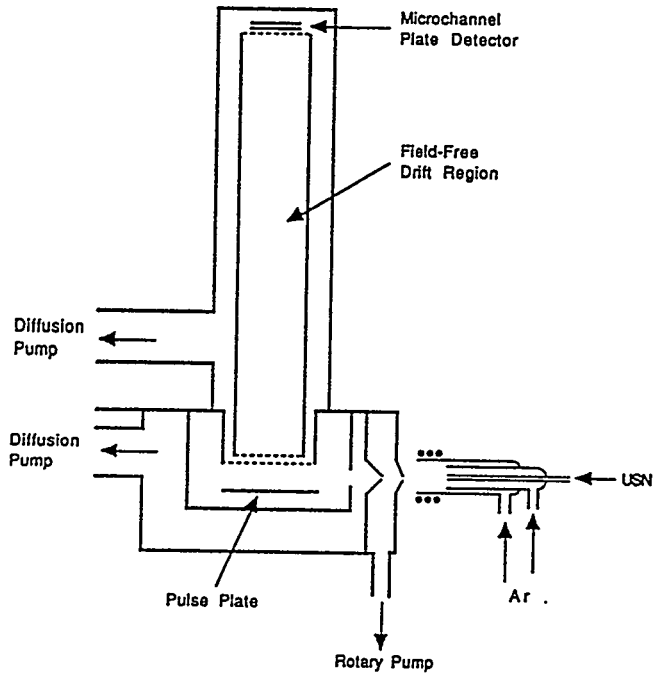

Figure 31. Schematic diagram of an interface design for ICP ion source coupling with TOF mass filter. Reproduced from with permission

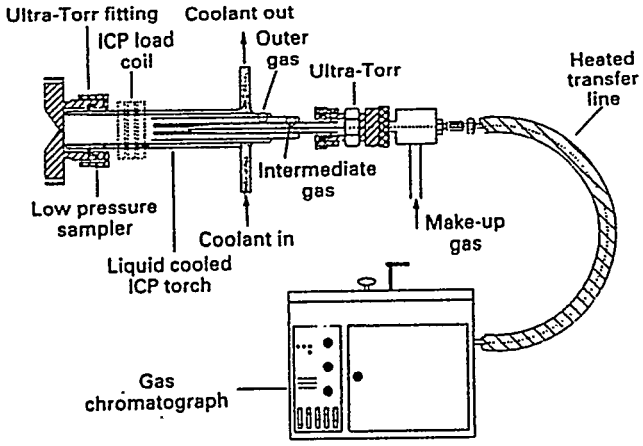

Figure 32. Schematic diagram of an interface design for low pressure plasma source mass spectrometry. Reproduced reference 215, from with permission

PAPER II

LANGMUIR PROBE MEASUREMENTS OF ELECTRON TEMPERATURE AND ELECTRON DENSITY BEHIND THE SKIMMER OF AN INDUCTIVELY COUPLED PLASMA MASS SPECTROMETER

INTRODUCTION

Throughout his career, Paul Boumans has insisted that the intelligent use of a spectroscopic method must be accompanied by an adequate understanding of the underlying fundamental principles. ICP-MS, although already a highly sensitive technique with widespread applications, is no exception to this caveat. To this end, a series of previous papers has addressed various basic aspects of ion extraction pertinent to ICP-MS. These studies include calculations of gas dynamic properties [1,2] and experimental studies via optical spectroscopy [3-7] and Langmuir probes [8-14] in the ICP near the sampling orifice and in the supersonic jet just behind the sampling orifice. This paper describes the basic feasibility of Langmuir probe measurements still further downstream between the skimmer and the entrance to the ion lens. OLIVARES and HOUK [15] briefly considered space-charge effects in this region to be a substantial source of ion loss. The detailed calculations of ion trajectories by GILLSON et al. [16] showed that space-charge effects caused both ion loss and matrix effects. The axially-resolved probe measurements described herein illustrate a possible way the study these phenomena.

EXPERIMENTAL

Apparatus

The instrument used is shown in Fig. 1. Instrumental components, important dimensions and operating conditions are identified in Table I. The entire third vacuum stage, including the mass analyzer, was removed from an ICP-MS device described previously [3]. A flange containing a linear motion feedthrough (5 cm travel) was mounted on the rear of the second stage to support and position the probe. The ICP was the same one used for the previous probe studies [12,13]. The load coil was grounded at the downstream turn as shown in Fig. 1. A mild secondary discharge is thought to persist with this geometry [9,12,13].

For some experiments, a "dry" ICP was desired, so the argon flow was passed directly from the flow controller into the injector tube of the torch, i.e., the nebulizer was bypassed completely. When a "wet" plasma was desired, a continuous flow ultrasonic nebulizer with desolvation was used [18]; operating conditions are listed in Table I. In the latter configuration, some water vapor reached the plasma, as determined by the vapor pressure of water at the temperature of the condenser.

Langmuir Probe

A single probe was used. The tungsten probe was insulated inside a drawn-out quartz tube supported by an outer ceramic sheath. The dimensions of the probe

construction and the component for the measurements were given in Table II. In the present work, the exposed probe tip was much thinner (0.12 mm diam.) and longer (5 mm) than the one used previously. This long, thin probe was desirable for two reasons. First, it conformed to the probe model of SONIN for a flowing, highly rarefied plasma [19]. This model required a probe that was much longer than its diameter so that end effects were negligible. Second, the probe did not heat appreciably and showed no signs of pitting or erosion. Thus, a thin wire probe could be used. Such a probe would probably melt or deteriorate rapidly if it were kept inside the supersonic jet from an ICP [12,13].

As shown in Fig. 1, the probe protruded through the ion lens along the centerline of the expansion. If the probe was more than 45 mm from the skimmer tip, the probe tip was actually inside the lens. Numerous I-V curves were obtained with the probe slightly inside the entrance to the lens. The sampler, skimmer and ion lens were kept grounded for all these experiments.

Measurement of T_e

I-V curves were obtained at various values of probe position, aerosol gas flow rate, and water loading. Three typical I-V curves are shown in Fig. 2. These curves will be discussed in more detail later in the Results and Discussion section. T_e was evaluated from each I-V curve as described previously [13]. SONIN [19] stated that this conventional method of determining T_e from an I-V curve was acceptable for the type of

plasma studied in this work.

A typical plot of probe response is given in Fig. 3. As was seen previously with probes in either the ICP [11] or in the jet [13], these probe response plots were often non-linear. If so, a roughly linear region was selected spanning low values of V, a line was drawn through these points only (as shown in Fig. 3), and T_e was calculated from the slope of the line.

Measurement of n_e

To determine n_e from the I-V curves, an appropriate probe model was necessary. This required estimates of mean free path (λ) and Debye length (λ_D) in the beam flowing out of the skimmer. The kinetic temperature of Ar neutrals in the beam was estimated to be ~ 200 K [1]. Mean free path was estimated as follows. The number density of neutrals (n_o) at the entrance to the skimmer was taken to be 8×10^{15} cm^{-3} [1]. The distance z was defined as the position downstream from the skimmer tip along the centerline of the beam. The number density n(z) of neutrals at position z was calculated by a similar equation as that used in the supersonic jet [1]:

$$n(z) = 0.161\ n_o\ (D_s/z)^2 \qquad (1)$$

Mean free path was then calculated at each position z [20]:

$$\lambda = (\sqrt{2}\quad \pi\sigma^2 n(z))^{-1} \qquad (2)$$

where σ = atomic diameter of Ar = 3.8×10^{-8} cm [21]. With the probe at z = 5 mm, the mean free path was 3.0 cm. Naturally, mean free path increased as the

beam flowed further from the skimmer to a limit of ~50 cm at the background pressure of 1 x 10^{-4} torr. These large values of mean free path indicate that the beam passing through the skimmer was essentially collisionless. This conclusion was expected because collisions are infrequent in the supersonic jet in front of the skimmer [1], and the density therein is much higher than that in the beam behind the skimmer. The Debye length is calculated from

$$\lambda_D = \left[\frac{\epsilon_o k T_e}{e^2 n_e}\right]^{1/2}$$

$$\lambda_D(\text{cm}) = 6.9\ (T_e/n_e)^{1/2} \qquad (3)$$

where ϵ_0 = permittivity of free space, k = Boltzmann constant, e = electron charge, T_e is in K, and n_e is in cm^{-3}. Based on the values for T_e and n_e reported below, λ_D was estimated to be in the range 0.02 - 3 mm. The probe radius (r_p) was 0.063 mm and was generally less than λ_D, with some important exceptions discussed in detail in Sect. 3.4. Thus, the relative magnitudes of λ, λ_D and r_p were: $\lambda >> \lambda_D \sim > r_p$.

According to this calculation, the probe was considered to be in a collisionless plasma in the orbital-motion-limit. For this probe regime, the basic theory of LAFRAMBOISE was suitable [22,23]. SONIN [19] adapted this theory and systematically studied its validity for a probe with length $l_p >> r_p$ aligned with the stream in a flowing plasma, which was appropriate for the present work (Fig. 1). Electron density was evaluated from the I-V curves by the following process based on SONIN's method [19]:

1). Calculate T_e as described in Sect. 2.3.

2). Measure the ion saturation current (I_i) at an applied voltage of $V_f - 10(kT_e/e)$, where V_f is the voltage corresponding to zero current (often called floating voltage).

3). Calculate the quantity β defined below:

$$\beta = (r_p/\lambda_D)^2 \alpha_i = (r_p^2/\epsilon_o) (2\pi m_i/e)^{1/2}(e/kT_e)^{3/2} (I_i/A_p) \qquad (4)$$

where m_i = ion mass and A_p = probe area (excluding the end) = $2\pi r_p l$. Eqn. (4) is convenient because n_e drops out; an appropriate value for n_e need not be assumed prior to the computation. In these experiments, the largest value of β was 12, which was well within the orbital-motion-limited regime [19].

4). Using the calculated value of β, read the appropriate value of α_i from Fig. 2 of ref. [19] for the case where $T_i/T_e \rightarrow 0$. Here T_i refers to the gas kinetic temperature of ions and is often called "ion temperature" in the plasma physics literature. This term should not be confused with the term "ionization temperature" common in spectrochemical literature, which refers to the results of temperature calculations from the Saha Equation. At any rate, since the heavy ions should be cooled to $\sim$ 200 K in the expansion while T_e stays close to that in the ICP, the assumption that $T_i < T_e$ is reasonable in the present work. We also note that the quantity we call α_i is referred to as I_i by SONIN [19]. In the present work, α_i was

generally 4.4 and, in fact, would not change greatly even if $T_i \sim T_e$.

5). Calculate n_e from:

$$n_e = \frac{I_i}{eA_p\alpha_i} \quad (2\pi m_i/kT_e)^{1/2} \qquad (5)$$

Some assumptions concerning the ion mass m_i are necessary, since both α_i and n_e depend on m_i. For a "dry" plasma or a "wet" plasma containing no matrix element, m_i was assumed to equal the mass of argon (40 g/mole, 6.67×10^{-23} g/atom). Incorporation of ions from a matrix element could change the average ion mass in the extracted beam. Therefore, two different n_e values were calculated from each I-V curve when a matrix element was added. First, m_i was assumed to be unchanged and still equal to the mass of argon, and one n_e value was calculated on that basis. Second, m_i was assumed to equal the arithmetic average of the mass of argon and the mass of the matrix element. For example, when uranium was present, the ion mass was assumed to equal $(40 + 238)/2 = 139$ g/mole $= 2.32 \times 10^{-22}$ g/atom. A second n_e value was then calculated based on this "average ion mass."

Standard Solutions

For experiments with a "wet" plasma, deionized distilled water was generally nebulized. Effects of sample matrix on T_e and n_e were evaluated with two sets of single-element standard solutions. The first set contained 0.14 M Li (i.e., 1000 ppm Li) and other solutions of Na, K and Rb, each at 0.14 M also. These concentrations

were chosen so that the effects of matrix elements could be compared to those seen in the earlier Langmuir probe studies in the jet [12,13]. The second set of solutions contained either Co or U at 1000 ppm, which is the common upper limit on solute concentration in ICP-MS. For each matrix solution, the solvent was 1% HNO_3 in deionized distilled water.

RESULTS AND DISCUSSION

Characteristic of I-V Curves

Some important qualitative observations can be made by simply inspecting the I-V curves in Fig. 1. First, the magnitude of current flow is small; the vertical scale is in μA, whereas the currents were in the mA range when a similar (though larger) probe was put inside the jet [13]. Since the currents observed are smaller, it follows that the charged particle densities behind the skimmer are smaller as well. This would be expected because the total density of all particles is smaller behind the skimmer as the gas flows into the high vacuum pumps. In some cases, particularly when a "wet" plasma was used, the ion saturation currents were below one nA. These low current values complicated the experiments. In particular, the voltage supply and ammeter were housed inside a grounded, copper-lined steel box to attenuate RF interference [11].

The three curves shown in Fig. 2 were obtained at the same probe position with three different values of aerosol gas flow rate. Despite the low currents, both the ion saturation current (shown in the inset) and the shape of the curves in the electron retarding region were different at the three different flow rates. Hence, the probe can sense variations in T_e and n_e as plasma operating conditions are changed.

Finally, at positive values of V, the electron current continued to rise and did not saturate. With the probe behind the skimmer, the electron current showed even

less tendency to saturate than when the probe was in the jet [13]. A similar effect has been seen in Langmuir probe measurements in other highly-rarefied, flowing plasmas [24,25].

Electron Temperature Measurements

1. Effect of water loading on T_e

Determined values for T_e are listed in Table 3 for a "dry" plasma and in Table 4 for a "wet" plasma. The measured values range from 2100 K to 11400 K. DOUGLAS and FRENCH [1,2] state that electrons should not be cooled during the supersonic expansion nearly as extensively as the heavy particles. Thus, T_e should remain in the range of several thousand degrees K, whereas heavy particles should be cooled to ~200 K. This precept was substantiated by our previous measurements in the jet [13] and was further corroborated by the relatively large values of T_e measured behind the skimmer.

Some other general trends are also apparent from these tables, although exceptions to each trend can be noted. T_e is lowest when the aerosol gas flow rate is zero, i.e., when there is no axial channel in the ICP. For a "dry" plasma, T_e increases with aerosol gas flow rate through 1.4 L/min. As in the previous experiments with the probe in the jet, this trend is thought to be due to an increase in plasma potential and intensity of the secondary discharge as the aerosol gas flow rate increases. For a "wet" plasma, a similar trend is seen, except that T_e is a maximum

at 1.0 L/min and then decreases as aerosol gas flow rate is increased further to 1.4 L/min. At aerosol gas flow rates of 0.6 and 1.0 L/min, T_e for a "wet" plasma is generally higher than that for a "dry" plasma. At 1.4 L/min, higher values of T_e are generally seen for the "dry" plasma.

Finally, all the T_e values measured behind the skimmer are substantially lower (by ~ 4000 K) than T_es measured in the jet under the same plasma conditions [13]. The fact that the probe was hot when it was in the jet but remained cool when it was behind the skimmer may contribute to this discrepancy.

2. Matrix effects on T_e

These results are shown in Table 5. First compare the results labelled "blank solution" with those for the same aerosol gas flow rate (1.0 L/min) in Table 4. The values in Table 5 are within 200 K to 1400 K of the corresponding values in Table 4. All but one of the values for the blank solution in Table 5 are lower than the corresponding values in Table 4. These two sets of T_e values were obtained on different days. Factors such as the difficulty of exactly reproducing aerosol gas flow rate and power from day to day, the generally low values of current observed (see Sect. 3.1), and differences in the linear ranges in the corresponding probe response plots (e.g., Fig. 3) probably contribute to this discrepancy.

To minimize the contribution of variable operating conditions, the T_e values in Table 5 were obtained in a single day. Addition of alkali metals either caused little

change or induced a slight decrease in T_e; this latter trend was more evident when the probe was further from the skimmer. Much greater decreases in T_e were seen in the presence of alkali matrix elements in the previous work [13]. Addition of Co or U induced a substantial increase in T_e, particularly when U was added. Little is known about whether T_e in the ICP is affected by matrix elements; the Thomson scattering measurements described by Hieftje and co-workers [26,27] may provide such information.

Electron Density Measurements

1. "Dry" plasma

These results are shown in Fig. 5. At each value of aerosol gas flow rate, n_e decreases as the probe is retracted further from the skimmer. This is expected, as the density of the supersonic beam flowing out of the skimmer decreases as the beam moves further downstream from the skimmer tip. However, the decrease in n_e shown in Fig. 4 is not as extensive as would be expected from the $1/z^2$ (z=distance behind skimmer tip) dependence usually seen for supersonic beams.

Fig. 4 also shows that, at each probe position, n_e decreases as aerosol gas flow rate increases. This trend is also expected because n_e at the sampling position in the axial channel of the ICP decreases as aerosol gas flow increases [28,29]. Electron density in the beam passing through the skimmer should follow changes in plasma conditions in the same fashion as n_e in the ICP.

2. "Wet" plasma

These results are shown in Fig. 5. Electron density follows similar trends with probe position and aerosol gas flow rate as were seen in Fig. 4 for a "dry" plasma. At low aerosol gas flow rates (0 and 0.6 L/min), the n_e results for a "wet" plasma do not differ greatly from those for a "dry" plasma (Fig. 4). At higher values of aerosol gas flow rate (1.0 and 1.4 L/min), n_e is substantially lower for a "wet" plasma. This trend agrees qualitatively with that seen for n_e in the axial channel of the ICP in recent measurements by OLESIK and DEN [30, Fig. 10]. There is some disagreement in the literature concerning the effects of water loading on n_e in the axial channel; some authors report increases of $\sim$30% in n_e in the axial channel when water is added [31,32], others report that n_e increases slightly when water vapor is added but n_e decreases when water droplets are added [33]. Although T_e behind the skimmer and in the jet [13] generally increases with water loading and/or aerosol gas flow rate, n_e shows the opposite trend. Apparently, a modest plasma potential and mild secondary discharge elevate T_e but do not affect n_e greatly [13].

3. Effects of matrix on n_e

These results are shown in Figs. 6 and 7. In each figure, two sets of plots are shown; one set (labeled A) is derived assuming the ion mass is unchanged when the matrix element is added. The other set (labeled B) is based on the assumption that the average ion mass changes when the matrix element is present (see Sect. 2.4).

These sets of data differ little when the matrix is Na, Rb or Co, but use of matrix elements such as Li or U with masses much different from that of argon could change the resulting n_e values somewhat.

Despite this uncertainty in ion mass, some interesting trends can be identified from Figs. 6 and 7. Addition of the matrix element did not change n_e much at probe positions near the skimmer (i.e., 5 to 20 mm). Close to the skimmer tip a modest increase in n_e was seen for a U matrix and a modest decrease in n_e was seen for a Li matrix if average ion mass was used (Fig. 6B). With the probe retracted from the skimmer tip by more than 20 mm, n_e was apparently substantially higher (by up to one order of magnitude) when a matrix element was present. The heavier matrix elements (Rb in Fig. 6 or U in Fig. 7) induced a more substantial increase in n_e than the lighter matrix elements.

These increases in n_e in the presence of a matrix element are qualitatively similar to the increases in ion current seen by GILLSON et al [16] and may be related to space-charge effects and matrix effects in ICP-MS in the following way. If space-charge repulsion causes defocusing and spreading of the ion beam [16], n_e may also change when matrix elements are added. Since the space-charge defocusing is thought to be more extensive for heavy matrix elements, such elements also affect n_e more extensively. In addition to the experiments and calculations of ion trajectories by GILLSON et al. [16] and the numerous studies of matrix effects in ICP-MS [34-39], these results also show that the properties of the beam leaving the skimmer

depend on the presence of matrix elements and on their mass.

It is also important to note that the concentrations of matrix elements used in this study are not high enough to induce large changes in n_e in the ICP [34]. Thus, the effects of matrix elements on n_e in the beam are attributable mainly to the ion extraction and beam formation processes rather than to changes in n_e in the ICP.

Finally, compare the n_e results obtained for the blank solution in Fig. 6A with those shown for the blank solution in Fig. 7A. Although these experiments were performed on different days, the n_e results for the blank solutions agree closely with each other, which indicates that the n_e results are reasonably reproducible from day-to-day.

Evaluation of Results

In this section, the overall validity of these T_e and n_e measurements is evaluated. The first step is to determine whether the probe drains a significant number of charge carriers from the beam. Consider the typical I-V curve in Fig. 2. The T_e and n_e values were measured using currents of 30 μA or less. The ion current (i.e., the current when the probe voltage is negative), which was used to measure n_e, was generally less than 1 μA. Since the total current through the skimmer is expected to be $\sim$1 mA [16], the current drawn by the probe is not considered a significant drain on the charge carriers in the beam.

The second step is to consider whether the beam passing through the skimmer

can be considered quasi-neutral, i.e., whether the number of positive charge carriers is roughly equal to the number of negative charge carriers. Alternatively, growth of an extended space-charge sheath around the skimmer could cause the extracted beam to deviate from neutrality. These possibilities can be evaluated by calculating the Debye length at the skimmer. From the calculations of DOUGLAS and FRENCH [1] and our previous measurements [13], T_e at the skimmer tip is estimated to be 10000 K and n_e is $\sim 5 \times 10^{11}$ cm^{-3}. From Eqn. (3), the Debye length under these conditions is ~ 0.01 mm. To verify this result, a single I-V curve was obtained with the probe thrust into the skimmer orifice, i.e. the probe position was 0 mm. The aerosol gas flow rate was 1.0 L min^{-1}, and a "dry" plasma was used. The measured T_e was 7500 K and n_e was 3×10^{11} cm^{-3}, so λ_D was 0.011 mm, in good agreement with the estimate described above.

These typical values of λ_D are much less than the diameter of the skimmer orifice (1.0 mm). The thickness of the sheath around the skimmer could well be several Debye lengths, but it is unlikely to be 50 Debye lengths thick [1,40]. Although there is no doubt that a sheath forms around the skimmer, the authors' opinion is that the sheath is not thick enough to perturb the neutrality of the beam substantially [40]. In addition, the sampler, skimmer, ion lens, and vacuum chamber were all kept grounded to minimize any applied electric fields that could alter the neutrality of the beam.

Sheath formation around the probe is another possible source of error. If the

sheath around the probe is large enough to intercept the inner wall of the skimmer, then the probe would not be in a quasineutral plasma. This problem would be most serious when the probe is close to the skimmer.

To address this question, values of λ_D were calculated for the T_e and n_e results reported above for the "dry" and "wet" plasma without matrix elements present. These values are presented in Table 5. At the probe position of 5 mm, n_e is still fairly large, so λ_D is small, and the sheath around the probe is obviously not large enough to reach the skimmer. Since T_e does not change greatly as the probe is retracted further, the change in λ_D with probe position is mainly determined by the decrease in n_e. Even at 40 mm, λ_D increases only to a few mm, so it is unlikely that the sheath around the probe greatly perturbs the neutrality of the extracted beam. Furthermore, if the size of the sheath around the probe is comparable to the diameter of the beam, the measured currents would be much higher, for virtually all the charge carriers in the beam would go into the sheath and reach the probe.

The λ_D results in Table 6 also allow evaluation of whether the condition $\lambda_D \sim > r_p$ from Section 2.4 is satisfied. Since the probe radius is 0.063 mm, there are several cases in which λ_D is comparable to or even less than the probe radius, particularly at a probe position of 5 mm and an aerosol gas flow rate of 0 or 0.6 L min^{-1}. However, as mentioned in Sect. 2.4, the present measurements were still within the orbital motion limited regime. LAFRAMBOISE [23] also showed that r_p can exceed λ_D substantially (by at least a factor of 10) without causing problems.

Thus, the fact that λ_D was occasionally less than r_p is not considered a serious source of error in these experiments.

Finally, the authors point out that Langmuir probe measurements are always subject to doubt, as reflected by the voluminous and often disheartening literature on deriving valid n_e measurements from I-V curves [25]. Both in this paper and in our previous work [13], the general magnitude and trends of the reported T_e and n_e values are considered to be reasonable approximations that provide interesting physical insight into ion beam formation, e.g., the electrons are not greatly cooled during extraction. The T_e and n_e values measured and the trends seen in n_e are all reasonable, which further supports the general validity of these Langmuir probe measurements.

CONCLUSION

These results illustrate the basic feasibility of measuring T_e and n_e behind the skimmer with a single Langmuir probe. Many further studies are suggested by these preliminary results, including a more extensive characterization of the effects of matrix elements on n_e. This apparatus permits three additional experiments that could prove valuable. First, the probe can be inserted through a different port along an axis perpendicular to the ion path. Such a probe would pass laterally through the gap between the base of the skimmer and the entrance to the ion lens. In this fashion, laterally-resolved profiles of T_e and n_e should be obtainable. Second, voltages can be applied to the ion lens and/or sampling interface (both sampler and skimmer) and the resulting effects on T_e and n_e measured. Finally, if the probe is inserted through a lateral port, the third vacuum stage and mass spectrometer [3] can be used with the probe to correlate T_e and n_e measurements with mass spectral observations. These types of studies should allow a thorough characterization of the region where space-charge effects are thought to cause ion loss and matrix effects in ICP-MS.

LITERATURE CITED

1. D. J. Douglas and J. B. French, *J. Anal. Spectrom.* **3**, 743 (1988).
2. D. J. Douglas, *"Fundamental Aspects of ICP-MS"*, ICPs in Analytical Atomic Spectrometry, Eds. A. Montaser and D. Golightlly, 2nd ed. VCH, New York (1991).
3. J. S. Crain, R. S. Houk and F. G. Smith, *Spectrochim. Acta* **43B**, 1355 (1988).
4. H. B. Lim, R. S. Houk, M. C. Edelson, and K. P. Carney, *J. Anal. Atom. Spectrom.* **4**, 365 (1989).
5. H. Kawaguchi, K. Asada and A. Mizuike, *Mikrochim. Acta* **3**, 143 (1988).
6. R. S. Houk and H. B. Lim, *Anal. Chem.* **58**, 3244 (1986).
7. A. L. Gray, *J. Anal. Atom. Spectrom.* **4**, 371 (1989).
8. D. J. Douglas and J. B. French, *Spectrochim. Acta* **41B**, 197 (1986).
9. A. L. Gray, R. S. Houk and J. G. Williams, *J. Anal. Atom. Spectrom.* **2**, 13 (1987).
10. R. S. Houk, J. K. Schoer and J. S. Crain, *J. Anal. Atom. Spectrom.* **2**, 283 (1987).
11. L. Pei-qi, G. Pei-zhong, L. Tie-zheng and R. S. Houk, *Spectrochim. Acta* **43B**, 273 (1988).

12. H. B. Lim, R. S. Houk and J. S. Crain, *Spectrochim. Acta* **44B**, 989 (1989).

13. H. B. Lim and R. S. Houk, *Spectrochim. Acta* **45B**, 453 (1990).

14. N. Jakubowski, B. J. Raeymaekers, J. A. C. Broekart and D. Stuewar, *Spectrochim. Acta* **44B**, 219 (1989).

15. J. A. Olivares and R. S. Houk, *Anal. Chem.* **57**, 2674 (1985).

16. G. R. Gillson, D. J. Douglas, J. E. Fulford, K. W. Halligan and S. D. Tanner, *Anal. Chem.* **60**, 1472 (1988).

17. R. H. Scott, V. A. Fassel, R. N. Kniseley and D. E. Nixon, *Anal. Chem.* **46**, 75 (1974).

18. B. R. Bear and V. A. Fassel, *Spectrochim. Acta* **41B**, 1089 (1986).

19. A. A. Sonin, *AIAA J.* **4**, 1588 (1966).

20. G. W. Castellan, Physical Chemistry. 2nd ed., Addison-Wesley, Reading MA (1971), p. 694.

21. L. Valyi, *Atom and Ion Sources*. Wiley, New York (1977), p. 388.

22. J. Laframboise, *Rarefied Gas Dynamics, Vol. II,* (Ed., J. H. de Leeur), Academic, New York (1965), pp. 22-43.

23. J. Laframboise, *Theory of spherical and cylindrical Langmuir probes in a collisionless,* Maxwellian plasma at rest, Univ. of Toronto, Inst. for Aerospace Studies, Report No. 100 (1966).

24. D. W. Koopman, Phys. *Fluids* **14**, 1707 (1971).

25. P. M. Chung, L. Talbot and K. J. Touryan, *Electric Probes in Stationary and*

Flowing Plasmas: Theory and Application. Springer-Verlag, New York (1975), p. 35.

26. M. Huang and G. M. Hieftje, *Spectrochim. Acta* **44B**, 739 (1989).

27. M. Huang, P. Y. Yang, P. S. Hanselman, C. A. Monnig and G. M. Hieftje, *Spectrochim. Acta* **45B**, 511 (1990).

28. J. S. Crain, F. G. Smith and R. S. Houk, *Spectrochim. Acta* **45B**, 249 (1990).

29. B. L. Caughlin and M. W. Blades, *Spectrochim. Acta* **40B**, 987, 1539 (1985).

30. J. W. Olesik and S.-J. Den, *Spectrochim. Acta* **45B**, 731 (1990).

31. J. F. Alder, R. M. Bombelka and G. F. Kirkbright, *Spectrochim. Acta* **35B**, 163 (1980).

32. S. Nowak, J. A. M. Ven Der Mullen, A. C. A. P. Van Lammeren and D. C. Schram, *Spectrochim. Acta* **44B**, 411 (1989).

33. S. E. Long and R. F. Browner, *Spectrochim. Acta* **41B**, 639 (1986).

34. J. A. Olivares and R. S. Houk, *Anal. Chem.* **58**, 20 (1986).

35. S. H. Tan and G. Horlick, *J. Anal. At. Spectrom.* **2**, 745 (1987).

36. J. J. Thompson and R. S. Houk, *Appl. Spectrosc.* **41**, 801 (1987).

37. H. Kawaguchi, T. Tanaka, T. Nakamura, M. Morishita and A. Mizuike, *Anal. Sci.* (Japan) **3**, 305 (1987).

38. D. Beauchemin, J. W. McLaren and S. S. Berman, *Spectrochim. Acta* **42B**, 467 (1987).

39. Y.-S. Kim, H. Kawaguchi, T. Tanaka and A. Mizuike, *Spectrochim. Acta*

45B, 333 (1990).

40. J. B. French, *Institute for Aerospace Studies*, University of Toronto, personal communication (1991).

Table I. Instrumentation and operating conditions

Component	Operation Condition
ICP generator:	
Type HFP-2500 with AMNPS-1 impedance matching network Loadcoil grounded at end nearest sampling orifice	Forward Power: 1.25 KW Frequency: 27.12 MHz
ICP Torch: Fassel-type [17] Precision Glass Co. Colorado	Ar Flow Rates: outer:15 l/MIN Auxiliary: 0.5 L/min
Ultrasonic Nebulizer: Model UNS-1 RF Plasma Products, Inc. Transducer mount, spray chamber and desolvation apparatus: Ames Laboratory design [18]	Sample uptake rate: 2.2 mL/min Transducer power supply: ~45 W Transducer frequency: 1.36 MHz Desolvation Temperatures: ~ 100 C Transducer and condenser cooled with ice water.
Ion Extraction Interface [33]:	Sampler orifice: 0.76 mm Skimmer orifice: 1.0 mm Sampling position: 10 mm from load coil, on center
Vacuum System: First stage: mechanical pump second stage: diffusion pump	First stage pressure: 800 mtorr measured by Convectron thermocouple gauge, Series 250 Granville-Phillips Second stage pressure: $1x10^{-4}$ measured by ionization gauges
Ion lens:	Stainless steel cylinder 13 mm diam. x 25 mm long located 45 mm from skimmer tip grounded

Table II. Measurement devices and operating conditions

Langmuir probe:	Tungsten curve Exposed section: radius (r_p) = 0.63 mm length (l^p) = 5 mm
Measurement device:	Model 177 multimeter Keithley Instruments, Inc.
Voltmeter	True Rms multimeter Model 8062A John Fluke Mfg. Co., Inc.
Power supply (in house)	-50v + 50v

Table III. T_e values for "dry" plasma

Probe distance (mm behind skimmer)	T_e(K) at indicated aerosol gas flow rates			
	0 L/min	0.6	1.0	1.4
5	2700 K	4500	8100	8900
10	3500	3000	8500	7800
15	2900	3400	9000	8100
20	3900	4500	8100	8500
30	2500	4900	8700	11000
40	3000	3400	8400	9000

Table IV. T_e values for "wet" plasma

Probe distance (mm behind skimmer)	T_e(K) at indicated aerosol gas flow rates			
	0 L/min	0.6	1.0	1.4
5	3700 K	8400?	10000	9400
10	2800	4900	9600	8500
15	2800	5400	9700	6800
20	2200	5600	11400	6400
30	2200	5500	8900	7700
40	3500	6600	9900	7000

Table V. Matrix effects on T_e

Probe Position[b]	Blank Solution	T_e(K) for indicated sample[a] Li (0.14 M)	Na (0.14 M)	Rb (0.14 M)	CO (1000 ppm)	U (1000 ppm)
5 mm	9800	9200	7400	8000	9600	12500
10 mm	8600	8100	7600	6800	8600	10000
20 mm	10000	6300	--	7600	11200	12200
30 mm	10000	6900	6000	--	11000	13000
40 mm	9500	7000	--	--	11000	13900

[a] Aerosol gas flow rate = 1.0 L/min

[b] Probe distance (mm) from the skimmer tip downstream of plasma flow

Table VI. Debye length values at various at probe locations

Type of Plasma	Probe Distance[a]	λ_D (mm) at indicated aerosol gas flow rates			
		0 L/min	0.6	1.0	1.4
Dry[b]	5	0.02	0.05	0.11	0.38
	20	0.07	0.08	0.23	0.64
	40	0.12	0.16	0.63	1.20
Wet[c]					
	5	0.02	0.04	0.4	0.7
	10	--	0.07	--	--
	20	0.05	0.09	1.2	1.4
	40	0.13	0.21	2.3	2.6

[a] Probe distance (mm) from the skimmer tip downstream of plasma flow
[b] Data from Table 2 and Fig. 4.
[c] Date from Table 3 and Fig. 5.

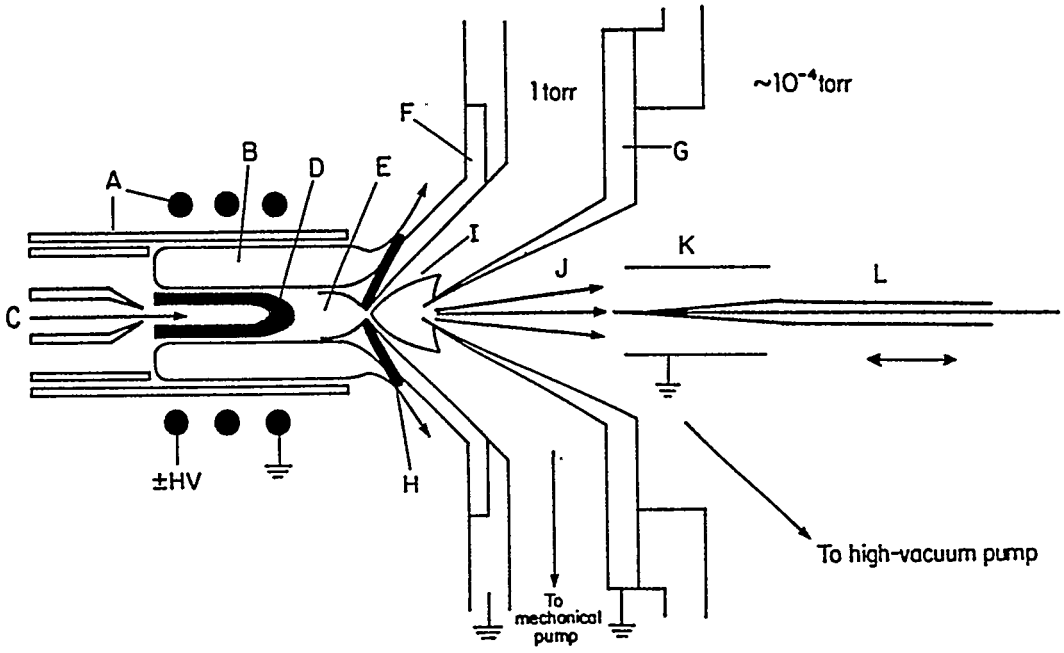

Fig. 1. Schematic diagram of ICP, ion extraction interface, and Langmuir probe (not to scale). See text and Table 1 for dimensions. A-E: ICP components and regions. F: sampling cone, G: skimmer cone, H: boundary layer outside sampling cone, I: supersonic jet, J: beam flowing through skimmer, K: cylindrical ion lens, L: Langmuir probe inside quartz sheath.

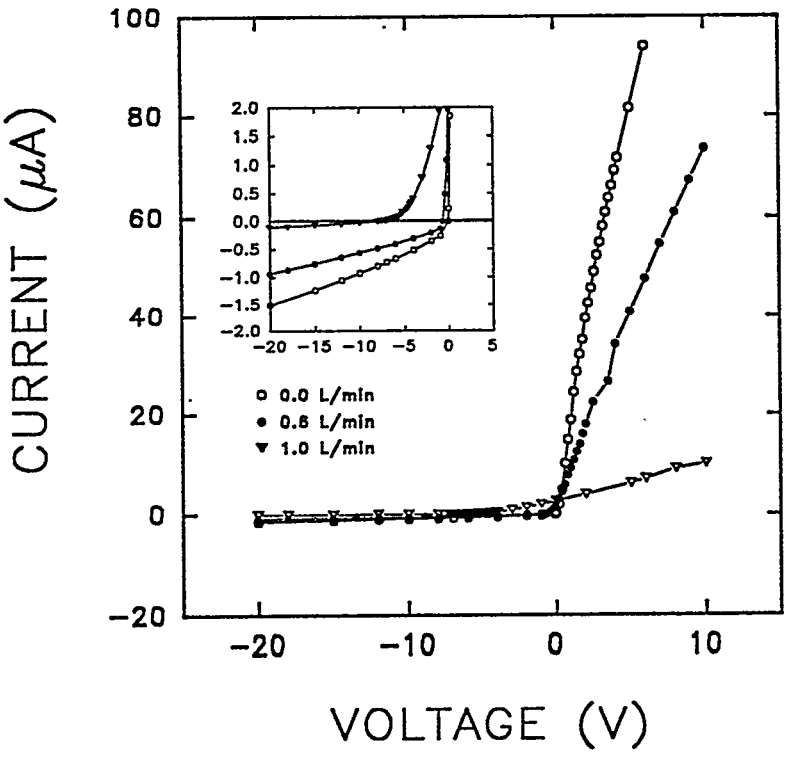

Fig. 2. Typical I-C curves for aerosol gas flow rates of 0 (○), 0.6 (●), and 1.0 L/min (▽). The probe position was 40 mm from the skimmer tip.

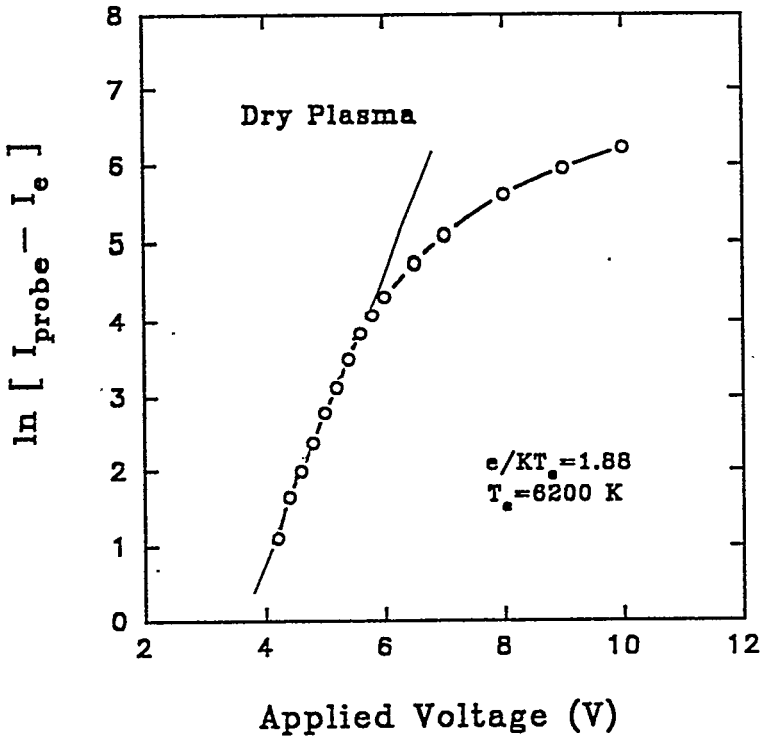

Fig. 3. Typical probe response curve showing linear region at low voltage and curvature at high voltage. The slope of the line show is $1/kT_e$.

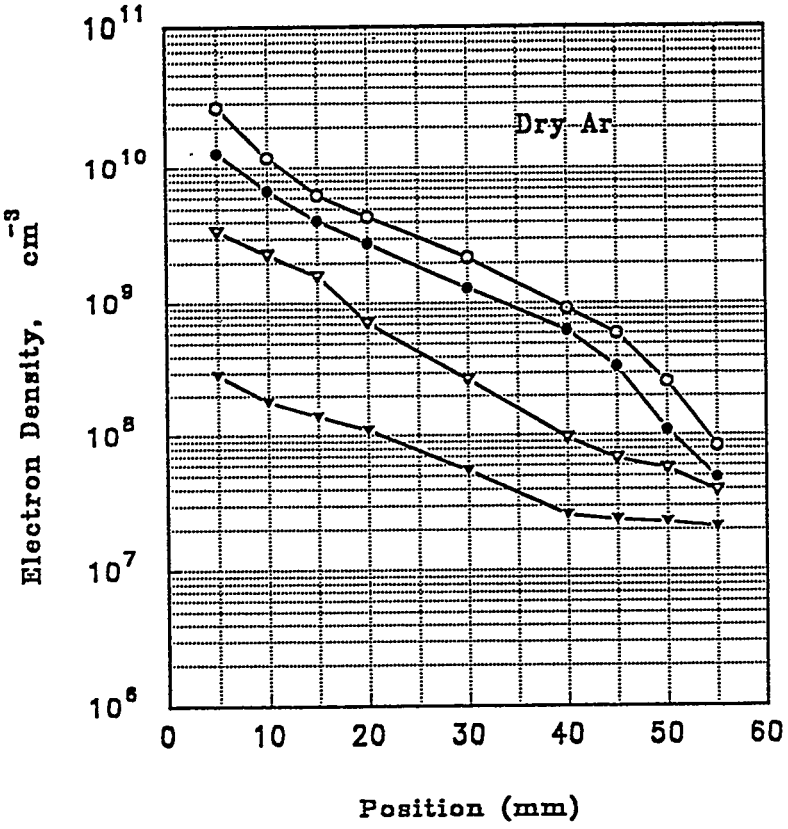

Fig. 4. Electron density at various probe positions for "dry" plasma at aerosol gas flow rates of 0 (○), 0.6 (●), 1.0 (▽) and 1.4 L/min (▾).

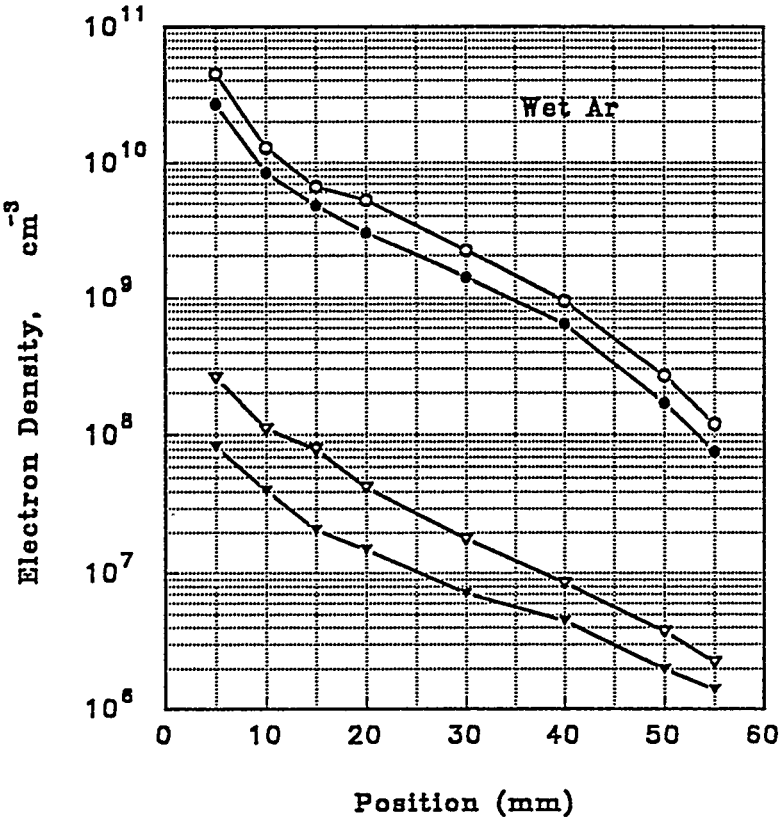

Fig. 5. Electron density at various probe positions for "wet" plasma at aerosol gas flow rates of 0 (○), 0.6 (●), 1.0 (▽) and 1.4 L/min (▾).

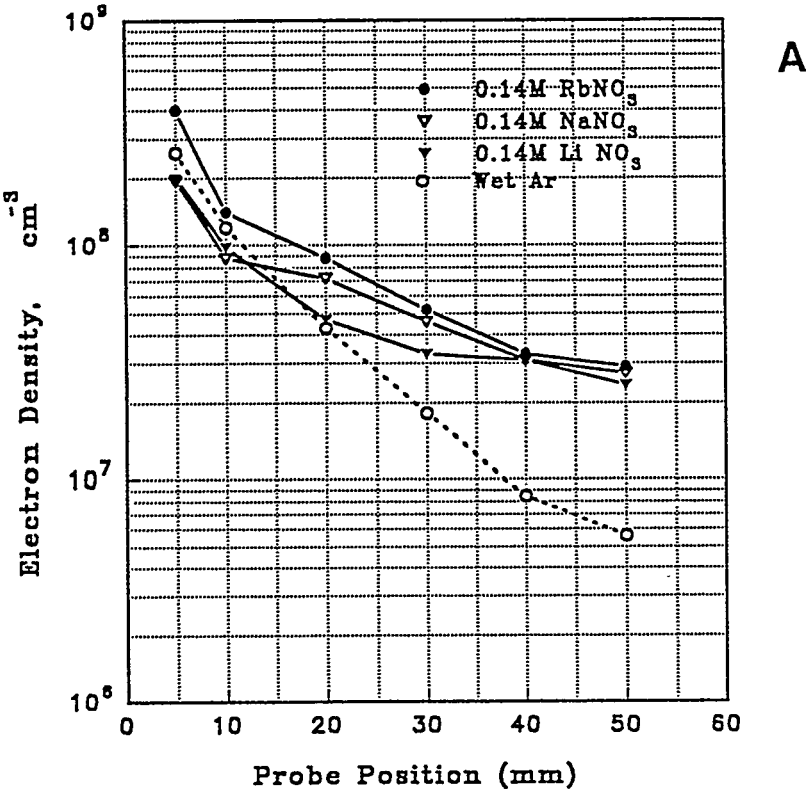

Fig. 6. Effect of matrix elements (0.14 M) on n_e: blank solution (○), $LiNO_3$ (▾), $NaNO_3$ (▽), and $RbNO_3$ (●). A: ion mass = 40 g/mole; B: ion mass = average of Ar and matrix element. The aerosol gas flow rate was 1.0 L/min.

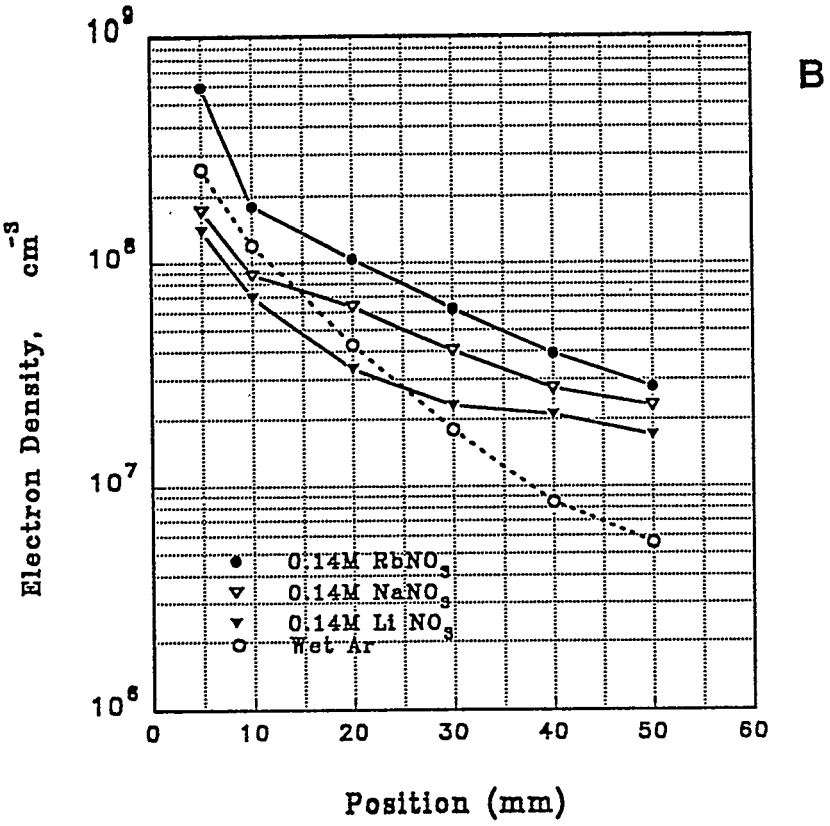

Fig. 6. (continued)

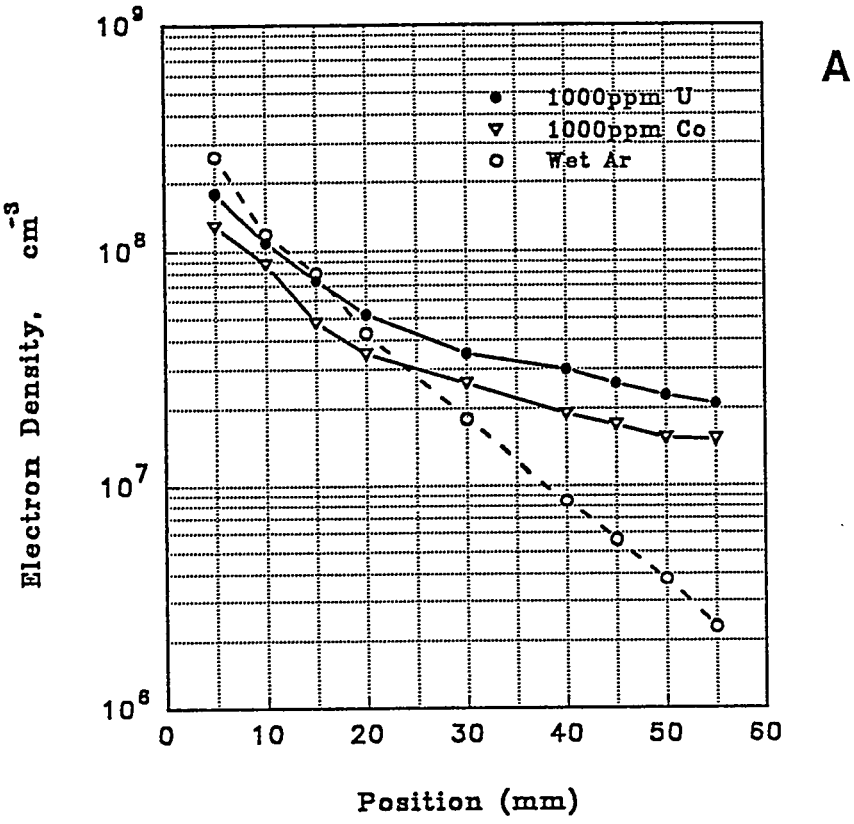

Fig. 7. Effect of matrix elements (1000 ppm) on n_e: blank solution (○), Co (▽), U (●). A: ion mass = 40 g/mole; B: ion mass = average of Ar and matrix element.

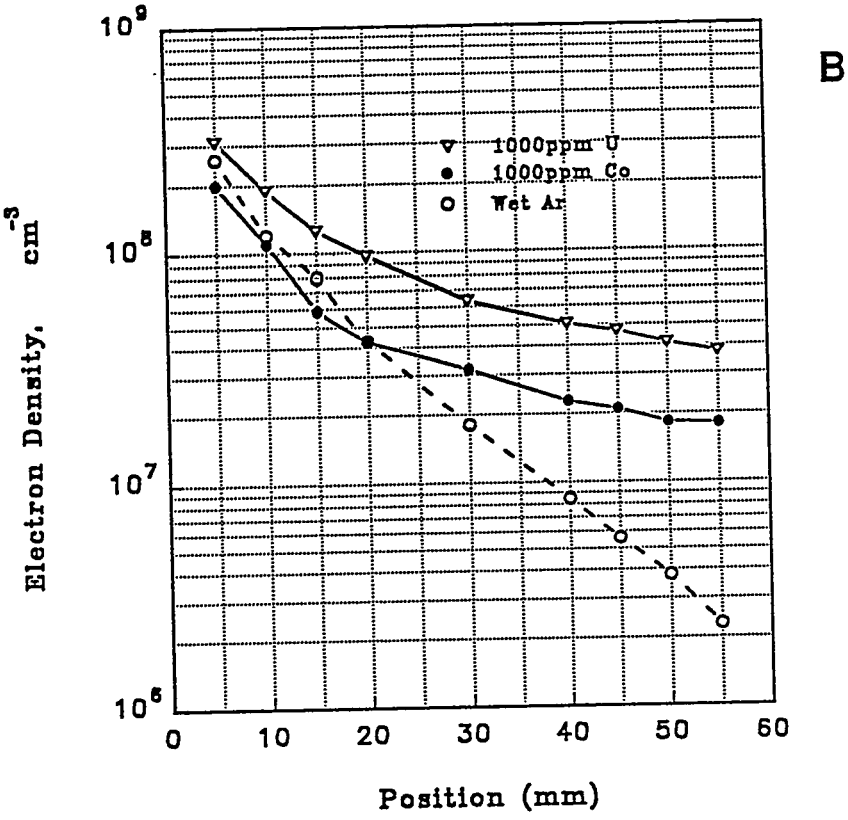

Fig. 7. (continued)

PAPER III

EXPERIMENTAL STUDIES OF THE PLASMA EXTRACTION AND ION BEAM FORMATION PROCESSES IN INDUCTIVELY COUPLED PLASMA-MASS SPECTROMETRY. I. SPATIALLY-RESOLVED DETERMINATION OF ELECTRON DENSITY AND ELECTRON TEMPERATURE

INTRODUCTION

The ion extraction process is obviously critical in ICP-MS. Several studies have characterized ion extraction from a fundamental viewpoint. These include studies of gas dynamics [1,2] emission, fluorescence and Langmuir probe measurements in the supersonic jet [3-10], the introduction of additional gases into the jet to evaluate its ionization capabilities [11], characterization of the dissociation of metal oxide ions [12-14], studies of the effects of the sizes of the sampler and skimmer apertures and the separation between them [15,16], ion kinetic energy measurements [13,17-19], and modeling and measurement of space charge effects [20-22]. A reasonable understanding of many of the main features of ion extraction has emerged from this work and from the consideration of the known properties of other supersonic expansions [23-25], including some jets extracted from plasmas similar to the analytical ICP [26].

The properties of free electrons are among the more important of these fundamental parameters. Previous studies have illustrated the feasibility of the Langmuir probe method for measuring electron temperature (T_e) and electron density (n_e) in a supersonic jet without the skimmer [8] and in the beam behind the skimmer [10]. The present work describes more complete T_e and n_e measurements with axial spatial resolution from near the sampler as far back as the entrance to the ion lens. Spatial resolution inside the supersonic jet is obtained by thrusting a small Langmuir

probe axially through the skimmer aperture, which is one novel aspect of the present work. Disturbances or perturbations in the supersonic jet due to the presence of the skimmer can be studied by this procedure.

The measured values of T_e and n_e are used to calculate Debye length (λ_D) at various spots in the extracted beam. These λ_D values are then used to evaluate the general question of charge neutrality in the extracted beam. Finally, the implications of these observations to ion sampling for ICP-MS are described.

EXPERIMENTAL

Apparatus

A diagram of the plasma, sampler, skimmer, and probe is shown in Fig. 1. Important components and operating conditions are identified in Table 1. The apparatus has been described previously [10]; it consists of a horizontal ICP and a conventional sampler and skimmer mounted on a two-stage vacuum chamber. The Langmuir probe was supported on a linear motion feedthrough mounted on the rear flange of the second stage.

As shown in Fig. 1, the exposed probe tip was solid tungsten and was 0.12 mm diam. x 2 mm long. Thus, the axial spatial resolution would be expected to be roughly the probe length, or 2 mm. Behind the exposed tip, the remainder of the probe was insulated by a drawn-out quartz pipet tip nested inside an alumina sleeve. The outside diameter of the pipet tip was approximately 0.3 mm, so it did not block the 1 mm hole through the skimmer appreciably. This probe assembly was mounted on a plastic connector and a stainless steel stand-off that was fastened to the linear motion feedthrough. Electrical signals from the probe ran through a connecting wire to an electrical feedthrough on the side wall of the second stage of the vacuum system.

Figure 1 also shows the coordinate system used to describe the probe position. The coordinate Z refers to distance from the sampler orifice to the middle of the

probe, i.e., 1 mm from the tip. The skimmer tip was 10 mm behind the sampler. This distance is roughly 2/3 of the way to the onset of the Mach disk [1,2] and corresponds closely to the sampler - skimmer distance generally used in most ICP-MS devices [1].

The probe could be inserted through the skimmer aperture into the supersonic jet between the sampler and skimmer. Thus, the shock waves formed on the outer wall of the skimmer, not on the probe. The increase in gas temperature and gas density behind such shock waves would probably melt the long, thin probe or cause it to become pitted or deteriorate in other ways. Instead, the heat was dissipated on the skimmer wall, so the probe stayed relatively cool. The theory used to interpret the current-voltage curves required a probe whose length was at least 30 times its radius [31-36], so a very thin probe was necessary to achieve the desired spatial resolution of $\sim$ 2 mm. This probe was not visibly damaged after 20 hours of use. In contrast, a single, thick (0.76 mm diam.) probe exposed to the shock waves did become pitted and corroded during the previous experiments [7,8]. Moving the probe axially through or behind the skimmer also allowed measurement of the properties of both the supersonic expansion and the beam leaving the skimmer for the same plasma during the same experiment.

The alignment of the probe was checked carefully several times with the sampler removed. In particular, care was taken to ensure that the probe tip was precisely in the center of the skimmer orifice at $Z = 10$ mm.

Both sampler and skimmer were grounded in these experiments. A cylindrical ion lens was mounted behind the skimmer. This lens was also grounded.

Operating Procedures

Standard operating conditions are given in Table 1. As shown by HORLICK and co-workers, aerosol gas flow rate exerts a strong influence on ion signal, stability and matrix effects in ICP-MS [37]. Therefore, aerosol gas flow rate was varied over a range of values found useful at the plasma power (1.25 kW) and sampling position (10 mm from load coil, on center) that would be employed if this device was used as a mass spectrometer.

The water loading was varied as well. For a "dry" plasma, the argon flow was injected directly into the injector tube of the torch; i.e., the usual nebulizer and spray chamber were bypassed. For a "wet" plasma, an ultrasonic nebulizer with desolvation was employed. Water droplets did not survive the desolvation step, so the water load reaching the plasma consisted solely of water vapor from the exit of the condenser. This water load was estimated to be either 2.9 or 4.8 mg/min at aerosol gas flow rates of 0.6 or 1.0 L/min, respectively. These values were calculated simply from the vapor pressure of water at 0 °C (4.58 torr) and the aerosol gas flow rate. The plasma had to be shut off to convert between "dry" and "wet" situations. No analyte or matrix elements were present in the sample in the present work.

Determination of T_e from I-V Curves

Several typical current - voltage (I-V) curves are shown for various probe positions in Figs. 2 and 3. These curves can be separated into the ion current saturation region at high negative probe voltages (i.e., the flat region at the left of each frame) and the electron retarding region where the current begins to rise as probe voltage becomes more positive (i.e., the curved region at the right). T_e is measured from the electron retarding part of the I - V curve, as described previously [8-10]. Basically, the current due to electrons is evaluated as a function of probe voltage. This involves subtracting the current contribution from ions (I_i) from the total measured current (I_p) at each voltage value. A plot of ln (I_p- I_i) versus probe voltage should then be a straight line with slope equal to e/kT_e where e=electron charge and k=Boltzmann constant.

Several typical plots are shown in Fig. 4 (with the probe in the jet) and Fig. 5 (with the probe behind the skimmer). Straight lines are drawn through the linear sections at low applied voltage, the slopes of which yield T_e. The particular curve shown in Fig. 5a had the narrowest linear region for any of the probe measurements. Most curves measured behind the skimmer had much longer linear regions, like that in Fig. 5b. This method of determining T_e should be valid under the temperature and flow conditions prevalent in either the supersonic jet or in the beam leaving the skimmer [8,10].

Determination of V_f and n_e

These parameters are evaluated from the same I-V curves used for T_e. V_f is simply the probe voltage at which the net current is zero, as shown in Figs. 2 and 3. Electron density is determined by an involved procedure similar to that described previously [10], with some important modifications. The following process is carried out for each I-V curve at each axial position [35,36]:

1. Evaluate T_e and V_f.
2. Measure the saturated ion current (I_i) at an applied voltage equal to (V_f - $10kT_e$). Fortunately, the I-V curve slopes only very gradually in the ion current saturation region. Thus, a small deviation between V_f and the true plasma potential (a very difficult parameter to evaluate [38]) does not cause much error in I_i.
3. Calculate r_p/λ_D where r_p = probe radius and λ_D (cm) = $6.9\ [T_e(K)/n_e(cm^{-3})]^{1/2}$. In general, n_e decreases and λ_D increases as the probe is retracted farther behind the sampler. The dependence of n_e on axial position z is estimated to be the same as that for the neutral gas density n [1,2]:

$$n(z) = 0.161\ n(z=0)\ (D_o/z)^2 \qquad (1)$$

$$n_e(z) = 0.161\ n_e(z=0)\ (D_o/z)^2 \qquad (2)$$

Modest deviations from these assumptions do not influence the eventual measured values of n_e greatly.

4. Estimate Knudsen number (Kn). Knudsen number is basically the ratio of

mean free path (λ) to the size of an object immersed in the flow. For this calculation

$$Kn = \lambda/r_p = \lambda/(\sqrt{2}\ \pi\ s^2\ n\ r_p) \qquad (3)$$

where s^2 = collision cross section for Ar atoms = 4.1×10^{-15} cm^2 [1,2]. Because the mean free path and flow characteristics of the expansion change with axial position, Kn also must be calculated separately at each position. The neutral density is assumed to drop proportionately to $1/z^2$, as described above.

5. For the appropriate value of Kn, read the corresponding value of a_i from the solid line in Fig. 6, which is derived from papers by KIRCHOFF et al. [33] and LAFRAMBOISE [36]. This figure shows correction factors for n_e measurements by Langmuir probes for various values of Kn. The dotted lines represent the curves given by KIRCHOFF et al.[33] except for the curve at Kn = 100, which is from LAFRAMBOISE [36]. The open circles are additional values of a_i that we calculated for Kn values intermediate between those shown. We used the a_i values shown in the solid line.

The electron density is high near the sampler, so λ_D is small and the ratio r_p/λ_D is large ($\sim$50). At these axial positions, the a_i values on the right side of the solid line in Fig. 6 are used. As the probe is moved downstream, r_p/λ_D decreases, so the value of a_i increases. Note that a_i is approximately constant at 4.4 when $r_p/\lambda_D < 3$, which is the situation at low n_e, i.e., well

downstream in the beam [10]. Here the probe is in the orbital-motion-limited regime [10,32].

6. Calculate n_e from the following equation:

$$n_e = \frac{I_i}{eA_p\alpha_i} \quad (2\pi m_i/kT_e)^{1/2} \qquad (4)$$

where A_p = probe area (excluding the end) and m_i = ion mass. As usual, m_i is not known exactly, because there is no mass spectrometer to identify the ions. The calculation assumes m_i equals the mass of argon (40 g/mole, 6.67 x 10^{-23} g/atom), which is certainly reasonable for a dry plasma. Even if all the ions from a wet plasma are O^+ (m_i = 16), which is unlikely, n_e would be lower by [1 - $(16/40)^{1/2}$] = 0.37. In other words, the potential error in n_e from the doubt about the ion mass is no greater than 37% and probably is substantially less.

RESULTS AND DISCUSSION

Profiles of Electron Density in Supersonic Jet

The dependence of neutral gas density (primarily argon in this case) on axial position in an ideal supersonic expansion is well-known and is given by Eqn. 1. Unlike most gas sources for supersonic expansions, the ICP contains a small fraction of charged particles. Since the original gas and sample is neutral, ionization creates equal numbers of positive and negative charges. Thus, the ICP is a quasineutral plasma, at least over distances long compared to the Debye length. DOUGLAS and FRENCH contend that the Debye length inside the sampler is small, so the plasma should flow through the sampler as a quasineutral plasma without significant separation of positive charges from negative ones [1,2]. Thus, electron density in the supersonic jet should also drop proportionally to $1/z^2$ as z increases, i.e., as the probe moves farther downstream.

To test this hypothesis, log-log plots of the measured n_e as a function of $1/z^2$ are provided in Figs. 7 and 8. For either a dry or wet plasma, these plots can be divided into two general regions. Near the sampler, i.e., at small values of z or large values of $1/z^2$, the plots are linear with slopes that are close to unity. Thus, the electron density in the early phases of the supersonic expansion does decay proportionally to $1/z^2$, just as expected if the supersonic jet is still a quasineutral plasma.

Ideally, the electron density should continue to fall in the same fashion near the skimmer tip. However, the measured values of electron density first rise above the expected line and then fall below it. This change of behavior is shown more clearly in the semilog plots in Figs. 9 and 10. These plots typify the behavior seen for the various aerosol gas flow rates tested. The solid curve represents a $1/z^2$ fall in n_e, fit through only the leftmost measured points. Beginning at z = 6 - 7 mm, the measured electron density rises above that predicted. Since the probe tip is 2 mm long, at z = 7 mm, the base of the probe tip is 8 mm behind the sampler, or 2 mm in front of the skimmer. Thus, the phenomenon that causes the rise in n_e above the predicted curve in Figs. 9 and 10 begins between 2 and 4 mm in front of the skimmer. At the skimmer tip (z = 10 mm), the measured electron density is below that predicted.

In previous work with a much thicker Langmuir probe (0.76 mm diam.) at z = 4 mm, the measured electron densities were $\sim 2 \times 10^{13}$ cm^{-3}, in good agreement with those reported in Figs. 9 and 10 [8]. Apparently, probe radius does not critically affect the measured n_e values, which is reassuring.

Electron Density at Sampler Tip

The curves in Figs. 9 and 10 can be extrapolated back to z=0 to estimate the electron density inside the sampling orifice. These extrapolated values are given in Tables 2 and 3, along with various literature values for n_e in the plasma. These

literature values were measured optically by either the Stark broadening method using the H_β or Ar(I) emission lines or by Thomson scattering. All but one of the literature values were measured in a regular ICP without a sampling orifice present.

Examination of these tables leads to several interesting observations. The electron densities estimated at the sampler are in the range 7×10^{14} to 9×10^{15} cm^{-3}, which is reasonable. The variation of n_e with changes in aerosol gas flow rate and water loading are also reasonable. In only one case was n_e measured optically in the gas flowing into the sampler, for a wet plasma at 1.0 L min^{-1}. Here the literature value (8×10^{14} cm^{-3}) agrees closely with the value extrapolated from n_e measurements behind the sampler (7.3×10^{14} cm^{-3}). This particular optical measurement was done here in our laboratory [41], and the plasma and sampler used were very similar to those employed for the present work.

Because the flow into the sampler alters the gas flow patterns in the ICP, the literature values for n_e measured for the "regular" ICP may not be strictly comparable to those determined in the present work. Nevertheless, the overall magnitude of the electron density values from the "regular" ICP agree reasonably well with those estimated from inside the jet, even though the work was done in different laboratories using different conditions (e.g., a MAK torch with much lower gas flow rates was used for many of the Thomson scattering results [39]).

Tables 2 and 3 therefore show that n_e at the sampler is similar in magnitude to and is clearly not vastly greater or lower than that in the ICP. This conclusion agrees

with that described by DOUGLAS and FRENCH [1,2]. It does not support the hypothesis of CHAMBERS et al. [9] that the plasma undergoes substantial charge separation as it flows through the sampler.

Electron Density at Skimmer Tip

Electron densities measured inside the skimmer tip are given in Tables 4 and 5. The measured n_e values are below those expected from the $1/z^2$ fall of n_e in the supersonic jet. The ratio n_e(measured)/n_e(expected) decreases as aerosol gas flow rate increases. Generally, this ratio also decreases when water is added to the plasma at constant aerosol gas flow rate. The conditions that cause the ratio to decrease also cause the plasma potential to increase [30], which is thought to intensify the secondary discharge between the plasma and the sampler [7,8].

These deviations of n_e from ideal behavior at and in front of the skimmer probably indicate the presence of some type of disturbance in the supersonic beam. With the probe removed, the Knudsen number at the skimmer is defined as l/D_S. The skimmer diameter (D_S) must be used here because the skimmer is now the obstruction to the flow. At the skimmer tip, Kn is approximately 0.2, in good agreement with DOUGLAS and FRENCH [1], who estimated Kn to be ~ 0.3 at the skimmer tip. The literature concerning supersonic expansions indicates that disturbances are to be expected when Kn at the skimmer is ≤ 1. Such disturbances include a) a thin shock in front of the skimmer, and/or b) perturbation of the straight

line beam flow by collisions of the beam with atoms reflected from the skimmer wall [24,25]. These problems don't change the total flow through the skimmer greatly, so the pressure behind the skimmer is not a sensitive indication of their occurrence. To our knowledge, these data represent the first indications of such disturbances in the sampling systems used for ICP-MS.

CHAMBERS et al. suggest that the plasma flowing through either the sampler or skimmer is not quasineutral because of formation of an extended sheath around these metal objects [9]. Generally, such sheaths are believed to contain an excess of positive ions compared to electrons, because electrons are so much more mobile that they flow to the conducting metal surface much more rapidly than the ions [45,46]. A thick positive ion sheath around the inside edge of the skimmer could conceivably account for the low values of n_e measured there. However, other evidence to be discussed below does not support CHAMBERS' proposed deviations from charge neutrality over large distances in the jet or near the skimmer, so this explanation is not considered likely.

Profiles of Electron Density Behind Skimmer

Electron densities behind the skimmer are given in Figs. 11 and 12. This time the horizontal axis is $1/(z')^2$, where $z' = 0$ at the skimmer tip. In most cases, n_e behind the skimmer is proportional to $1/(z')^2$. The exceptions are the two plots obtained from the wet plasma at high aerosol gas flow rates in Fig. 12. The

curvature in these log-log plots indicates that there is no simple relationship between n_e and z' in these cases, although n_e does continue to decrease as $1/(z')^2$ decreases, i.e., as z' increases. Again, plasma conditions that result in a higher plasma potential and stronger secondary discharge result in non-ideal behavior, this time in the beam leaving the skimmer. The trends in n_e with aerosol gas flow rate are reasonable, as is the agreement with n_e values measured previously [10].

Electron Density Throughout the Extracted Beam

The results described above are combined in Figs. 13 and 14. A solid line fitted to one particular set of n_e values with no aerosol gas flow from 2 mm to about 6 mm is also shown for comparison. For an ideal skimmer, the electron density behind the skimmer would continue to drop with the same dependence, as indicated by the dotted line. Instead, the measured values of n_e behind the skimmer are much lower than those expected. If the beam passes through the skimmer as a quasineutral plasma, then the ion densities behind the skimmer are also much lower than expected. Suppose the entrance to an ion lens is located 40 mm behind the sampler. The ion density there is some 10^3 to 10^4 less than if the skimmer behaved ideally! Quadrupole-based ICP-MS devices measure roughly one analyte ion for every 10^4 to 10^6 analyte ions through the skimmer [47], depending on the vintage of the device. The low n_e values behind the skimmer represent one possible contribution to ion loss and overall inefficiency in ion extraction in ICP-MS.

These measurements also show that n_e first rises as the beam approaches the skimmer, then n_e becomes substantially less than expected at and behind the skimmer. The solid curves beginning at z = 10 mm in Figs. 13 and 14 represent a $1/(z')^2$ drop in n_e, starting with the n_e value measured at the skimmer. In most cases, the measured n_e values fall off with roughly the same dependence as that shown for the solid curve. Thus, the extraction system behaves as if there is a new expansion source at the skimmer. The electron density then decays proportionately to $1/(z')^2$ behind the skimmer (Figs. 11 and 12), except for the special case of a wet plasma at high aerosol gas flow rate. Thus, the discontinuity in the curves in Figs. 13 and 14 at z=10 mm is also consistent with some disturbance that starts just in front of the skimmer tip.

A diagram suggesting the difference between this extraction system and an ideal one is given in Fig. 15. In the ideal case (Fig. 15a) the beam expands from the sampler directly through the skimmer, and n_e decays proportionally to $1/z^2$ through both sampler and skimmer. The presence of the skimmer tip has little effect on the beam properties other than to provide differential pumping and a lower background pressure, which prevents formation of a Mach disk. However, our measurements suggest that the beam first passes through a disturbance in front of the skimmer, depicted schematically by the dotted lines in Fig. 15b. After this disturbance, the beam diverges more extensively than in the ideal case, so n_e behind the skimmer is lower than expected, at least for the skimmer used in the present work.

The apparent presence of a disturbance in front of the skimmer is moderately surprising in view of two earlier photographic studies of supersonic beam formation. GRAY shows visual emission from the outside of the skimmer region in an ICP-MS device. The sampler and skimmer diameters and spacing are similar to those used in the present work. There is no visual evidence of a shock wave in front of the skimmer tip unless the pumping speed is reduced to the point where the stagnation pressure behind the sampler is 5 - 10 torr. At high stagnation pressure, the whole supersonic expansion contracts, and the Mach disk forms in front of the skimmer [6]. McMICHAEL and FRENCH use an electron beam to excite luminescence from a free jet. They do not see a detached shock in front of the skimmer at a Knudsen number of ~ 0.2, which is similar to the Knudsen number at the skimmer in the present work [48].

For the wet plasma (Fig. 14), the n_e values behind the skimmer for the curves obtained at high aerosol gas flow rate are substantially below the others. If the early phases of this beam are quasineutral, then the ion densities here are also much lower than expected when the plasma potential is substantial. Several laboratories have observed that plasma operating conditions that promote a high plasma potential and strong secondary discharge lead to poor ion transmission [45,49]. For example, several workers have found that reducing water loading can improve analyte sensitivity substantially with an ICP-MS device with an unbalanced load coil such as the one used in the present work [50,51]. The general dearth of ions in ICP-MS

devices with a substantial plasma potential is consistent with the lower electron densities seen in the present work for the wet plasma at high aerosol gas flow rate.

Estimated Error in n_e

The random error in n_e was estimated from Equation (4) via propagation of error. The uncertainty in T_e was estimated to be ± 100 K, and the standard deviation of I_i was calculated from the I-V curves. Typical uncertainties are shown in Table 6. In general, the relative standard deviation in n_e was estimated to be $\sim 2\%$ near the sampler, 3% near the skimmer, and up to 7% behind the skimmer. These uncertainties are small compared to the changes in n_e with axial position. Of course, there may be systematic errors in any of these n_e values, either from the uncertainty in ion mass (see Sect. 2.4) or to other problems common in Langmuir probe measurements [8-10,34-36], but we are confident that our results faithfully represent at least the trend of n_e with axial position.

Electron Temperatures

Measured values of T_e are shown in Figs. 16 and 17. First, consider the behavior of T_e in the supersonic jet, i.e., between z=0 and z=10 mm. Essentially, T_e increases with aerosol gas flow rate and is higher for a wet plasma than for a dry one. The magnitude of the T_e values is generally 4000 to 12000 K. A T_e range of 4000 - 8000 K is reasonable for the ICP [39,44]. For the wet plasma at the highest

aerosol gas flow rate, the measured T_e is much higher (16,000 to 18,000 K). These elevated T_e values are again attributed to the secondary discharge, which is thought to increase the velocities and velocity spread of the electrons to artificially high values as they are extracted [8].

There is no consistent trend of T_e with axial position in the jet. Sometimes, T_e drops smoothly by $\sim$2000 K as the beam nears the skimmer. In other cases, there is a $\sim$1000 K increase in T_e near the skimmer, which could be caused by the same disturbance that affects n_e, as discussed above.

In general, the T_e results agree with the expected behavior of T_e in the jet described by DOUGLAS and FRENCH [1,2] and FRASER et al. [26] and with our previous probe measurements [8] Under plasma conditions that yield a low plasma potential and secondary discharge, the electrons may cool somewhat in the jet, but they still remain at temperatures above 4000 K, which is much hotter than the stagnation temperature of the neutrals (expected to be $\sim$150 K) [1,2]. Plasma conditions that cause a high plasma potential and secondary discharge elevate T_e drastically to values much higher than would be expected from the ICP alone. Thus, T_e changes with water loading and aerosol gas flow rate in the opposite direction expected from the behavior of T_e as these parameters are changed in the ICP alone [39,44]. Electron temperature is apparently much more sensitive to plasma potential than n_e, as if a mild secondary discharge can readily affect the velocities of existing free electrons but does not create many new electrons by further ionization.

Behind the skimmer ($z > 10$ mm), a surprising result is obtained. T_e drops drastically to values as low as 2000 K at $z = 20$ mm. T_e then increases again at $z > 30$ mm. A similar, though less pronounced drop in T_e behind the skimmer was seen in the preliminary work [8] One possible explanation for this trend been suggested by TANNER [51]. McDANIEL describes a phenomenon called diffusional cooling [52]. In a beam containing electrons, the faster ones tend to diffuse farther from the center and are progressively depleted from the central axis as the beam moves farther away from the source. A smaller spread of velocities corresponds to a lower numerical value of T_e. Thus, removal of some of the faster electrons would diminish the measured T_e value in the center as the beam travels further downstream, which explains the drop in T_e seen between $z = 8$ and $z = 20$ mm in Figs. 16 and 17. However, this rationale does not account for the subsequent rise in T_e observed after $z > 25$ mm, which remains unexplained. Perhaps the rise in T_e after $z > 25$ mm (Figs. 16 and 17) represents the breakdown of quasineutrality in the extracted beam. As discussed in the next section, the Debye length becomes large (~ 1 mm) here, so perhaps external fields (such as the floating potential) can accelerate and re-heat electrons when the beam gets well behind the skimmer.

Debye Length and Charge Neutrality

The measured values of T_e and n_e allow estimation of the Debye length (λ_D) at various points in the extraction process. Basically, λ_D is $\sim 10^{-4}$ mm inside the

sampler and $\sim 10^{-2}$ mm inside the skimmer. Both these values are much smaller than the diameter of the holes through the sampler or skimmer, which are typically 1 mm. An electric sheath forms inside the inner edges of the sampler and skimmer orifices. Within such a sheath, the plasma is not quasineutral, as charge carriers of different sign reach the probe at different rates. These sheaths should be no more than a few Debye lengths thick [1,2,22,46] so the bulk of the flow should remain quasineutral as it passes through either the sampler or skimmer.

As the beam leaves the skimmer and nears the ion lens, n_e decays to the point where λ_D increases to $\sim$ 2 mm. Here the Debye length is significant compared to the size of the beam and the dimensions of the ion lens, and the extracted beam is no longer quasineutral.

This picture of the ion extraction process agrees closely with that described by DOUGLAS and FRENCH [1,2] and TANNER [22]. It does not support the contention of CHAMBERS et al. that substantial charge separation takes place in the supersonic jet [9]. This latter point is also pertinent to V_f measurements, which are discussed in more detail in a separate paper [53].

The ratio r_p/λ_D must be > 0.1 throughout the beam for the probe model used to calculate n_e to remain valid. Generally $r_p = 0.12$ mm $>> \lambda_D$, except for the largest λ_D values far downstream in the beam near the ion lens. Even here, the largest value of λ_D is $\sim$ 2 mm and $r_p/\lambda_D \sim 0.03$, which is close enough to 0.1 for the conditions of the probe model to be just satisfied.

Estimate of Sheath Thickness

AXFORD and HAYHURST have recently discussed electrical sheaths in great detail [46]. They sampled an atmospheric pressure flame seeded with Cs ($n_e \sim 10^7$ to 10^{10} cm^{-3}) through a relatively small sampler (80 to 200 μm diam.). The sheath thickness was found to be substantial compared to the sampler diameter, particularly when the flame was operated at low n_e, i.e., no Cs dopant was added.

Application of the concepts from AXFORD and HAYHURST'S paper to the extraction system in ICP-MS is instructive. The approach can be visualized by referring to the cross-sectional diagram in Fig. 18. Basically, the edge of the sampler is considered analogous to a spherical Langmuir probe of radius r, as indicated by the solid circle inside the lower lip of the sampler in Fig. 18. For the samplers used in ICP-MS, a typical value of r is $\sim$0.05 mm. We extend the approach inside the vacuum system to the tip of the skimmer, which is also considered to be a Langmuir probe. The various regimes for probe operation described by SMY [54] are then invoked, much as we did during Langmuir probe measurements in the ICP [55]. This step involves estimation of the electric Reynolds number (R_e) and the dimensionless quantities a (not to be confused with a_i in Eqn. 4) and c. These parameters are defined and typical values are given for them in Table 7. Since the mobility (μ_i) of the ions can only be estimated, a range of R_e values are employed. The crucial quantities are the products $R_e a^2 \chi^2$ and $R_e a^2$.

Table 7 shows that $R_e a^2 \chi^2 << 1$ at the sampler for any reasonable R_e values.

The sampler behaves like a Langmuir probe in the diffusion-convection regime, in which the sheath is much thinner than the boundary layer around the inner edge of the sampler [46,55,56]. This boundary layer is, in turn, thin compared to the hole diameter, because the flow through the hole is of a continuum nature. Thus, a relatively thin sheath forms along the inner edge of the sampler.

The skimmer tip is also analogous to a Langmuir probe but in a different probe regime. Here l_D is longer and the flow velocity (V_f) is substantially higher (see Table 7), assuming the beam still passes through the skimmer under supersonic flow. The skimmer is usually more sharply pointed than the sampler, hence r = 0.02 mm.

At the skimmer $R_e a^2 \chi^2 > 1$ and $R_e a^2 \approx 1$ to 10. These conditions are borderline for the sheath-convection regime, in which the sheath thickness is comparable to boundary layer thickness. The sheath thickness (Y_s) now is [46]

$$Y_s = (r_s/R_e^{1/2}) (R_e a^2 \chi^2)^{1/4} \qquad (5)$$

For the conditions given in Table 7, we estimate Y_s to be 0.03 to 0.04 mm, i.e., several Debye lengths, just as proposed by DOUGLAS and FRENCH [1,2]. Thus, AXFORD and HAYHURST's treatment yields precisely the same practical result as DOUGLAS and FRENCH, that the sheaths around the inner edges of the sampler and skimmer are much thinner than the corresponding hole diameters.

CONCLUSION

The main findings from the present work can be summarized as follows:

1. Electron densities estimated inside the sampling orifice are similar to those expected outside in the ICP. Simultaneous optical measurements of n_e just in front of the sampler and Langmuir probe measurements in the jet are necessary to further validate this point.

2. The measured values of T_e, n_e and λ_D, as well as the observation that n_e generally falls off proportionally to $1/z^2$, indicate that the plasma remains quasineutral as it passes through both the sampler and skimmer.

3. The electrons stay hot ($T_e > 4000$ K) in the supersonic jet. In some cases, T_e then drops as the beam passes through the skimmer, for reasons that may be related to diffusional cooling seen by other investigators in beams containing electrons [53].

4. A disturbance in front of the skimmer causes the electron density there to be substantially higher than expected. The electron density in the beam behind the skimmer then drops as if the beam comes from a new expansion source at the skimmer tip.

5. Behind the skimmer, the electron density in the beam center falls off with axial position much more rapidly than expected if the skimmer behaved ideally. Near the ion lens, the electron density is less than expected by a factor of 10^3 to 10^4.

Assuming the ion density also decays in a similar manner, this phenomenon could be a major source of the overall inefficiency of ion transmission in ICP-MS. With typical quadrupole instruments, only 1 ion reaches the detector for every 10^4 to 10^6 ions through the skimmer [47].

6. Use of plasma operating conditions that induce a high plasma potential cause various deviations from expected behavior in the extracted beam.

Some additional interesting studies are suggested by these results. Is the disturbance in front of the skimmer a general phenomenon seen in other ICP-MS devices or is the disturbance unique to the skimmer geometry and gas flows used in this study? Optical measurements [3-5] of the basic properties of this disturbance at various skimmer cone angles and skimming positions should prove interesting in this regard. If indeed the ion density behind the skimmer is several orders of magnitude below that expected for an ideal quasineutral beam, what happened to the lost ions? We have been attempting to deposit ions behind the skimmer onto spatially separated solid targets to address this issue [56] as has FARNSWORTH's group [57]. Can anything be done to mitigate the extensive loss of ions in the beam behind the skimmer? How are the beam properties affected by highly concentrated matrix elements and by the application of various voltages to the ion lenses? Clearly, important questions remain in our basic understanding of the ion extraction process in ICP-MS.

LITERATURE CITED

1. D. J. Douglas and J. B. French, *Anal. Atom. Spectrom.* **3**, 743 (1988).
2. D. J. Douglas, *"Fundamental Aspects of ICP-MS"*, ICPs in Analytical Atomic Spectrometry, eds. A. Montaser and D. Golightly, 2nd Edn., VCH, New York 1991.
3. H. B. Lim, R. S. Houk , M. C. Edelson, and K. P. Carney, *J. Anal. Atom. Spectrom.*, **4**. 365 (1989).
4. H. Kawaguchi, K. Asada, and A. Mizuike, *Mikrochim. Acta* **3**, 143 (1988).
5. R. S. Houk and H. B. Lim, *Anal. Chem.* **58**, 3244 (1986).
6. A. L. Gray, *J. Anal. Atom. Spectrom.* **4**, 371 (1989).
7. H. B. Lim, R. S. Houk, and J. S. Crain, *Spectrochim. Acta,* **44B**, 989 (1989).
8. H. B. Lim and R. S. Houk, *Spectrochim. Acta*, **45B**, 453 (1990).
9. D. M. Chambers, J. Poehlman, P Yang, G. M. Hieftje, *Spectrochim. Acta*, Part B, **46B**, 741 (1991).
10. H. S. Niu, K. Hu, and R. S. Houk, *Spectrochim. Acta, Part B*, **46B**, 805 (1991).
11. H. Togashi, A. Hashizuma, and Y. Niwa, *Spectrochim. Acta, Part B,* **47B**, 561 (1992).
12. H. P. Longerich, *J. Anal. Atomic Spectrom.*, **4**, 491 (1989).
13. S. D. Tanner, *J. Anal. Atomic Spectrom.*, 1993, submitted.

14. N. Shibata, N. Fudagawa, and M. Kubota, *Spectrochim. Acta Part B*, **48B**, 1127 (1993).

15. J. W. H. Lam and G. Horlick, *Spectrochim. Acta Part B*, **45B**, 1327 (1990).

16. M. A. Vaughan and G. Horlick, *Spectrochim. Acta, Part B*, **45B**, 1289 (1990).

17. D. M. Chambers and G. M. Hieftje, *Spectrochim. Acta, Part B*, **46B**, 761 (1991).

18. J. E. Fulford and D. J. Douglas, *Appl. Spectrosc.*, **40**, 971 (1986).

19. J. A. Olivares and R. S. Houk, *Appl. Spectrosc.*, **39**, 1070 (1985).

20. J. A. Olivares and R. S. Houk, *Anal. Chem.*, **57**, 2674 (1985).

21. G. R. Gillson, D. J. Douglas, J. E. Fulrod, K. W. Halligan and S. D. Tanner, *Anal. Chem.*, **60**, 1472 (1988).

22. S. D. Tanner, *Spectrochim. Acta, Part B*, **47B**, 809 (1992).

23. R. Campargue, *High Intensity Supersonic Molecular Beam Apparatus*, in IV Symposium on Rarefied Gas Dynamics, J. H. De Leeuw, Ed., Academic: New York, pp. 279-298.

24. H. C. Beijerinck, R. J. F. Van Gerwen, E. R. T. Kerstel, J. F. M. Martens, E. J. W. Van Vliembergen, M. R. Th. Smits, and G. H. Kaashoek, *Chem. Phys.*, **96**, 153 (1985).

25. G. A. Bird, *Phys. Fluids*, **19**, 1486 (1976).

26. R. B. Fraser, F. Robben and L.Talbot, *Phys. Fluids*, **14**, 2317 (1971).

27. K. W. Olson, W. S. Haas, Jr. and V. A. Fassel, *Anal. Chem.*, **49**, 632 (1977).

28. B. R. Bear and V. A. Fassel, *Spectrochim. Acta, Part B*, **41B,** 1089 (1986).

29. R. H. Scott, V. A. Fassel, R. N. Kniseley and D. E. Nixon, *Anal. Chem.*, **46,** 75 (1974).

30. A. L. Gray, R. S. Houk, and J. G. Williams, *J. Anal. Atom. Spectrom.*, **2,** 13 (1987).

31. S. Lederman, M. H. Bloom and G. F. Widhopf, *AIAA J.* **6,** 2133 (1968).

32. M. G. Dunn and J. A. Lordi, *AIAA J.*, **7,** 1458 (1969).

33. R., H. Kirchoff, E. W. Peterson and L. Talbot, *AIAA J.* **9,** 1686 (1971).

34. A. A. Sonin, *AIAA J.*, **4,** 1588 (1966).

35. A. A. Sonin, "*The Behavior of Free Molecule Cylindrical Langmuir Probes in Supersonic Flows and Their Application to the Study of Blunt Body Stagnation Layers,*" Institute of Aerospace Studies, University of Toronto, Ontario, Canada, Rep. **109** (1965).

36. J. Laframboise, "*Theory of spherical and cylindrical Langmuir probes in a collisionless, Maxwellian plasma at rest,*" Institute of Aerospace Studies, Rep. **100** (1966).

37. S. H. Tan and G. Horlick, *J. Anal. Atomic Spectrom.*, **2,** 745 (1987).

38. R. M. Clements and P. R. Smy, J. Phys. D; *Appl. Phys,* **7,** 551 (1974).

39. M. Huang and G. M. Hieftje, *Spectrochim. Acta, Part B,* **44B,** 739 (1989).

40. B. L. Coughlin and M. W. Blades, Spectrochim. Acta, Part B, **42B,** 353 (1987).

41. J. S. Crain, F. G. Smith and R. S. Houk, *Spectrochim. Acta, Part B*, **45B,** 249

(1990).

42. X. Jian, L. Qingyuan, L. Wenchang, Q. Haowen and Z. Zhanxia, *J. Anal. Atomic Spectrom.* **1**, 131 (1992).

43. B. L. Coughlin and M. W. Blades, *Spectrochim. Acta, Part B,* **40B** 987 (1985).

44. D. S. Hanselman, N. N. Sesi, M. Huang and G. M. Hieftje, *Spectrochim. Acta Electronica,* submitted (1994).

45. R. S. Houk, V. A. Fassel and H. J. Svec, *Dynamic Mass Spectrom.* **6**, 234 (1981).

46. S. D. T. Axford and A. N. Hayhurst, *Int. J. Mass Spectrom.* Ion Processes, 110, 31 (1991).

47. R. S. Houk, S. C. K. Shum and D. R. Wiederin, *Anal. Chim. Acta*, **250**, 61 (1991).

48. A. L. Gray, personal communication (1983).

49. R. C. Hutton and A. N. Eaton, *J. Anal. Atomic Spectrom.*, **3**, 547 (1988).

50. N. Jakùbowski, I. Feldmann and D. Stuewer, *J. Anal. Atomic Spectrom.*, **8**, 969 (1993).

51. S. D. Tanner, personal communication (1993).

52. E. W. McDaniel, *Collision Phenomena in Ionized Gases,* Wiley: New York, 1964, pp. 512-521.

53. H. Niu and R. S. Houk, *Spectrochim. Acta Part B*, **49B**, submitted (1994).

54. P. R. *Smy, Adv. Phys.*, **25**, 517 (1976).

55. P.-Q. Lu, P.-Z Gong, T.-Z. Lin and R. S. Houk, *Spectrochim. Acta Part B*, **43B**, 273 (1988).

56. R. S. Houk, *Pittsburgh Conf. on Anal. Chem. and Appl. Spectros.*, Atlanta, GA, Page No. 982, (1993).

57. P. Farnsworth, Y. Chen, M. Lee, M. Wu and J. Sin, *Pittsburgh Conf. on Anal. Chem. and Appl. Spectros.*, Chicago, IL, February-March, Paper No. 7, (1994).

Table I. Instrumentation and operating conditions

Component	Operation Condition	
Ultrasonic Nebulizer [27,28]:		
Model U-5000	Sample uptake rate:	2.2 mL/min
Cetac Technologies	Transducer power:	45 W
Omaha, NE	Frequency:	1.36 MHz
	Desolvation Temp.	140 °C
	Condenser temp.	-5 °C
ICP generator:		
Type HFS-3000D with	ForwardPower:	1.25 KW
MN-3000E matching network	Frequency:	27.12 MHz
Plasma-Therm, Inc.	Loadcoil grounded at downstream	
(now RF Plasma Products	end nearest sampling orifice	
Kresson, NJ)	see Fig. 2x of ref. [30]	
ICP Torch:	Argon Flow Rates (L/min):	
Fassel-type [29]	Outer:	15
Precision Glass Co.	Auxiliary:	0.5
Englewood, Colorado	Aerosol:	0-1.5
Sampling cone:	Material: nickle	
Ames Lab construction	Orifice diam.:	0.76 mm
	Internal angle:	90°
	External angle:	100°
	Sampling position:	10 mm
	from load coil, on center	
Skimmer cone:	Material: stainless steel	
Ames Lab construction	Orifice diam.:	0.76 mm
	Internal angle:	50°
	External angle:	60°
	Skimmer tip 10 mm behind sampler tip	

Table I. (continued)

Vacuum System:	
First stage:	Rotary pump, speed: 10 l/s pressure: 0.8 torr measured by Convectron thermocouple gauge, Series 250 Granville-Phillips, Boulder, CO
Second stage:	Diffusion pump with liquid N_2 trap Pumping speed, 1600 l/s Second stage pressure: $2x10^{-4}$ measured by ionization gauges
Ion lens:	Stainless steel cylinder 13 mm diam. x 25 mm long located 45 mm from skimmer tip grounded
Ammeter and voltage supply	Model 177 multimeter Model 487 picoammeter/voltage source Keithley Instruments, Inc. Cleveland, OH

* conditions: 10 mm from load coil, on center, 1.25 kw.

Table 2. Extrapolated values for electron density at sampler entrance for dry ICP.

	Electron Density (cm^{-3})		
Aerosol gas flow rate (L/min)	At sampler Langmuir Probe	In ICP Thomson scat.[39]	In ICP emission [40]
0	$8.8x10^{15}$	--	--
0.5	--	$5.0x10^{15}$	--
0.6	$4.4x10^{15}$	--	--
0.9	--	--	$1.5x10^{15}$
1.0	$2.1x10^{15}$	--	--
1.35	$1.4x10^{15}$	--	--
1.5	$1.1x10^{15}$	--	--

* conditions: 10 mm from load coil, on center, 1.25 kw.

Table 3. Extrapolated values for electron density at sampler entrance for wet ICP.

	Electron Density (cm^{-3})				
Aerosol gas flow rate (L/min)	At sampler Langmuir Probe	At sampler H_β line	In ICP H_β line	In ICP Ar(I)	In ICP Thomsom scat.
0	9.1×10^{15}	--	--	--	--
0.6	2.8×10^{15}	--	--	--	--
0.8	--	--	0.8×10^{15} [42]	--	1.0×10^{15} [44]
0.9	--	--	1.7×10^{15} [43]	1.0×10^{15} [40]	--
1.0	0.7×10^{15}	0.8×10^{15} [41]	--	--	--
1.2	--	--	0.7×10^{15} [43]	--	< 0.1 [44]

Table 4. Measured electron density at the skimmer entrance for dry ICP.

Aerosol Gas Flow (L/min)	Number Density (cm^{-3})		
	Measured	Expected	Ratio
0	5.7×10^{12}	9.4×10^{12}	0.61
0.6	2.5×10^{12}	4.1×10^{12}	0.61
1.0	0.55×10^{12}	2.1×10^{12}	0.26
1.3	0.23×10^{12}	1.3×10^{12}	0.18
1.5	0.16×10^{12}	1.1×10^{12}	0.15

Table 5. Measured electron density at the skimmer entrance for wet ICP.

Aerosol Gas Flow (L/min)	Number Density (cm^{-3})		
	Measured	Expected	Ratio
0	$1.1x10^{13}$	$1.1x10^{13}$	1.0
0.6	$1.9x10^{12}$	$2.9x10^{12}$	0.65
1.0	$8.6x10^{10}$	$6.0x10^{11}$	0.14

Table 6. Fundamental parameters and conditions at sampler and skimmer [54, 55].

Quantity	Symbol and Definition	Value at Sampler	Value at Skimmer
Dimensionless quantity	$\alpha = \lambda_D/r$	2 x 10-3	0.5
Electron density	n_e	1 x 1015 cm-3	1 x 1013 cm-3
Radius of metal at edge of sampler or skimmer	r	0.05 mm	0.02 mm
Electric Reynolds number	$R_e=2\nu r/\mu_i(kT_e/e)$	0.18 - 0.48	14-39
Electron Temperature	T_e	8000	8000
Ion mobility	μ_i	$3x10^{-3}$ - $8x10^{-3}$ ($m^2v^{-1}s^{-1}$)	$3x10^{-3}$ - $8x10^{-3}$ ($m^2v^{-1}s^{-1}$)
Flow velocity	V_f	103 cm^{-3}	$2x10^5$ cm s^{-1} [1]
Dimensionless quantities	$x = eV/kT^e$	7.2 for V=5 volts	7.2
	$Re\alpha^2\chi^2$	$4x10^{-5}$ - $1x10^{-4}$	180-500
	$Re\alpha^2$	not necessary	3-10

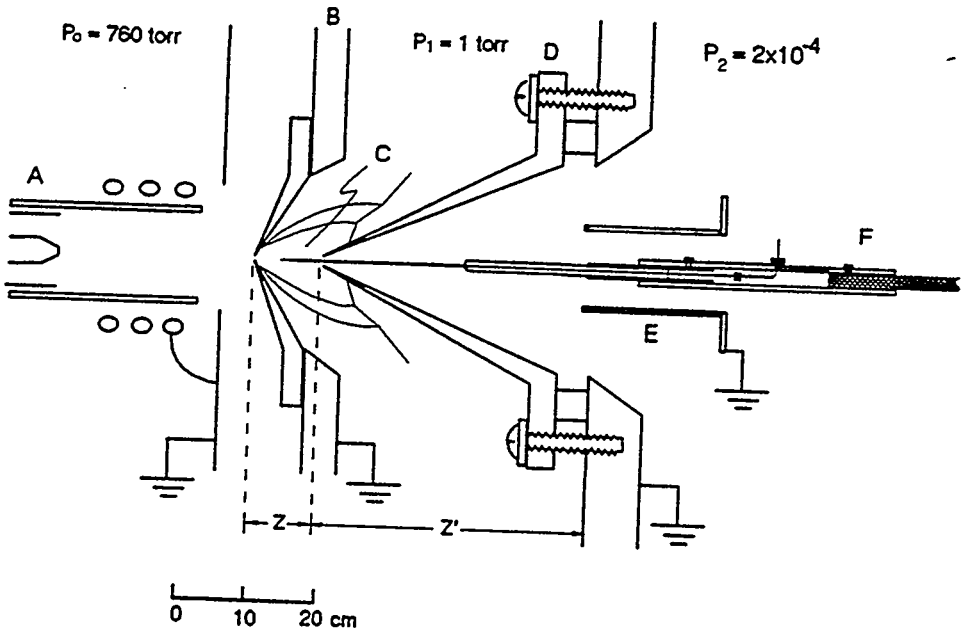

Fig. 1. Scale diagram of apparatus. A: ICP showing arrangement of load coil and metal shielding plate; B: sampler cone; C: zone of silence of supersonic jet; D: skimmer: E: cylindrical ion lens; F: Langmuir probe on shaft driven by linear motion feedthrough.

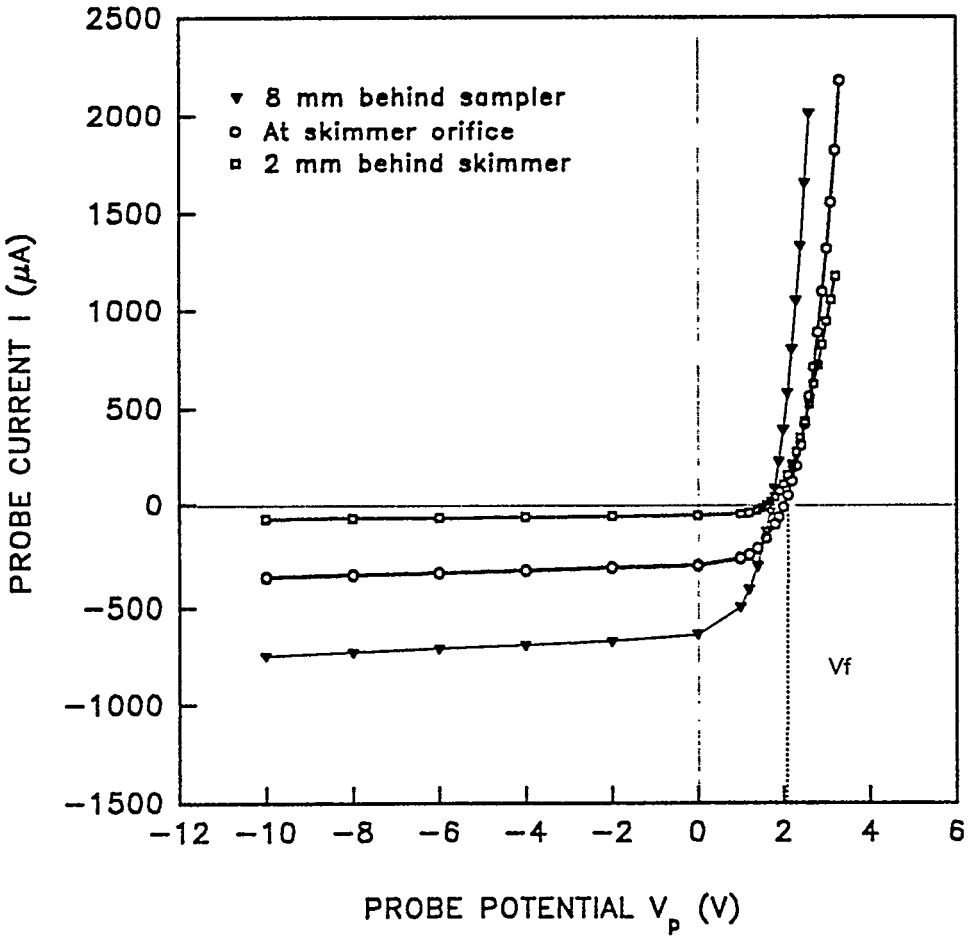

Fig. 2. Typical current-voltage curves obtained at 8 mm behind sampler (▽), at skimmer tip (○), and at 2mm behind skimmer (▫).

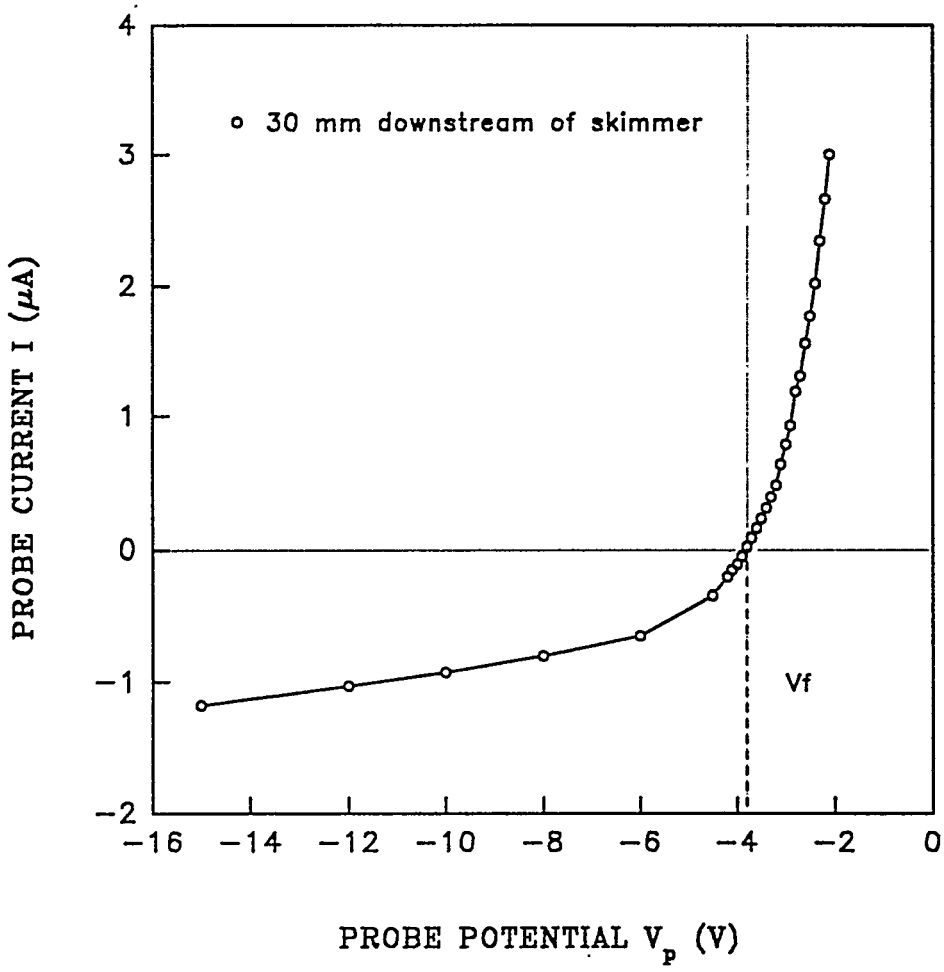

Fig. 3. Typical I-V curve obtained at 30 mm behind skimmer.

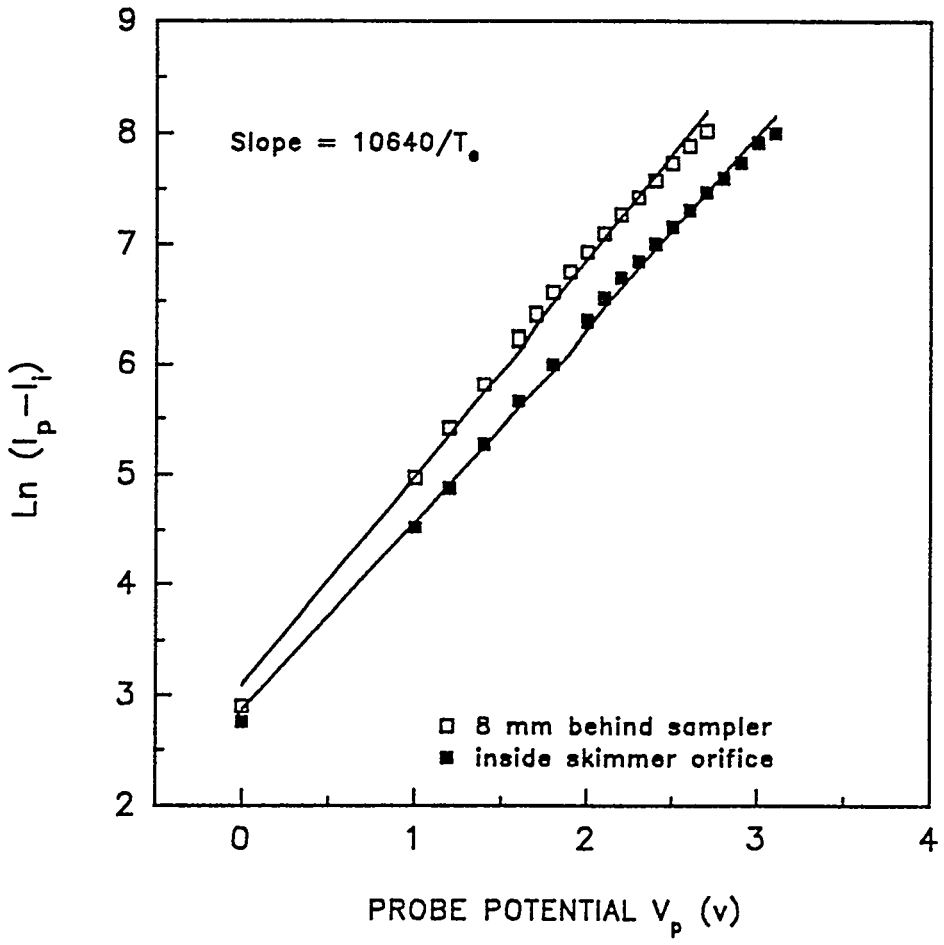

Fig. 4. Plot for determining T_e at two axial positions: 8 mm behind sampler (□) and inside skimmer tip (■).

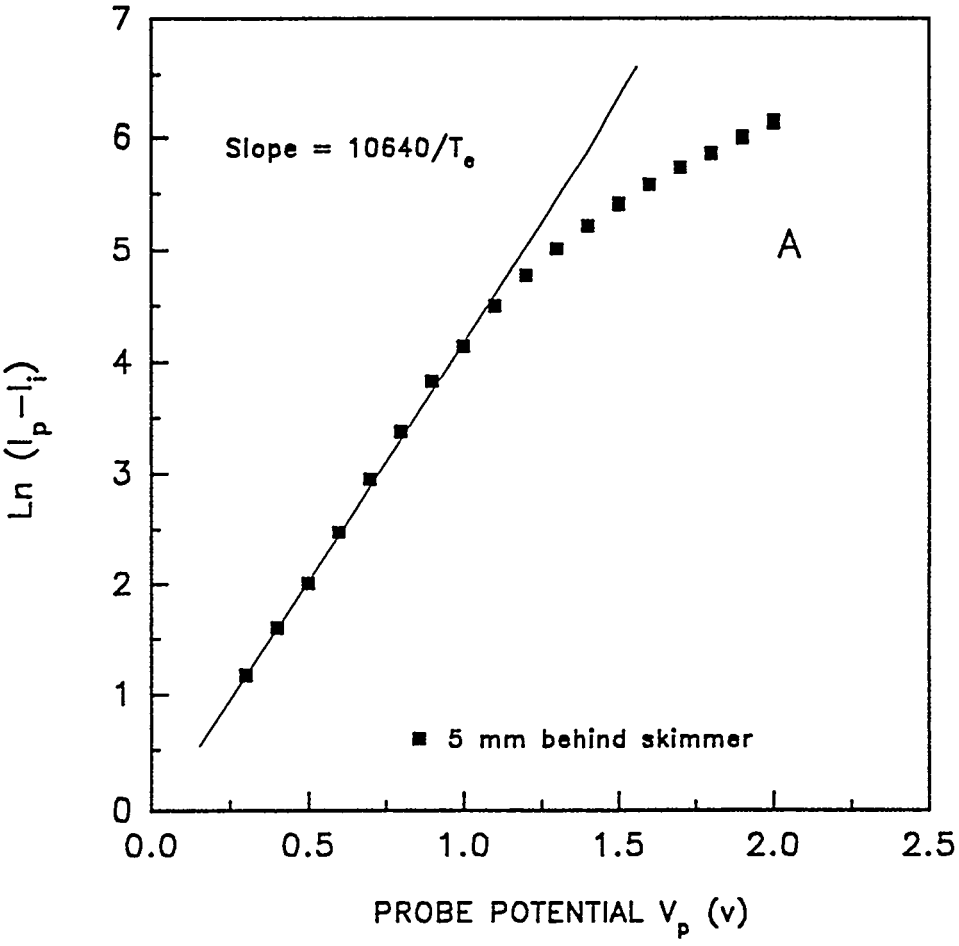

Fig. 5. Typical plots for determining T_e at two axial position: 5 mm behind skimmer (A) and 30 mm behind skimmer (B).

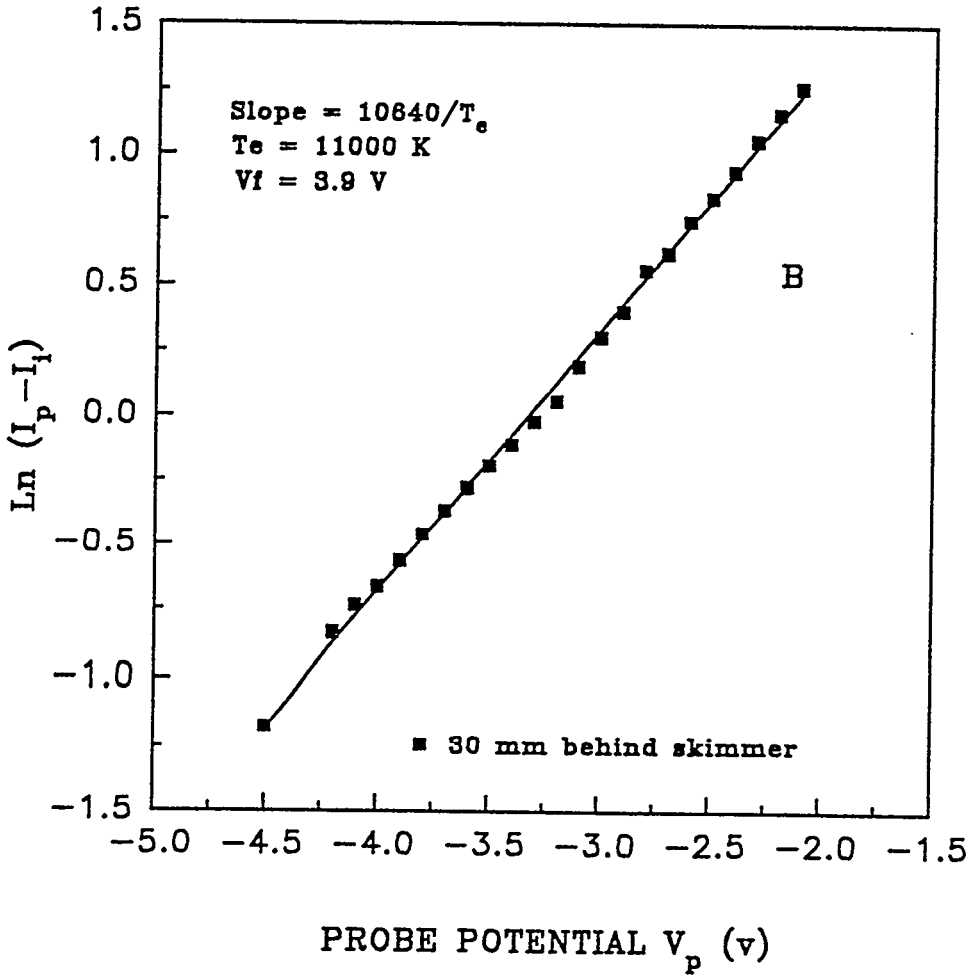

Fig. 5. (Continued)

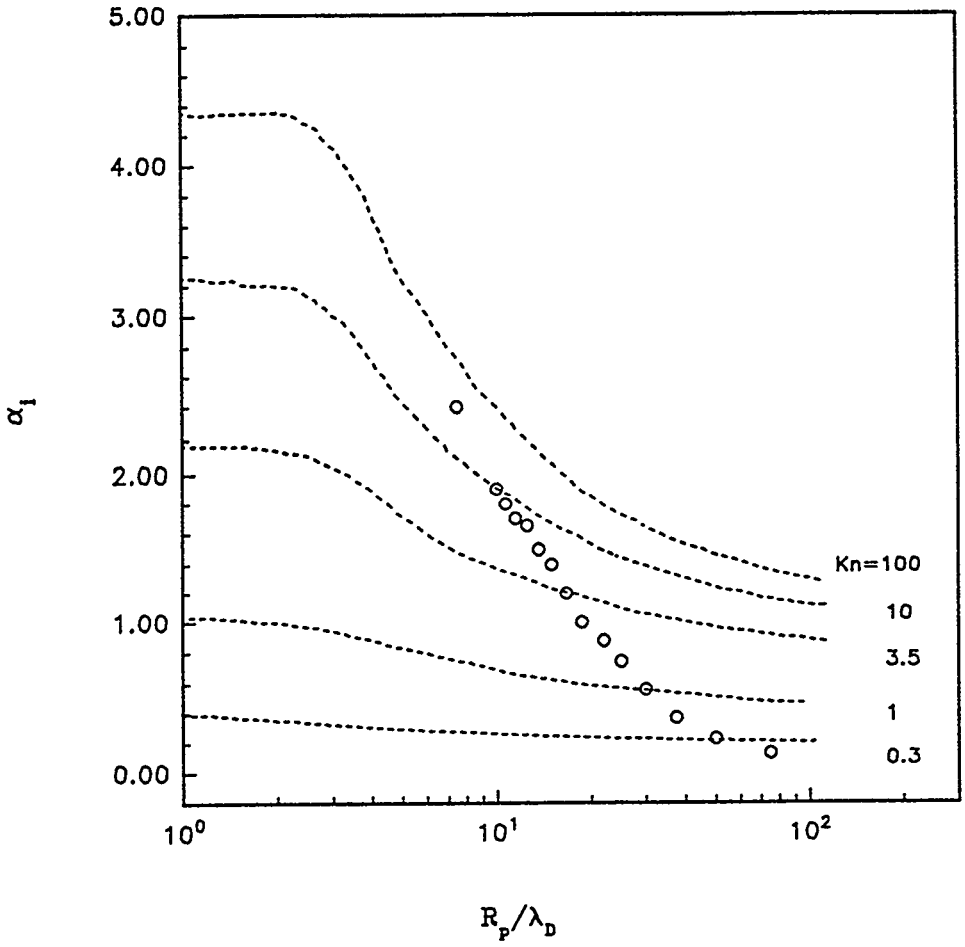

Fig. 6. Plots for determining α_i to calculate ne at various axial positions. Dotted lines represent values given by Laframboise [36]. Points represent values calculated by us based on Laframboise's model. Solid line represents values used in present work. See text for explanation.

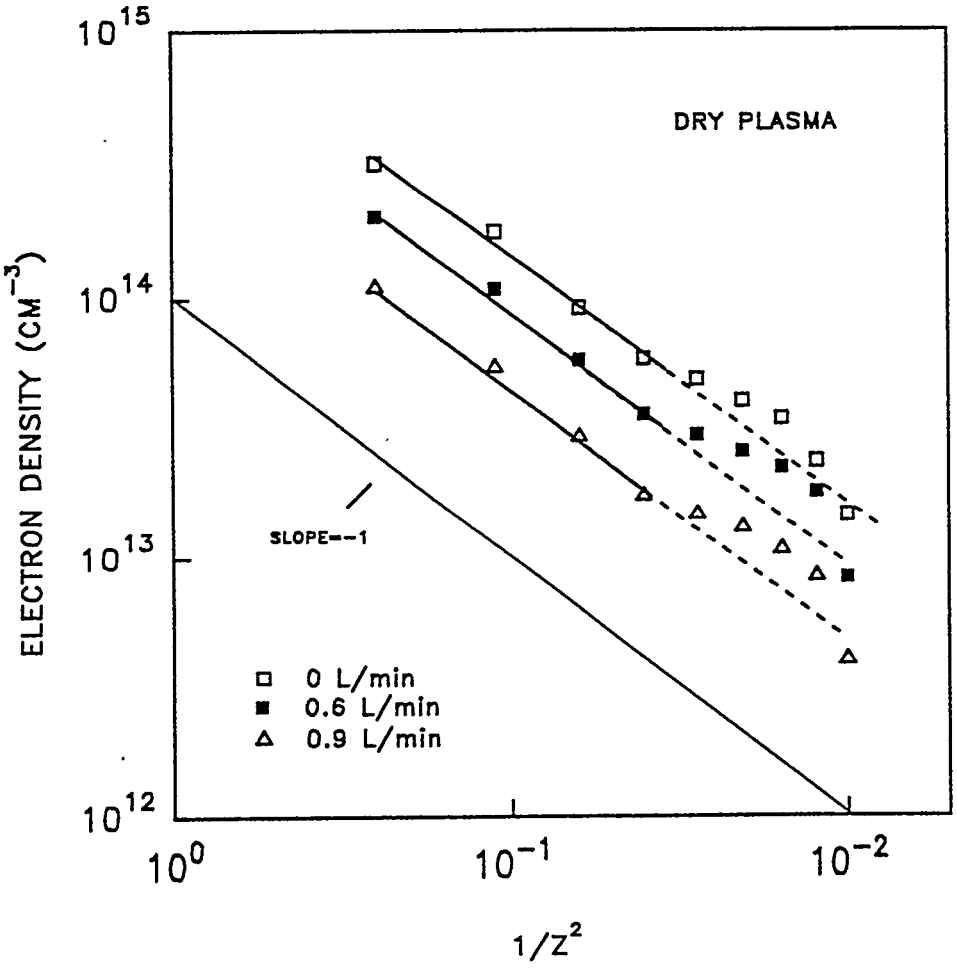

Fig. 7. Measured values of electron density plotted vs. axial position between sampler and skimmer $1/z^2$ for dry plasma. The leftmost point is 2 mm behind the sampler. The rightmost point is at the skimmer tip.

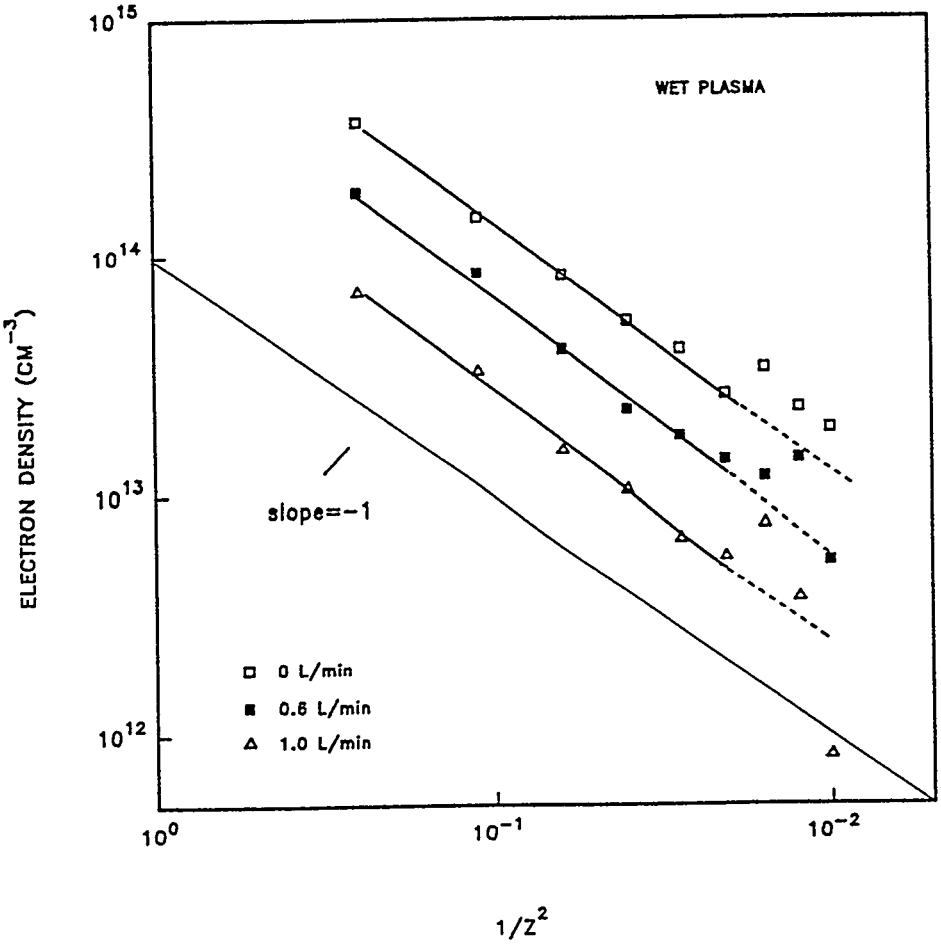

Fig. 8. Measured values of electron density plotted vs. $1/z^2$ between sampler and skimmer for wet plasma

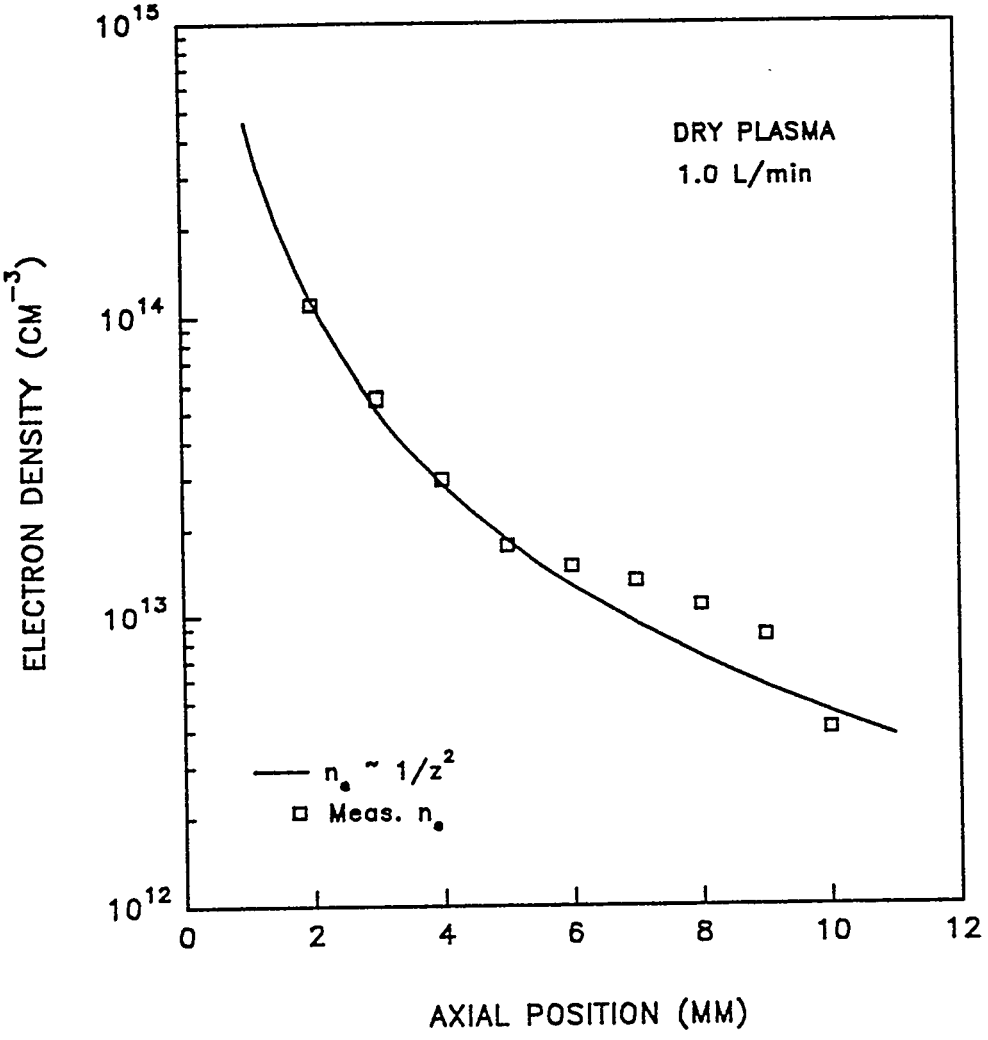

Fig. 9. Measured values of electron density plotted vs. axial position between sampler and skimmer. Conditions: dry plasma at aerosol gas flow rate = 1.0 L/min. The solid curve represents a $1/z^2$ dependence fitting to the four leftmost points.

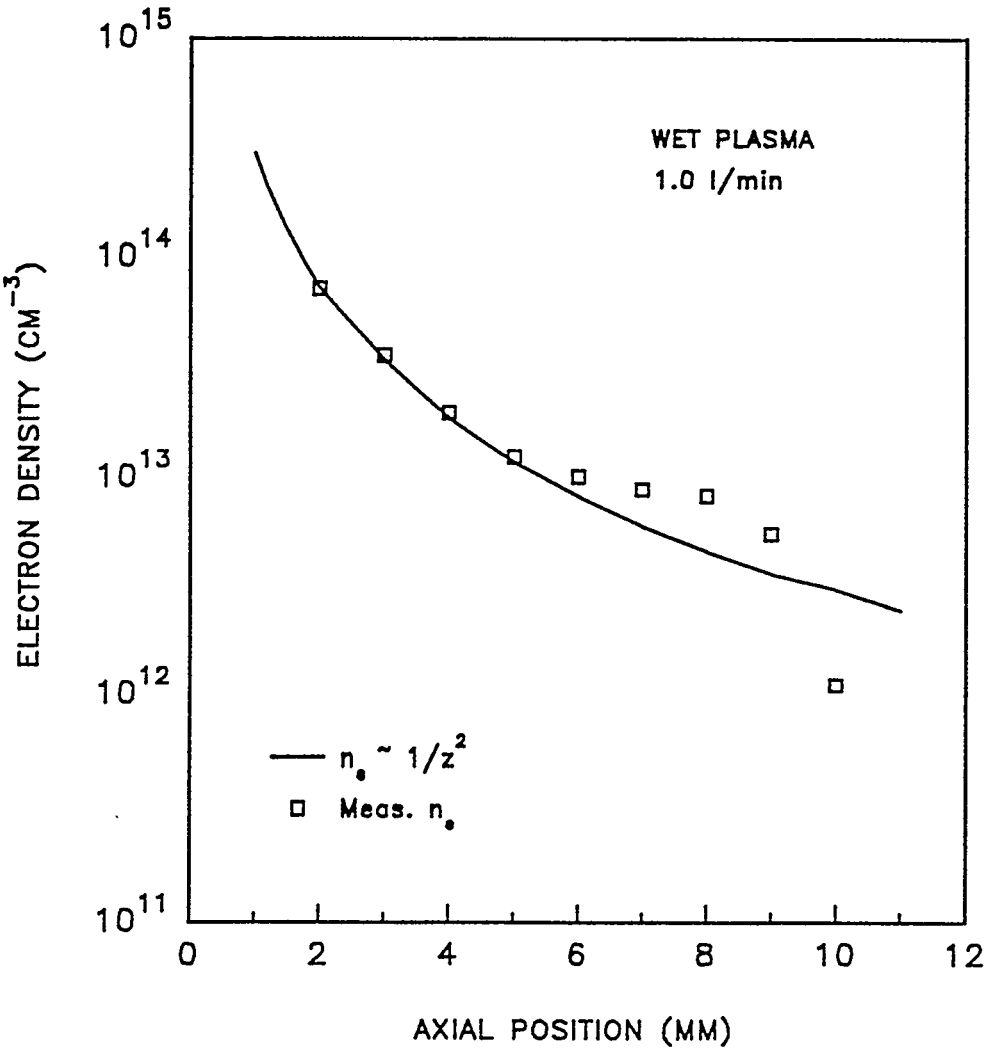

Fig. 10. Measured values of electron density plotted vs. axial position between sampler and skimmer. Conditions: wet plasma at aerosol gas flow rate = 1.0 L/min. The solid curve represents a $1/z^2$ dependence fitting to the four leftmost points.

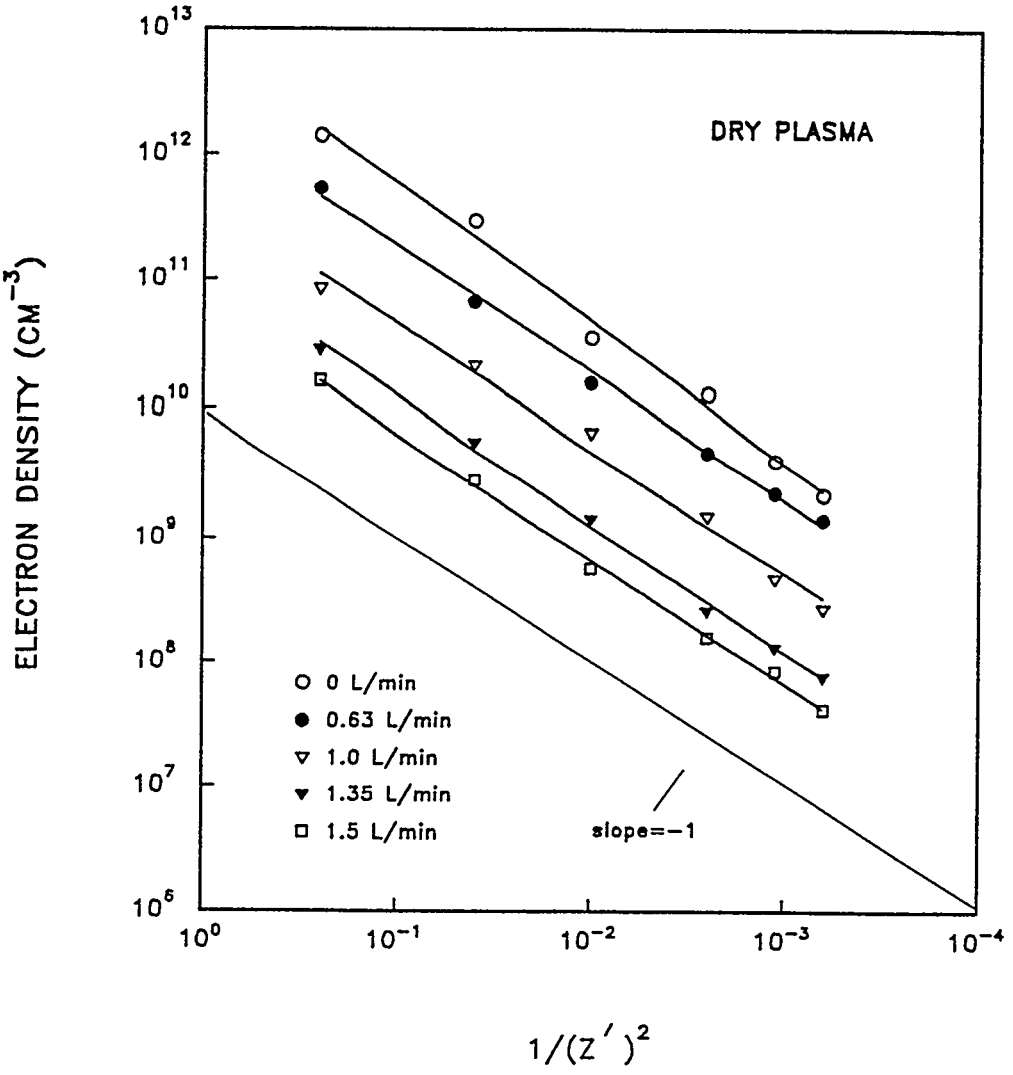

Fig. 11. Measured values of electron density behind skimmer plotted vs. $1/(z')^2$ for dry plasma at various aerosol gas flow rates: 0 (○), 0.63 (●), 1.0 (▽), 1.35 (▼) and 1.5 L min^{-1} (□). The leftmost point is 2 mm behind the skimmer.

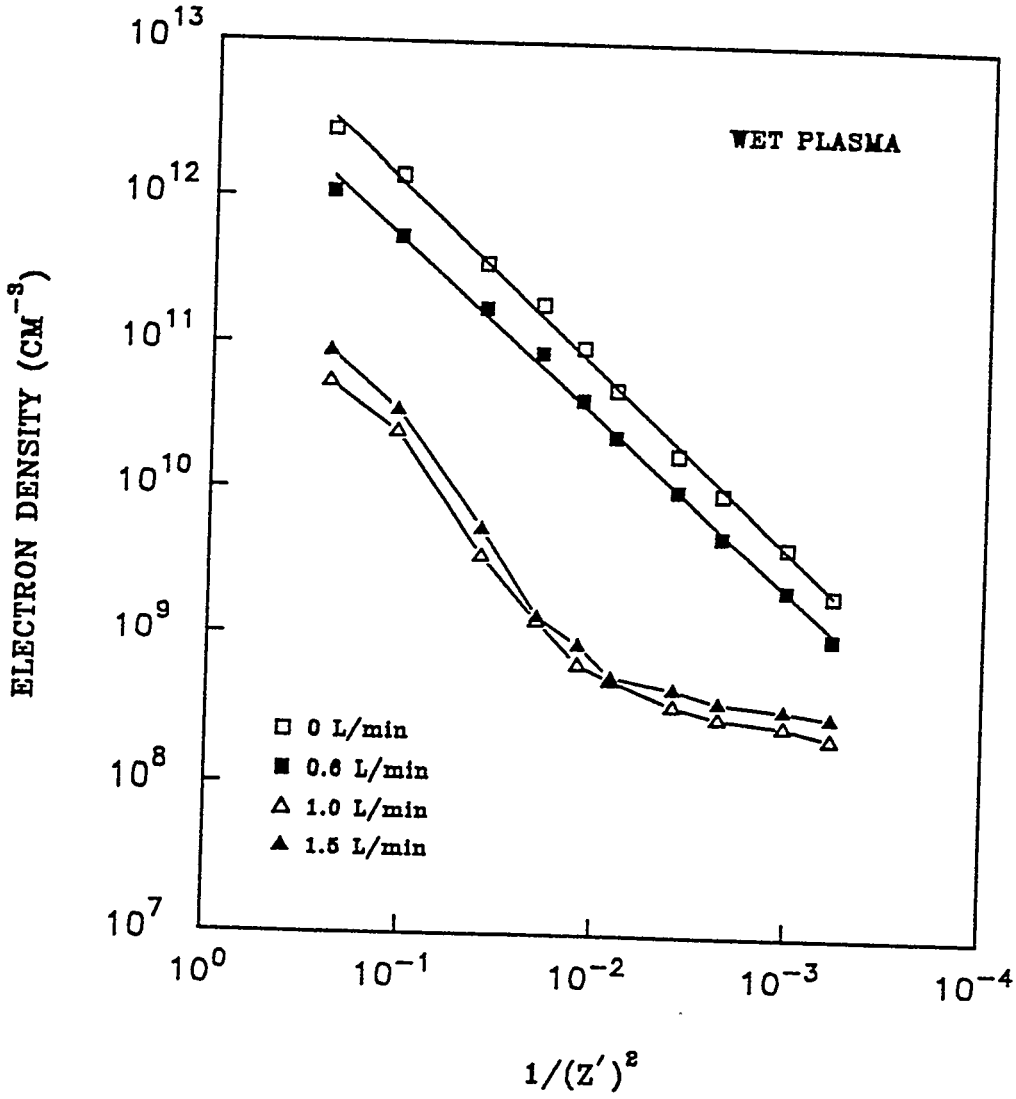

Fig. 12. Measured values of electron density behind skimmer plotted vs. $1/(z')^2$ for wet plasma at various aerosol gas flow rates: 0 (□), 0.63 (■), 1.0 (▽), and 1.5 L min^{-1} (▲).

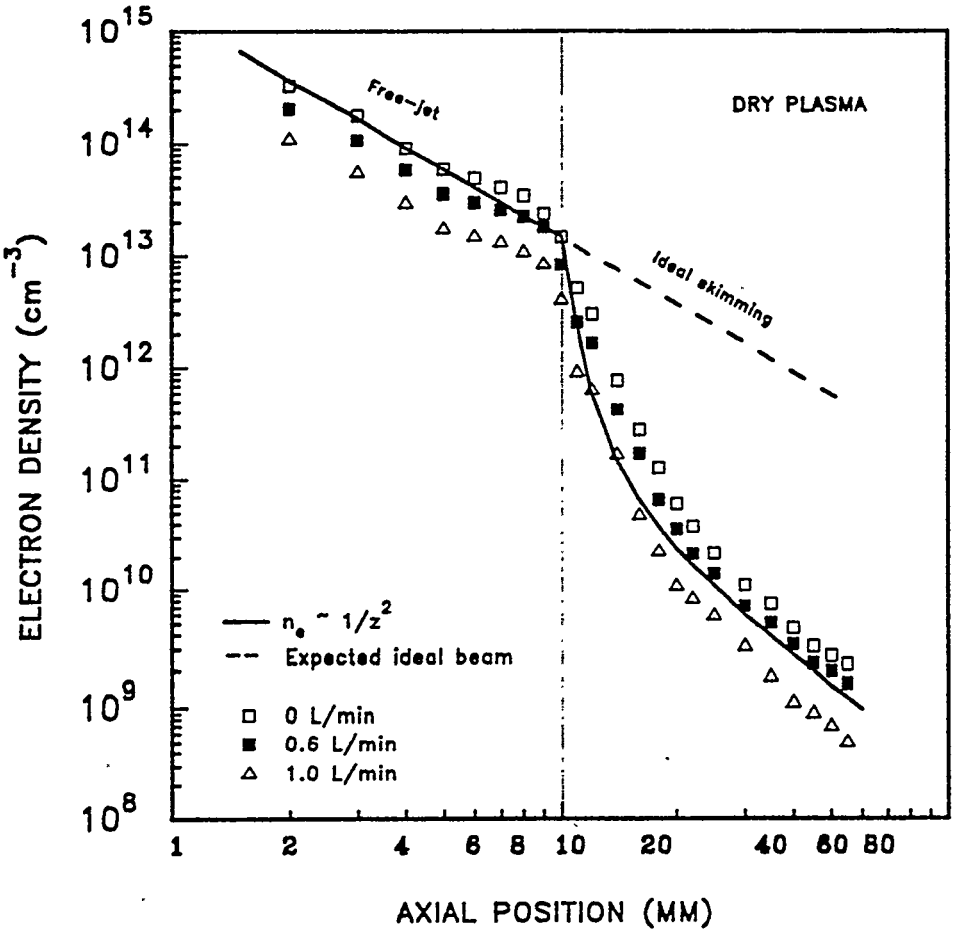

Fig. 13. Composite plot of electron density vs. axial position for dry plasma. The skimmer tip is at 10 mm. The aerosol gas flow rate was 0 (□), 0.63 (■), and 1.0 (▽) L min^{-1}. The solid line and curve represent $1/z^2$ dependence of n_e on axial position. The dotted line represents the electron densities expected if the skimmer behaved ideally. See text for discussion.

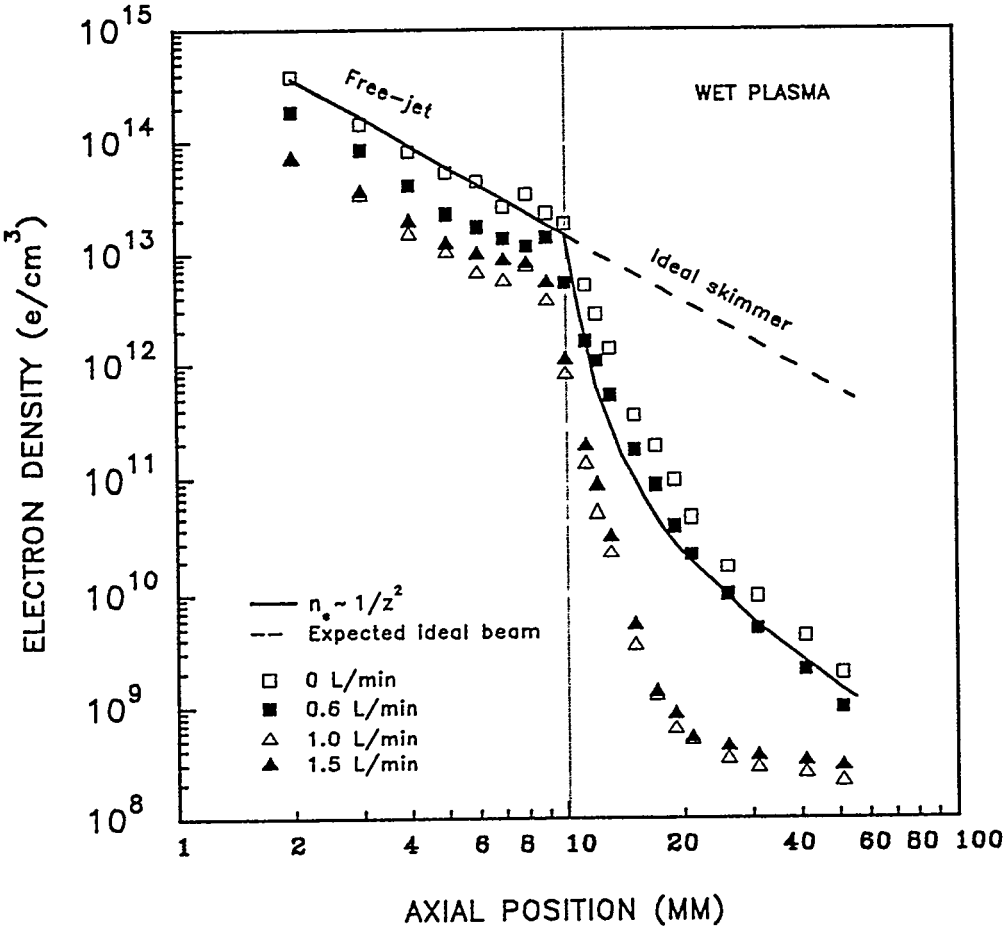

Fig. 14. Composite plot of electron density vs. axial position for wet plasma. The aerosol gas flow rate was 0 (▫), 0.63 (▪), 1.0 (▽), and 1.5 L min^{-1} (▲). The solid lines represent $1/z^2$ dependence of n_e on axial position. The dotted line represents the electron densities expected if the skimmer behaved ideally. See text for discussion.

A

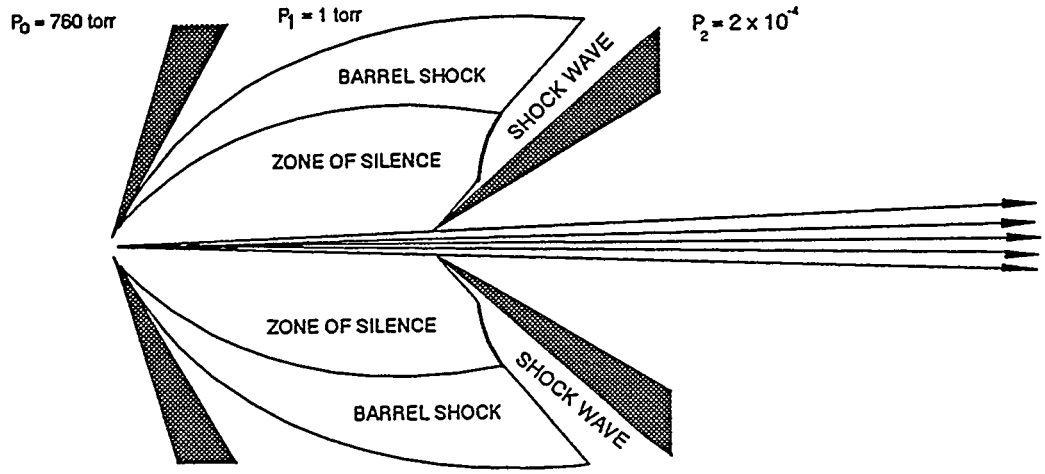

Fig. 15. Suggested depiction of the effect of the skimmer tip on the supersonic beam. A: ideal case with no disturbance at skimmer; B: real case in which disturbance at skimmer acts as new expansion source and disperses beam behind skimmer.

B

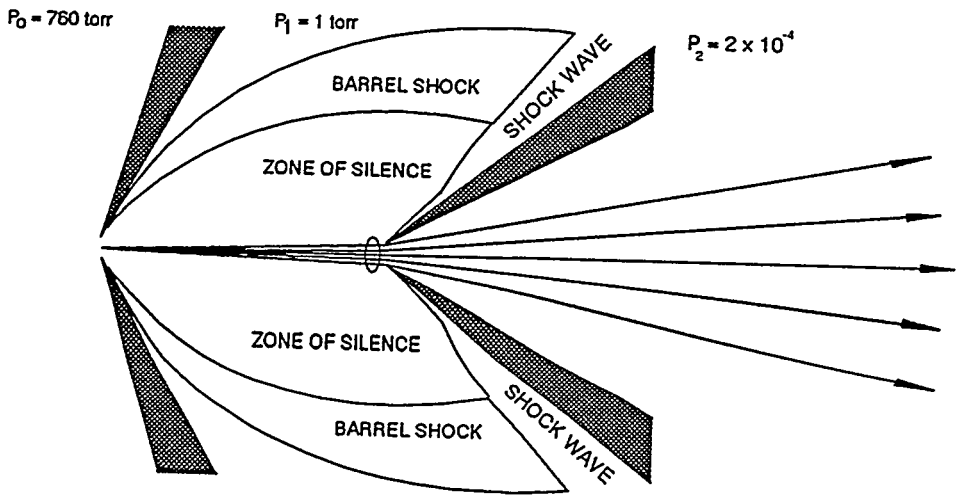

Fig. 15. (Continued)

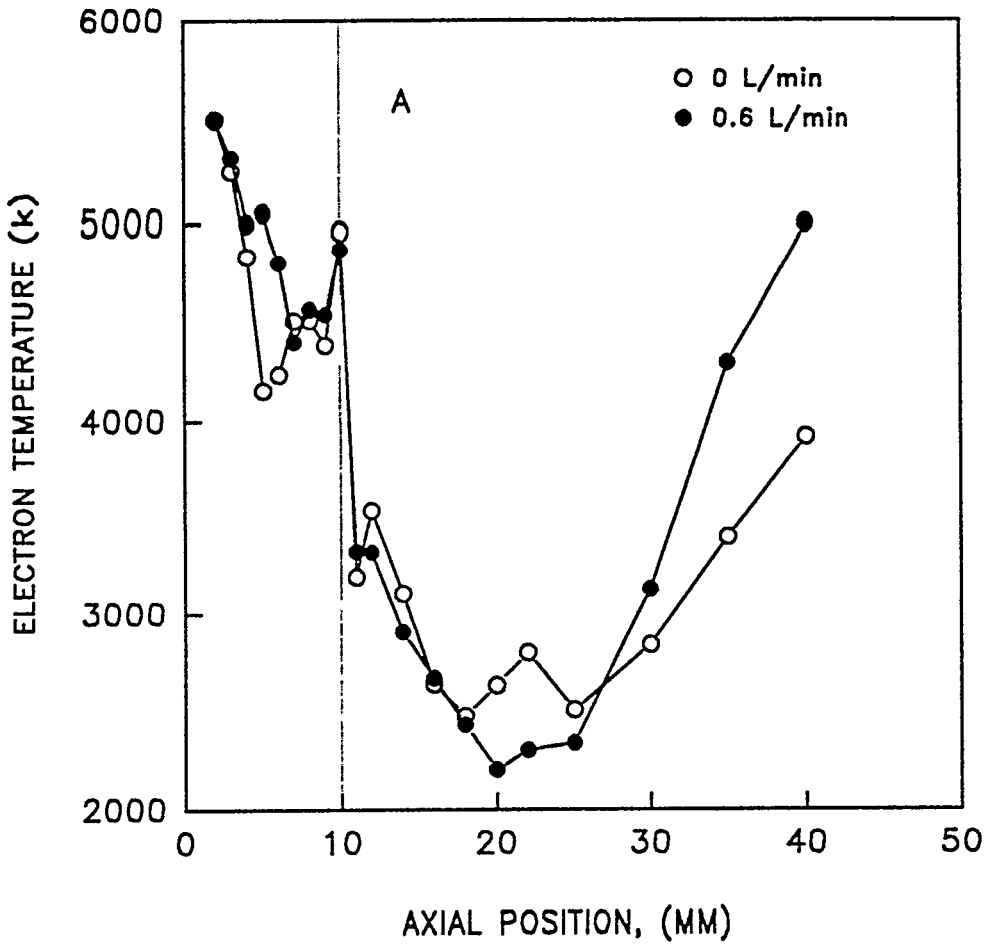

Fig. 16. Measured electron temperature for dry plasma. The aerosol gas flow rate was 0 (○), 0.63 (●), 1.0 (▫), and 1.5 L min^{-1} (▪). The skimmer tip is at 10 mm.

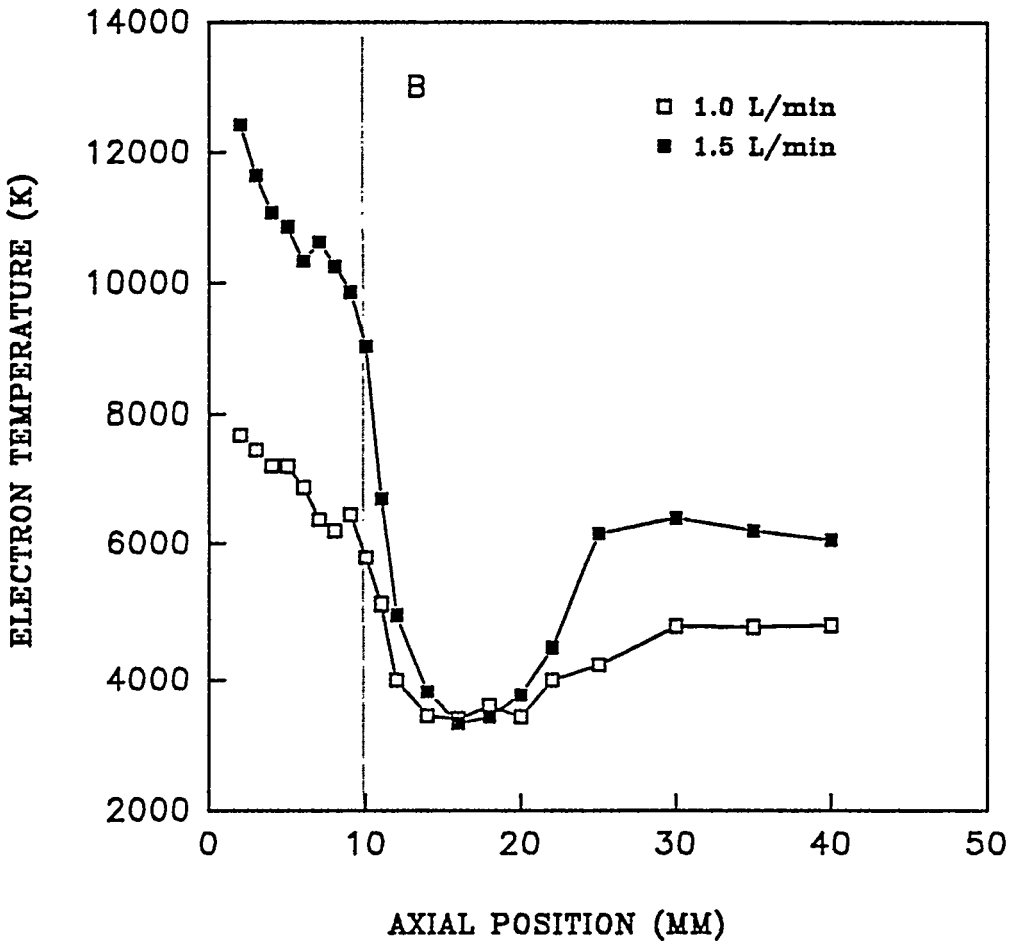

Fig. 16. (continued)

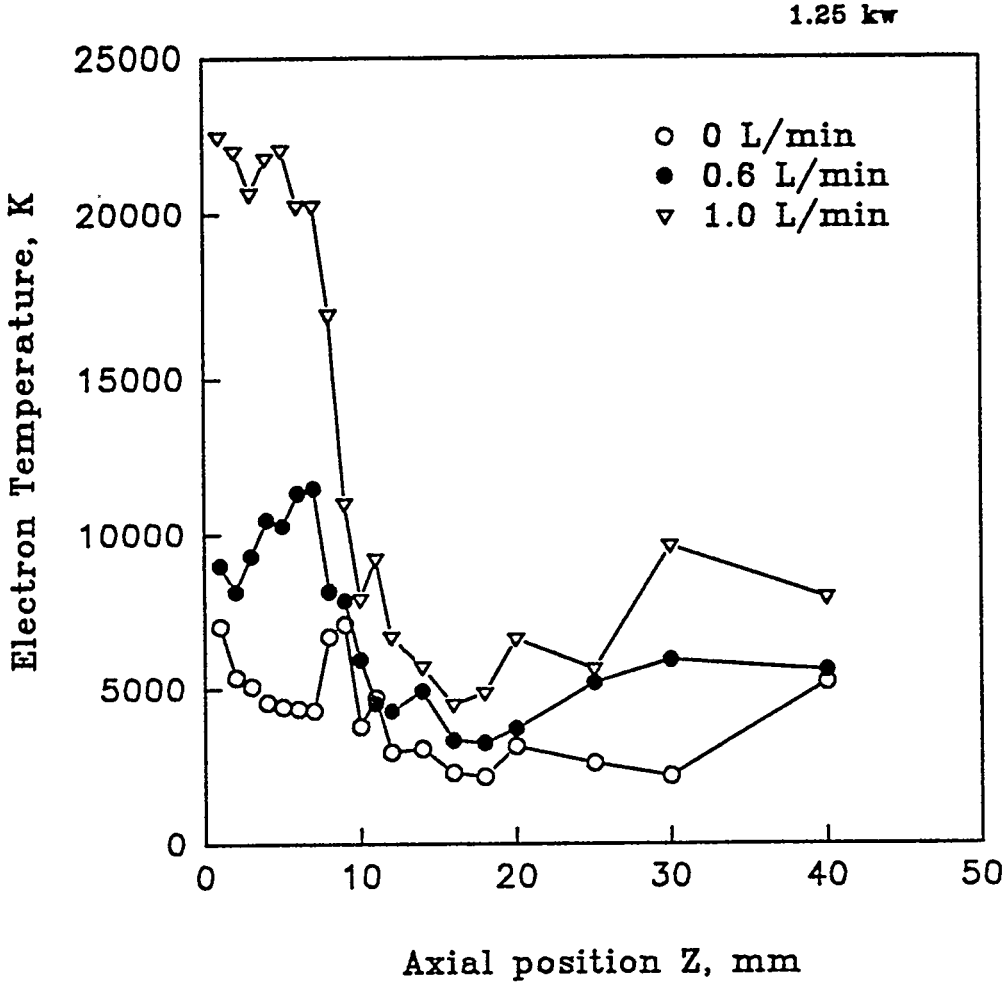

Fig. 17. Measured electron temperature for wet plasma. The aerosol gas flow rate was 0 (○), 0.63 (●), 1.0 L min^{-1} (▽).

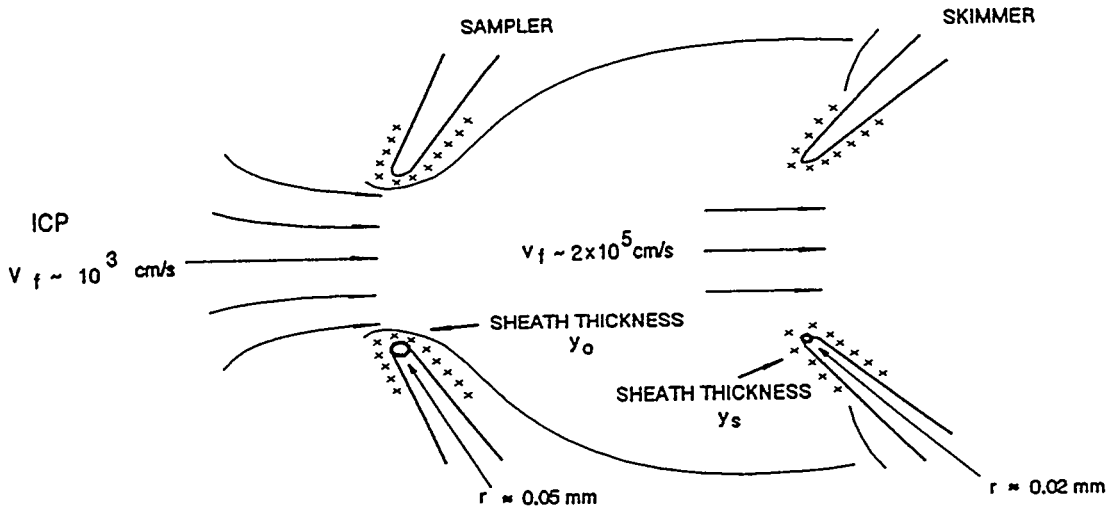

Fig. 18. Conceptual diagram illustrating how the edgers of the sampler and skimmer are analogous to spherical Langmuir probes of radius r. See text for explanation.

PAPER IV

EXPERIMENTAL STUDIES OF THE PLASMA EXTRACTION AND ION BEAM FORMATION PROCESSES IN INDUCTIVELY COUPLED PLASMA-MASS SPECTROMETRY. II. FLOATING VOLTAGE AND RF VOLTAGE

INTRODUCTION

ICP-MS has developed into a highly sensitive and selective technique for elemental and isotopic analysis. Despite its analytical success, ICP-MS still suffers from certain weaknesses such as matrix effects [1-6] and mass bias [2,7-9]. In addition, for common quadrupole devices, the overall ion transport efficiency is only roughly 1 ion detected for 10^6 to 10^7 ions passing through the sampler [10-12].

Conceivably, these problems could be rectified to some extent based on an improved understanding of the processes responsible for ion extraction and ion beam formation. Several important theoretical studies of the ion extraction process include definitive papers on gas dynamics by Douglas and French [13] and on space charge effects by Gillson et al. [14] and Tanner [15]. These studies are supported by a variety of measurements, including optical spectroscopy [16-20], ion kinetic energy measurements [21-24], ion deposition [25], and high speed photography [26-28]. Langmuir probe studies in the plasma [29-33], behind the sampler [34-38], and behind the skimmer [38,39] have also been reported..

This paper accompanies a recent one in which a single Langmuir probe is used to determine electron density and temperature in the supersonic jet and behind the skimmer during the same experiment [38]. Measurements of floating voltage on a biased probe and RF voltage on a floating probe are reported and discussed.

EXPERIMENTAL

V_f Measurements

The apparatus for these measurements is described in the companion manuscript [38]. It consists of an ultrasonic nebulizer and desolvator [40], a 27 MHz fixed-frequency ICP sustained in argon, a grounded sampler and skimmer on a two-stage vacuum system, and a tungsten Langmuir probe. This probe is positioned axially in either the supersonic jet or the beam leaving the skimmer. For a so-called "dry" plasma, the nebulizer is bypassed and the aerosol gas is added directly to the injector tube of the torch.

The load coil has the RF voltage applied to the upstream end, i.e., the end closest to the inner tubes of the torch. The downstream end of the coil is grounded both to a copper block on the wall of the impedance matching network and by a copper strap soldered to the copper box used to shield the torch. This coil arrangement reduces the plasma potential and secondary discharge substantially but does not totally eliminate them as shown in previous Langmuir probe experiments [30,34] and measurements of ion kinetic energies [21-23].

Floating voltage is measured from the intercept of a plot of current vs. applied voltage, as illustrated by the typical I-V curve in Fig. 1. We also measured the voltage on a floating probe by connecting it to a voltmeter with high input impedance. When the probe was in the supersonic jet, these latter voltages were similar to the V_f

values, as shown before [39]. However, the floating probe yielded erratic results when used behind the skimmer. In many cases, the probe apparently assumed a voltage of only several mV. Other times, the voltage drifted erratically and did not stabilize. In both these cases the probe acted as if there was no reference electrode in the circuit. For this reason, only the Vf method was used.

RF Voltage Measurements

In the course of other experiments designed to intensify emission from the Mach disk, an RF voltage was measured on a floating graphite electrode positioned behind the Mach disk. This apparatus is shown in Fig. 2, and operating conditions and components are described in Table 1. Note that the plasma and vacuum chamber were very different from those used for the other results described below. The other apparatus used previously for the Vf measurements was not available for RF voltage experiments, and these latter results are pertinent to the theme of this paper, so these initial RF voltage results are described here.

RESULTS AND DISCUSSION

Floating Potential

The V_f values described in this section are derived from the same I-V curves used in the companion paper in number density measurement [38] and are directly comparable to them. Results are shown for various axial positions (denoted by coordinate z) for a dry plasma in Fig. 3.

First, consider the following trends in V_f with axial position. As the probe is moved between the sampler and skimmer (z = 2 to 10 mm), V_f drops slightly, which agrees with the observation of Chambers et al. [37] that voltage doesn't change much with axial position inside the supersonic jet. At low values of aerosol gas flow rate ($<= 0.65$ L/min), V_f also drops only gradually as the probe is retracted back through the sampler into the beam behind the skimmer (z = 10 to 50 mm). However, at high aerosol gas flow rate (≥ 0.65 L/min), V_f drops substantially behind the skimmer and changes to negative polarity.

Fig. 3 also shows that V_f inside the jet (z = 2 to 10 mm) increases at first as aerosol gas flow rate increases up to 1.0 L/min. Floating voltage then decreases as aerosol gas flow rate increases above this value. The same trend in V_f is seen if the probe is in the ICP (i.e., outside the sampler) for a plasma operated with the same type of load coil used in the present work [30].

Floating voltages for the beam extracted from a wet plasma are shown in

Figure 4. In this case, V_f in the supersonic jet essentially increases with aerosol gas flow rate. There is a sharp drop in V_f near the skimmer tip (z=10 mm) at the two higher values of aerosol gas flow rate (1.0 and 1.35 L/min). Chambers et al. found that probe voltages dropped when the probe was moved into either the barrel shock or Mach disk [37]. Thus, the drop in V_f near the skimmer may be caused by a disturbance in front of the skimmer, as discussed in the companion paper [38]. If so, the disturbance is apparently more severe for a wet plasma at high aerosol gas flow rate. Finally, the V_f values behind the skimmer for the wet plasma do not go nearly as far negative as those for a dry plasma.

The general range of V_f values in the supersonic jet (+2 to +6 V) agrees closely with those measured previously with Langmuir probes without the skimmer present [35,37]. When this instrument was configured as a mass spectrometer, the best aerosol gas flow rate was in the range 0.65 to 1.0 L/min. A plot of ion kinetic energy vs. ion mass would intercept the energy axis at +3 to +5 volts [41], in good agreement with the range of V_f values reported here. Thus, the offset of several eV seen in such plots of ion energy vs. mass can be caused by small residual voltages inside the sampler, as suggested by Fulford and Douglas [22], although space charge effects can also displace the measured energies for light ions to high values as well.

RF Voltage

Results for these measurements are shown in Figs. 5 and 6. In each case, a wave at approximately 40 MHz is seen, which is the nominal operating frequency for the plasma used. This generator is free-running, so the actual frequency changes with forward power and aerosol gas flow rate in such a way as to minimize reflected power [42].

In this discussion, we are mainly concerned with the amplitude of the RF signal from the probe. As shown in Fig. 5, the RF amplitude increases with aerosol gas flow rate up to 0.6 L/min and then decreases. The RF amplitude increases slightly with forward power (Fig. 6). Summation of each of these curves yields the average voltages shown in Table 2. These average voltages are in the range +1 to +4 volts and are similar to the V_f values seen between the sampler and skimmer. This particular plasma operates with a balanced circuit and probably has a lower plasma potential than the one used for the V_f measurements.

Close examination of the curves shows that the negative-going peaks are more rounded off than the positive ones. Presumably, ions try to flow to the probe when the probe is negative, but the ion current may reach a limit because of the low mobility of ions, or ions response to the RF filed change more slowly by moving through the electrical double layer on the probe surface.

A "blank" experiment was performed with the pump valved off and the chamber allowed to vent with argon from the plasma. The plasma was positioned

against the sampler as usual, but there was no gas flow through the sampling orifice. As shown in Fig. 7, only a small RF voltage is seen in this case, and it is distributed symmetrically about V = 0. This signal is primarily RF pickup in the cable used to connect the probe to the oscilloscope. This RF pickup is small compared to the voltages observed when the plasma was flowing through the sampler, so the signals shown in Figs. 5 and 6 are not merely due to RF interference in the cable. This observation shows that the plasma must flow though the sampling orifice for there to be a substantial RF voltage behind the sampler.

Plasma Rectification

These voltage measurements can be reconciled with previous ones with the aid of Fig. 8, which compares voltage measurements inside and outside the interface. The discussion concentrates on apparent DC voltages measured by slow circuits, but the reader should note that these DC values are actually caused by RF voltages from the plasma. The discussion also presumes that the voltage measured on a floating probe is similar to the floating voltage, i.e., the intercept of an I-V curve from a biased probe.

First, a probe is inserted into a "normal" ICP that is not in contact with a sampler (Fig. 8a). Both ions and electrons go to the probe. Electrons flow to the probe faster than ions, so the probe builds up a negative DC voltage, as seen by Gray et al. [38]. Without contact between the plasma and a reference such as the sampler,

the probe simply floats at ~ -40 V. Such a probe also sees a significant RF voltage determined by the extent of capacitive coupling between the load coil and plasma, as described by Douglas and French [29].

In the next scenario, the probe is inserted into a plasma that is also in contact with the sampler (Fig. 8b). Now the plasma is in electrical contact with ground through the sheath around the sampler. An equivalent circuit that describes the coupling of the plasma to the sampler has been described by Koppenaal [43]. Essentially, the sheath acts like a capacitor, and the plasma is rectified through it. This rectification effect causes the plasma to float to an apparent positive potential, which is sensed by the probe [30].

With the types of load coils used for the V_f measurements reported in this paper, this offset DC voltage is typically a few volts. However, when in the plasma, the probe operates in a collision-dominated regime. Cooling of electrons and recombination of electrons with ions in the boundary layer around the probe can affect the measured voltage [44], which does not necessarily equal the voltage actually present. However, the change in voltage with modest changes in aerosol gas flow rate, power or solvent loading is consistent with changes in mass spectral characteristics such as ion kinetic energies, abundance of doubly charged ions, etc. [30]. Thus, the trends of probe voltage as plasma operating parameters change are probably reasonably representative of the corresponding changes in the plasma, even if the voltages measured do not equal those actually plasma potential.

Next, the probe is put through the skimmer into the supersonic jet (Fig. 8c). The flow through the sampler carries an electron current of ~0.5 mA, as well as an equivalent ion current [14,45]. The ions and electrons present in this gas flow make it a good conductor, and the RF potential from the plasma readily passes through the sampler into the supersonic jet. There is an electrical sheath around the inner edge of the sampler, and this sheath shields the extracted plasma from the electrically-conducting sampler. The sheath inside the edge of the sampler is only ~ 10^{-4} mm thick [38], so the fluctuating RF voltage in the plasma is conducted right through the orifice by the flow of charged particles in the sampled gas. The observation of a reasonable RF potential behind the sampler is further proof that the sheath around the sampler is relatively thin, a point which is belabored at length in electron density and electron temperature studies reported in the companion paper [38].

The RF potential inside the jet can rectify to either the sampler or skimmer, maybe both, in the same way as in the plasma. The conditions inside the jet are reminiscent of those in RF glow discharges, which operate in a similar pressure regime (~ 1 torr) [46].

Finally, the probe is retracted through the skimmer (Fig. 8d). Here the electron density is much lower than in the supersonic jet. In principle, the RF potential from the jet should still pass through the skimmer, because the sheath around the inner edge of the skimmer is ~ 10^{-2} mm thick and is still much smaller than the diameter of the orifice. However, the rectification effect requires enough

charge carriers for a low impedance path from the RF source through the skimmer. Thus, the rectification effect still occurs, and V_f stays positive, when the aerosol gas flow rate is 0 or 0.65 L/min for a dry plasma (Fig. 3), because a low aerosol gas flow rate corresponds to a high electron density in the plasma, the jet and in the beam behind the skimmer [32,35,38].

At higher aerosol gas flow rate or for a wet plasma, the electron density is too low and there is effectively no reference electrode for the rarefied beam behind the skimmer. Therefore, Vf drifts to a negative value for the same reasons a negative voltage is seen with the probe outside the interface in a plasma that is not in contact with a sampler. This explanation also accounts for the unsuccessful attempts to measure voltage with a floating probe behind the skimmer described in last section.

Calorelectric Effect

The probe voltage measured in these experiments is probably also influenced by the calorelectric effect described by Klein [47] and von Engel and Cozens [48]. If two probes are immersed in a flame or plasma, a potential difference develops between the probes if they are at different temperatures. The colder probe is at the more positive potential. This potential difference is suggested to be caused by changes in the electron energy due to collisions and cooling of electrons in the sheath and boundary layer surrounding each probes.

When the ICP is in contact with the sampler, the sampler serves as a second

electrode. If a relatively thick probe (diam. ~ 1 mm) is now swung through the ICP, the boundary layer around the probe is probably thicker and cooler than that at the inner edge of the sampler, because there is no gas flow through the solid probe. Thus, the electrons cool more extensively as they go to the probe, so the calorelectric effect contributes a positive component to the overall probe voltage, measured relative to the grounded sampler. The situation is similar inside the sampler in the supersonic jet. The probe is now immersed in the cold supersonic flow, while both the sampler and skimmer tip are hot. Indeed, Gray's photographs show that the shock waves on the outside of the skimmer make the skimmer tip nearly as hot as the sampler [49]. In the beam behind the skimmer, the probe is also undoubtedly cooler than the skimmer. Hence, the calorelectric effect would be expected to make the probe positive with respect to either the sampler or skimmer.

If the probe is moved into the barrel shock or Mach disk, or into the disturbance thought to exist in this particular system just in front of the skimmer, the probe is heated and its temperature increases. Thus, the probe temperature moves closer to the temperature of the sampler and skimmer, and the measured voltage on the probe becomes less positive, as seen experimentally [38].

Von Engel and Cozens provide a formula for estimating the magnitude of the calorelectric effect.

$$V \sim -(kT_e/2e)\ln(T_e m_+/T_+ m_e)$$

Here T_e = electron temperature (typically 8000 K), T_+ = gas kinetic temperature of

ions (typically 6000 K), m_e = electron mass and m_+ = ion mass (40 g/mole for an argon ICP). Insertion of these typical values into this equation yields a voltage of + 4 volts. Clearly, this phenomenon could readily contribute to the measured DC offset voltages in the ICP and the interface.

Charge Neutrality

Chambers *et al.* have argued that the measurement of a positive voltage in the supersonic jet indicates that the plasma therein deviates from overall charge neutrality. They estimate that a 1% excess of positive ions relative to electrons would suffice to generate the observed potential of several volts [37]. In contrast, the mechanisms discussed above (plasma rectification and the thermoelectric effect) can generate a non-zero voltage on a probe even if the surrounding plasma remains quasineutral. In our opinion, the measurement of a non-zero potential on a probe simply indicates that the probe is surrounded by a cloud of charge carriers whose overall composition is non-neutral, as is the case for an electrode immersed in an electrolyte solution.

Electron densities and temperatures inside the supersonic jet are remarkably like those in the negative glow of a glow discharge, which is commonly considered quasineutral even though a non-zero voltage is seen when a probe is immersed therein. Although we cannot measure electron density and ion density accurately enough to discern a 1% imbalance in overall charge neutrality, we do point out that there are numerous other reasons why a probe in a plasma can float to a non-zero

voltage other than charge imbalance in the bulk of the plasma.

In a plasma beam, electrons play an important role in sustaining positive charged particles. If a plasma is disturbed from neutrality for any reason, naturally there will be large resorting forces striving to re-establish the status of neutrality. Electrons move faster and more likely to lose by diffusion or collision on the metal surface. However, the electrostatic field will be build and tend to keep charge neutrality.

The sampling cone is an electrical conductor. As the sampler is inserted into the plasma, an electrostatic double layer will build up next to the surface of the cone. It is no longer electrically neutral inside the sheath and charge carriers from the plasma can be neutralized as encountered with the sheath on the surface. The charged double layers around the sampler and skimmer have been discussed in our previoues papers (38,39). The space-charge sheath is much thinner than the orifice diameters of the sampler and sampler. It is therefore reasonable to believe that charge separation is not significant as the plasma beam proceeds through the sampler and skimmer. Experimental studies of the supersonic beam properties with RF induced plasma in physics field have demonstrated that the plasma could retain bulk characteristics after sampling through the orifice into a low-pressure chamber (50,51). The movement of the ion beam simply follows the behavior of the neutrals.

In the part I of this serial paper, we have demonstrated that the profiles of electron number densities measued along the axial position as the beam expansion

downstream of the sampler and the skimmer. The evidence of n_e fall-off with $1/z^2$ along the beam axial flow indicates that the movements of ions or electrons are very similar to the neutral beam expansions in the interface of the ICP-MS. The experimental results support the hypothesis that the charged particles flow though the sampler and the skimmer as a quasineutral plasma without significant separation of positive and negative charges.

CONCLUSION

The experimental results demonstrated the correlation of floating voltage and the RF voltage in the ICP-MS interface. The floating voltage V_f generally decreases between the sampler and skimmer and can assume negative polarity downstream of skimmer. The raise of V_f near the skimmer is consistent with the electronnumber density measurements, which may indicate a disturbance in front of the skimmer.

As the plasma flows through the sampler, the RF potential from the ICP source readily passes through the sampler into the supersonic jet. The RF voltage profiles reveal the potential in the extracted beam oscillates at the same frequency as as in the plasma source. As expected, the magnitude of the RF voltage in the extracted beam shows a net positive potential in the supersonic expansion. The observation of a reasonable RF potential behind the sampler is also further proof that the sheath around the sampler is relatively thin and the plasma flows into the ICP-MS by bulk sampling.

LITERATURE CITED

1. S. H. Tan and G. J. Horlick, *Anal Atom. Spectrom.* **2**, 745-763 (1987).
2. B. S. Ross and G. M. Hieftje, *Spectrochim. Acta.* **46B**, 1263-1273 (1991).
3. G. M. Hieftje and L. A. Norman, *Int. J. Mass Spectrom. Ion Phys.* **118/119,** 519-573 (1992).
4. J. S. Crain, R. S. Houk and F. G. Smith, *Spectrochim. Acta.* **43B**, 1355-1364 (1988).
5. D. C. Gregoire, and G. Horlick, *Appl. Spectrosc.* **41**, 897 (1987).
6. B. S. Sheppard, W. L. Shen, and J.A. Caruso, *Anal. Chem.*, **63**, 1491 (1991).
7. G. M. Hieftje and L. A. Norman, *Int. J. Mass Spectrom. Ion Phys.* **118/119,** 519-573 (1992).
8. B. S. Ross, D. M. Chambers, and G. M. Hieftje, *Microchim. Acta.* **11**, 287 (1990)
9. P. J. Turner, *In Applications of Plasma Source Mass Spectrometry,* Holland, Eaton, A. N. (Eds.), Thomas Graham House. Science Park. Cambridge, (1991)
10. G. M. Hieftje and G. H. Vickers, *Anal. Chim. Acta* **216**, 1-24 (1989).
11. R. S. Houk, S. C. K. Shum, D. R. Wiederin, *Anal. Chim. Acta.* **250**, 61-70 (1991)
12. D. J. Douglas, *"Fundamental Aspects of ICP-MS"*, ICPs in Analytical Atomic Spectrometry, eds. A. Montaser and D. Golightly, 2nd Edn., VCH, New York

1991.

13. D. J. Douglas and J. B. French, *Anal. Atom. Spectrom.* **3**, 743 (1988).

14. S. D. Tanner, *Spectrochim. Acta, Part B*, **47B**, 809 (1992).

15. G. R. Gillson, D. J. Douglas, J. E. Fulford, K. W. Halligan and S. D. Tanner, *Anal. Chem.*, **60**, 1472 (1988).

16. J. S. Crain, R. S. Houk and F. G. Smith, *Spectrochim. Acta* **43B**, 1355 (1988).

17. H. B. Lim, R. S. Houk, M. C. Edelson, and K. P. Carney, *J. Anal. Atom. Spectrom.* **4**, 365 (1989).

18. H. Kawaguchi, K. Asada and A. Mizuike, *Mikrochim. Acta* **3**, 143 (1988).

19. R. S. Houk and H. B. Lim, *Anal. Chem.* **58**, 3244 (1986).

20. A. L. Gray, *J. Anal. Atom. Spectrom.* **4**, 371 (1989).

21. D. M. Chambers and G. M. Hieftje, *Spectrochim. Acta, Part B*, **46B**, 761 (1991).

22. J. E. Fulford and D. J. Douglas, *Appl. Spectrosc.*, **40**, 971 (1986).

23. J. A. Olivares and R. S. Houk, *Appl. Spectrosc.*, **39**, 1070 (1985).

24. S. D. Tanner, *J. Anal. Atomic Spectrom.*, 1993, submitted.

25. R. S. Houk, Ion Deposition

26. R. K. Winge, J. S. Crain and R. S. Houk, *J. Anal. At. Spectrom.*, **6**, 601 (1991)

27. N. Furuta, *J. Anal. At. Spectrom.*, **6**, 199 (1991).

28. A. T. Ince, J. G. Williams and A. L. Gray, *J. Anal. At. Spectrom.*, **8**, 899

(1993)

29. D. J. Douglas and J. B. French, *Spectrochim. Acta* **41B**, 197 (1986).

30. A. L. Gray, R. S. Houk and J. G. Williams, *J. Anal. Atom. Spectrom.* **2**, 13 (1987).

31. R. S. Houk, J. K. Schoer and J. S. Crain, *J. Anal. Atom. Spectrom.* **2**, 283 (1987).

32. L. Pei-qi, G. Pei-zhong, L. Tie-zheng and R. S. Houk, *Spectrochim. Acta* **43B**, 273 (1988).

33. N. Jakubowski, B. J. Raeymaekers, J. A. C. Broekart and D. Stuewar, *Spectrochim. Acta* **44B**, 219 (1989).

34. R. S. Houk and H. B. Lim, *Anal. Chem.* **58**, 3244 (1986).

35. H. B. Lim, R. S. Houk and J. S. Crain, *Spectrochim. Acta* **44B**, 989 (1989).

36. H. B. Lim and R. S. Houk, *Spectrochim. Acta* **45B**, 453 (1990).

37. D. M. Chambers, J. Poehlman, P Yang, G. M. Hieftje, *Spectrochim. Acta*, Part B, **46B**, 741 (1991).

38. H. Niu and H. S. Houk, *Spectrochim. Acta.* in press, (1994).

39. H. Niu, K. Hu and R. S. Houk, *Spectrochim. Acta.* 46B, 805-817, (1991)

40. Ultrasonic Nebulizer, Model U-5000, Cetac Technologies, Omaha, NE.

41. R. S. Houk, "Instrumentation for ICP-MS", in *Handbook of Inductively Coupled Plasma Mass Spectrometry*, Ed. by K. E. Jarvis, A. L. Gray and R. S. Houk, Blackie, London (1992).

42. S. Greenfield and A. Montaser, *Inductively Coupled Plasma in Analytical Atomic Spectrometry,* A. Montaser and D. W. Golightly, (Eds.), 2nd Edition, VCH, New York, Ch. 4, (1992)

43. D. W. Koppenaal, and L. F. Quinton, *J. Anal Atom. Spectrom.*, **3**, 667 (1988).

44. R. M. Clements and P. R. Smy, *J. Phys. D: Appl. Phys.*, **7**, 551 (1974).

45. J. A. Olivares and R. S. Houk, *Anal. Chem.* **57**, 2674 (1985).

46. B. Chapman, *Glow discharge Processes*, Chapters 3 and 5, John Wiley & Sons, New York (1980).

47. S. Klein, C. R. Acad. Sci., Paris, **251**, 657, 2492 (1960).

48. A. von Engel and J. R. Cozens, *Proc. Phys. Soc.*, 1963, Vol. **82** (1963).

49. A. L. Gray, *Anal. At. Spectrom.* **4**, 371-373, (1989).

50. R. B. Fraser, F. Robben, and L. Talbot, *Phys. Fluids,* **14**, 2317-2327 (1971).

51. R. H. Kirchoff and L. Talbot, *AIAAJ.* **9**, 1098 (1971).

Table 1. Instrumental components used in RF voltage measurements

Component	Manufacturer/description
ICP generator	
Perkin-Elmer Optima 3000 free-running RF generator with True Power Control (TPC)	RF power: 1100 W Frequency: 40-MHz
ICP torch	
Perkin-Elmer Optima 3000 demountable torch with 2.0-mm i.d. alumina injector	Plasma argon flow: 15 L/min Auxiliary argon flow: 1.0 L/min Torch mouth shortened by 10 mm
Nebulizer	
GemTip™ cross-flow nebulizer	Nebulizer argon flow: 1.000 L/min
Spray chamber	
Ryton Scott-type, double-pass spray chamber with pumped drain	
Peristaltic pump	
Gilson Minipuls 3 two channel peristaltic pump	Liquid uptake rate: 1.0 mL/min pump tubing i.d. : 0.76 mm
Extraction system	
Ames Laboratory construction (See Fig. 2)	Sampler Orifice diameter: 1.02 mm Orifice centered on the ICP source Sampling position: 15.0 mm above top of load coil (*ca.* 10 mm from tip of initial radiation zone when Y was introduced at 1000 mg/L)

Table 1. (continued)

Component	Manufacturer/description
Pressure measurement	
Granville-Phillips series 275 analog readout convectron vacuum gauge (calibrated for N_2)	Operating pressure: 1.8 torr (converted to argon pressure) while sampling ICP
Inline valve	
MDC KIV-150 high vacuum inline valve	
Vacuum pump	
Edwards E2M18 rotary vacuum pump	Speed (pneurop): 20.4 m^3/h
Oscilloscope	
Hewlett Packard 54503A 500-MHz digitizing oscilloscope	Coupling: d.c. Waveforms stored in non-volatile memories of the oscilloscope and then transferred to PC via IOtech MP488CT IEEE bus interface board using ASYST 4.01 software

Table 2. Average voltage values from RF potential measurements shown in Figs. 5 and 6.

Aerosol gas flow rate (L/min)	Forward power (kW)	Average voltage (V)
0.000	1.10	3.00
0.200	1.10	3.63
0.400	1.10	3.63
0.500	1.10	4.10
0.600	1.10	2.92
0.800	1.10	1.74
1.000	1.10	1.18
1.200	1.10	0.95
1.000	0.90	1.26
1.000	1.10	1.18
1.000	1.30	1.10
1.000	1.50	1.18

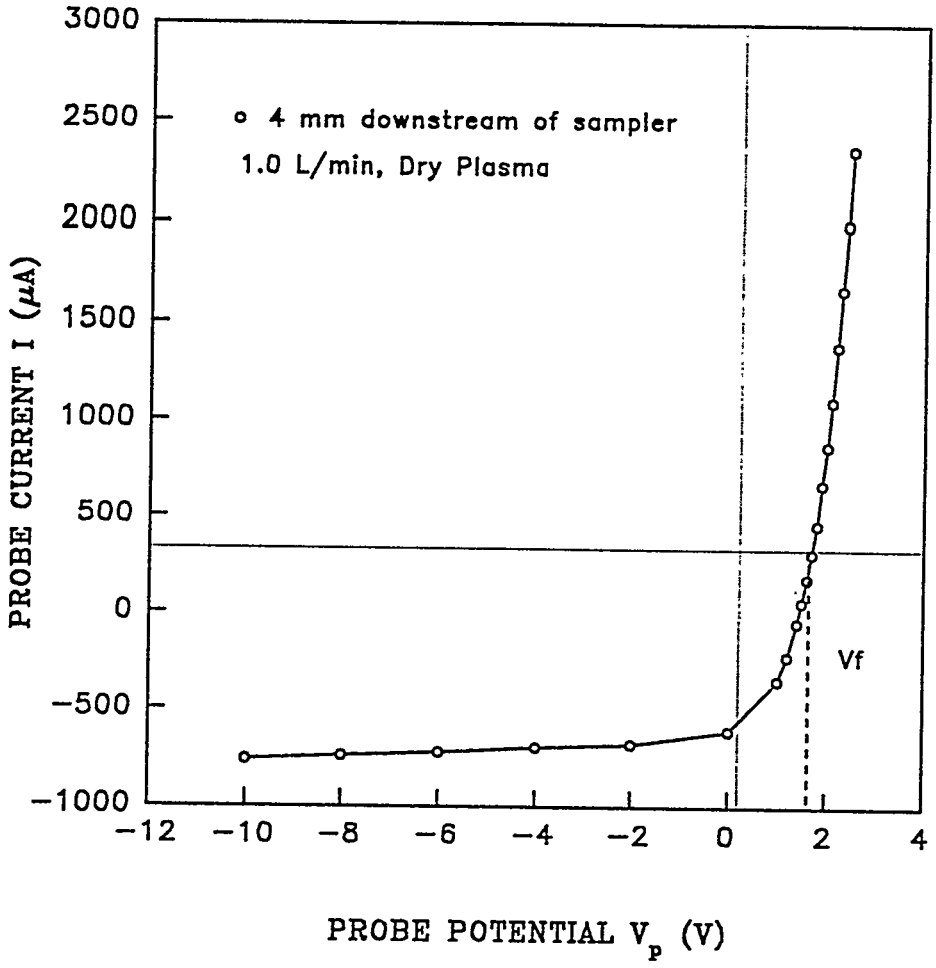

Fig. 1. Typical I-V curve. The intercept with the horizontal axis is the V_f value.

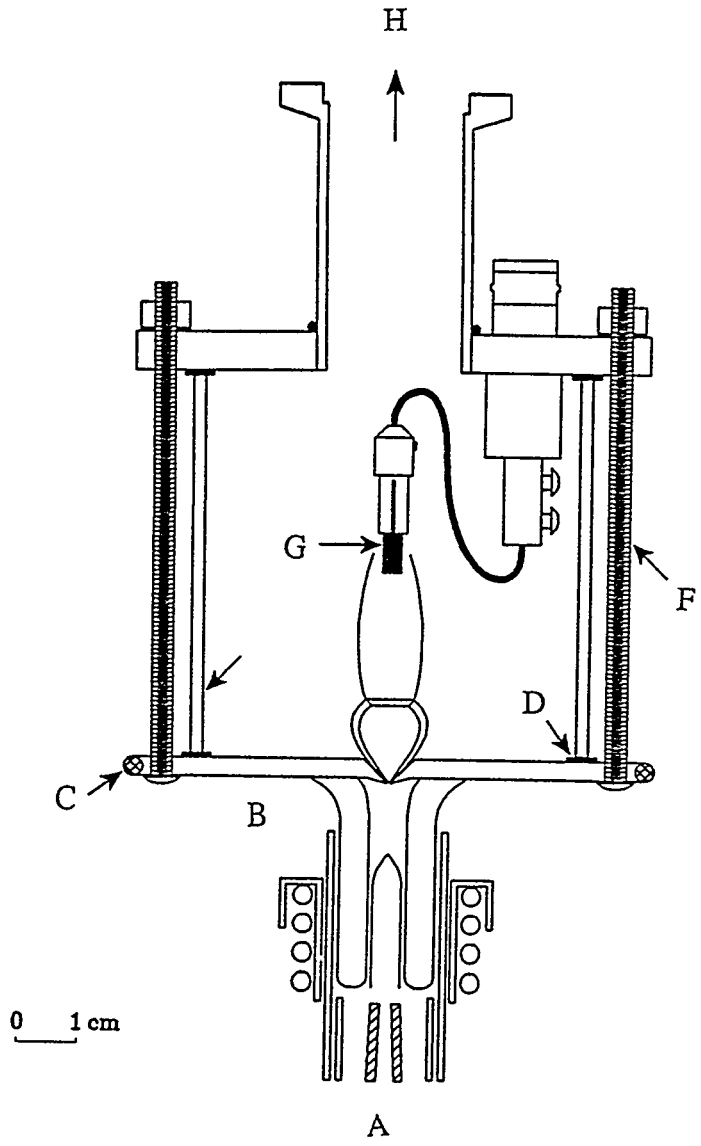

Fig. 2. ICP and extraction system for RF voltage measurements. A: ICP torch, load coil and bonnet; B: copper sampling disk; C: water cooling coil; D: Viton gasket; E: cylindrical quartz wall; F: threaded retaining rods; G: graphite electrode with connection to electrical feedthrough; and H: pumping port.

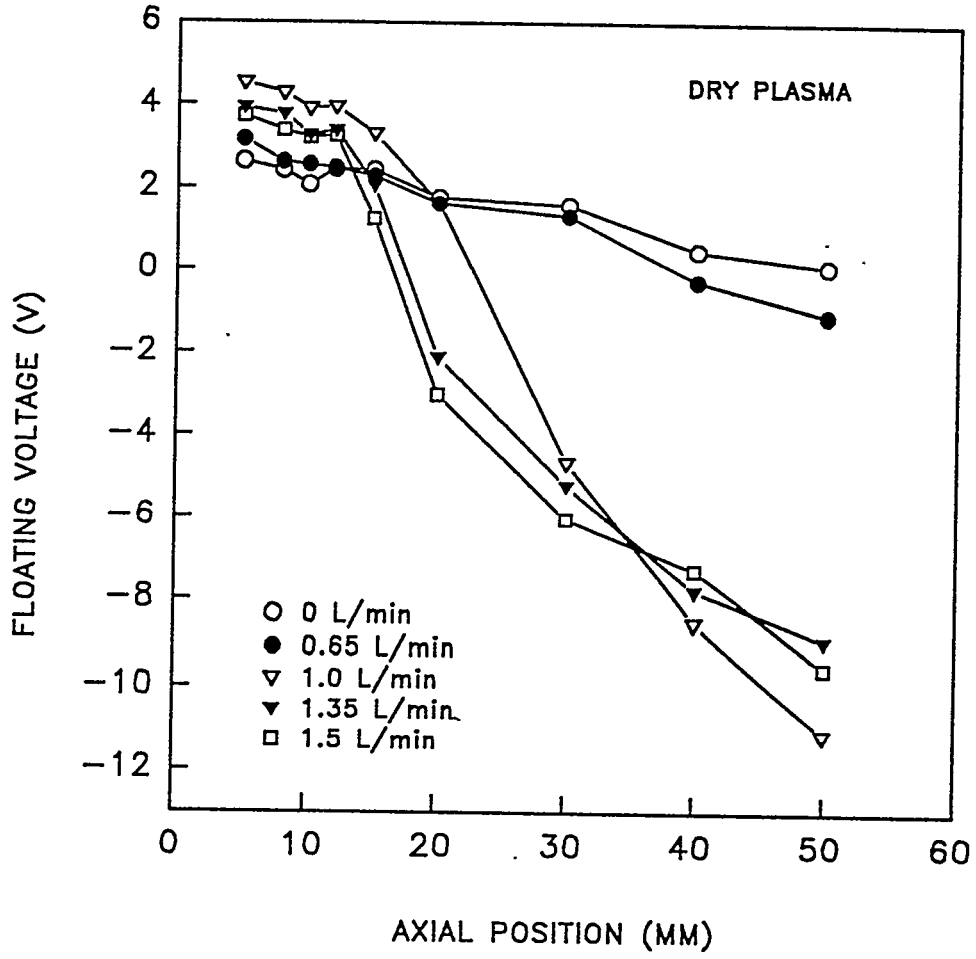

Fig. 3. Measured values of V_f for dry ICP at various aerosol gas flow rates (shown in caption). The sampler orifice is at 0 mm. The skimmer tip is at 10 mm. The forward power is 1.25 kw.

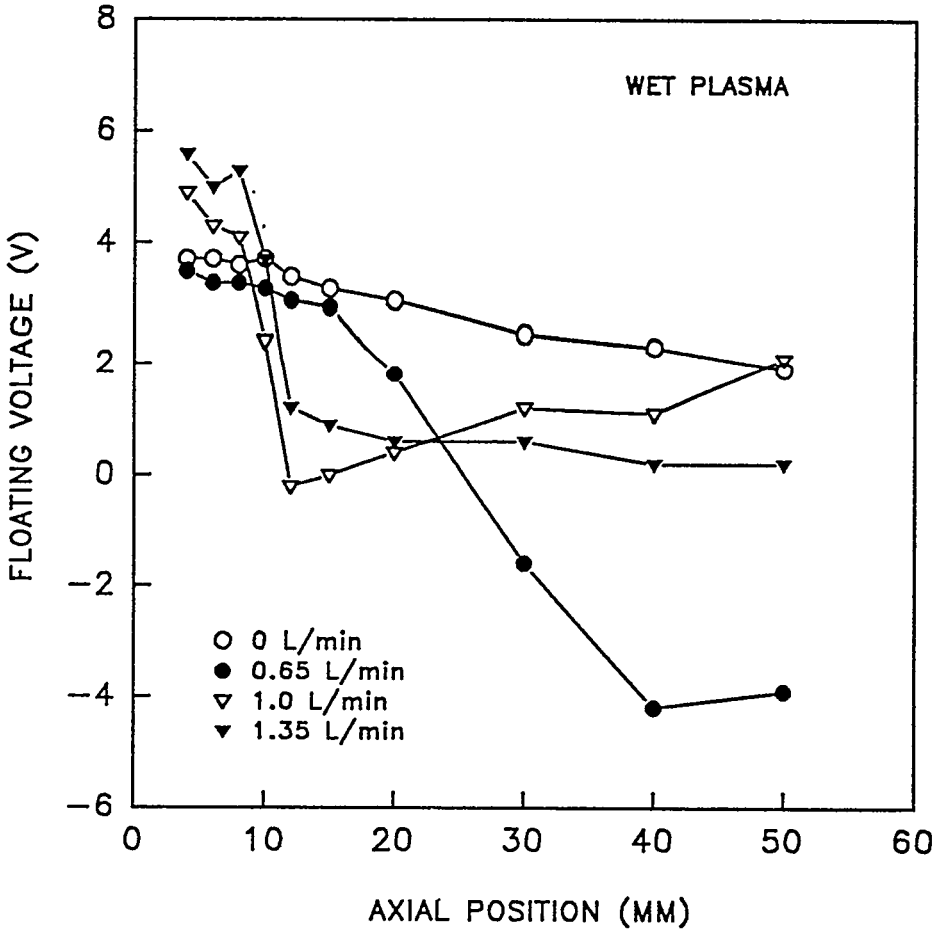

Fig. 4. Measured values of V_f for wet plasma at various aerosol gas flow rates.

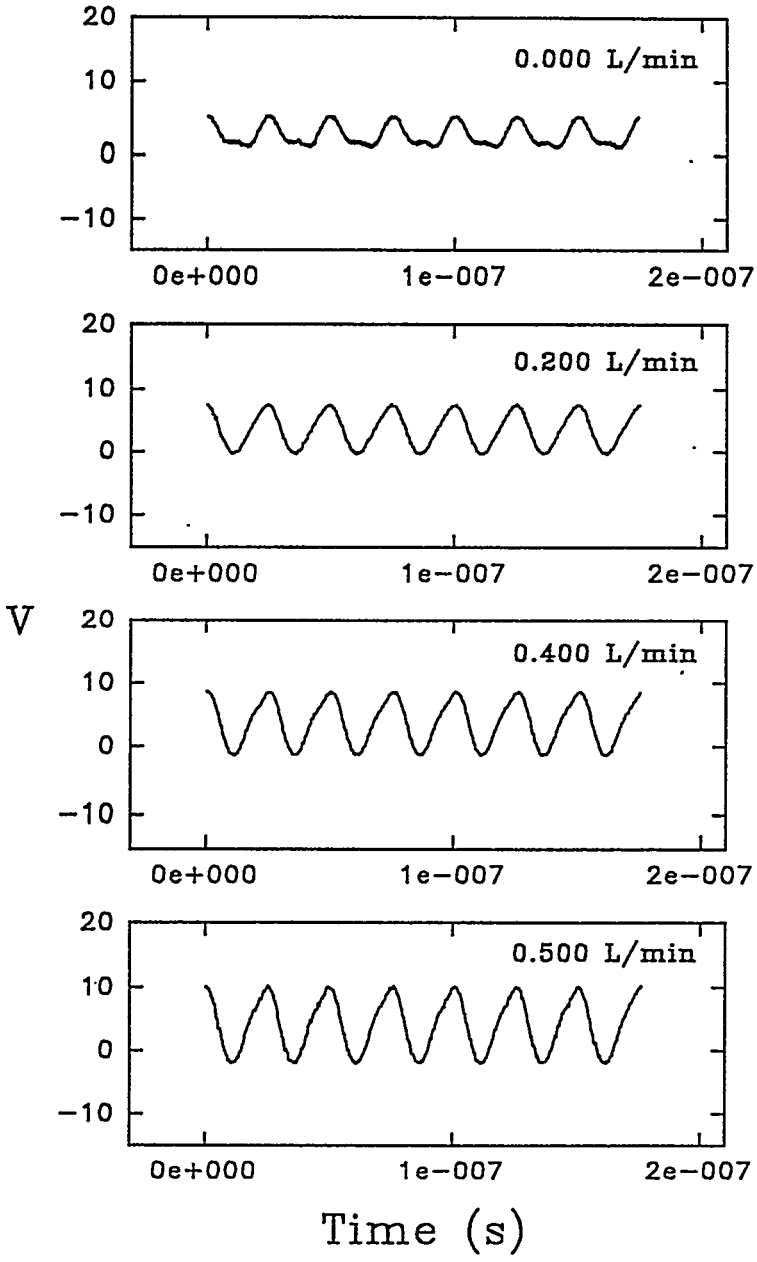

Fig. 5. Measured RF voltage waveforms at various values of aerosol gas flow rate. The forward power is 1.1 kW.

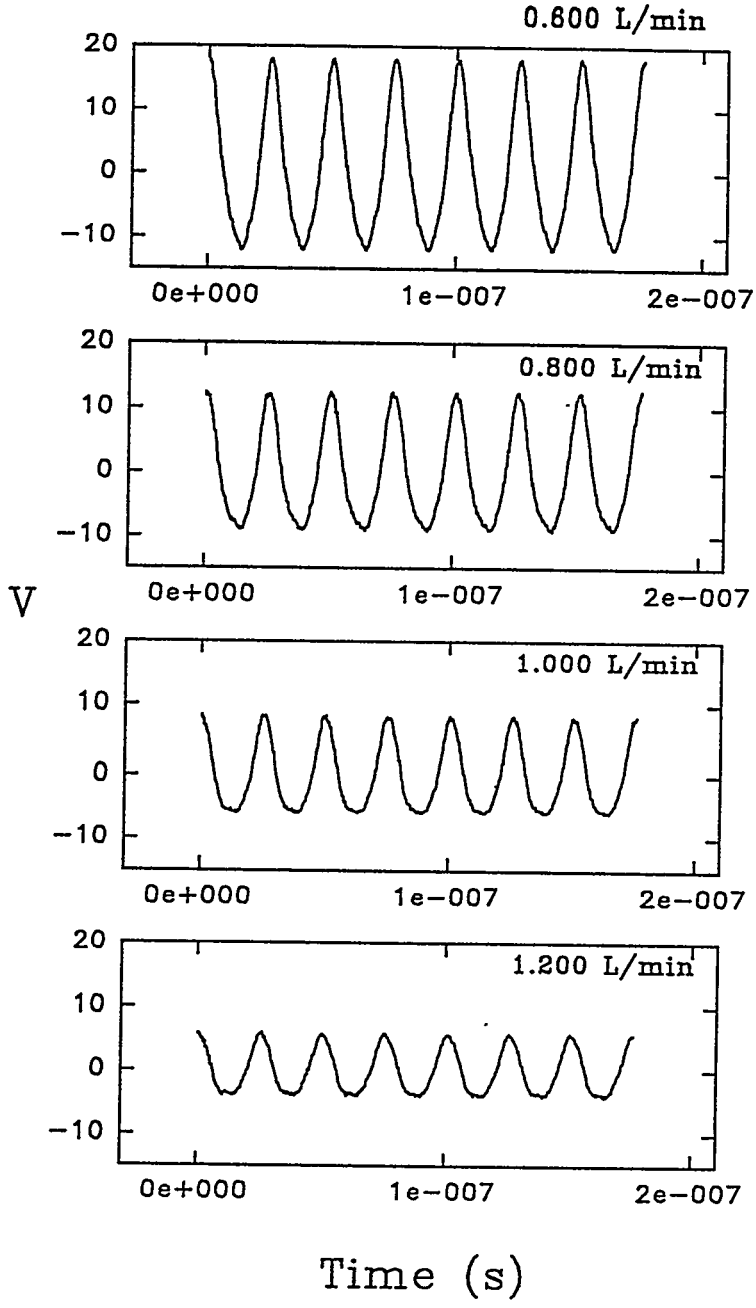

Fig. 5. (continued)

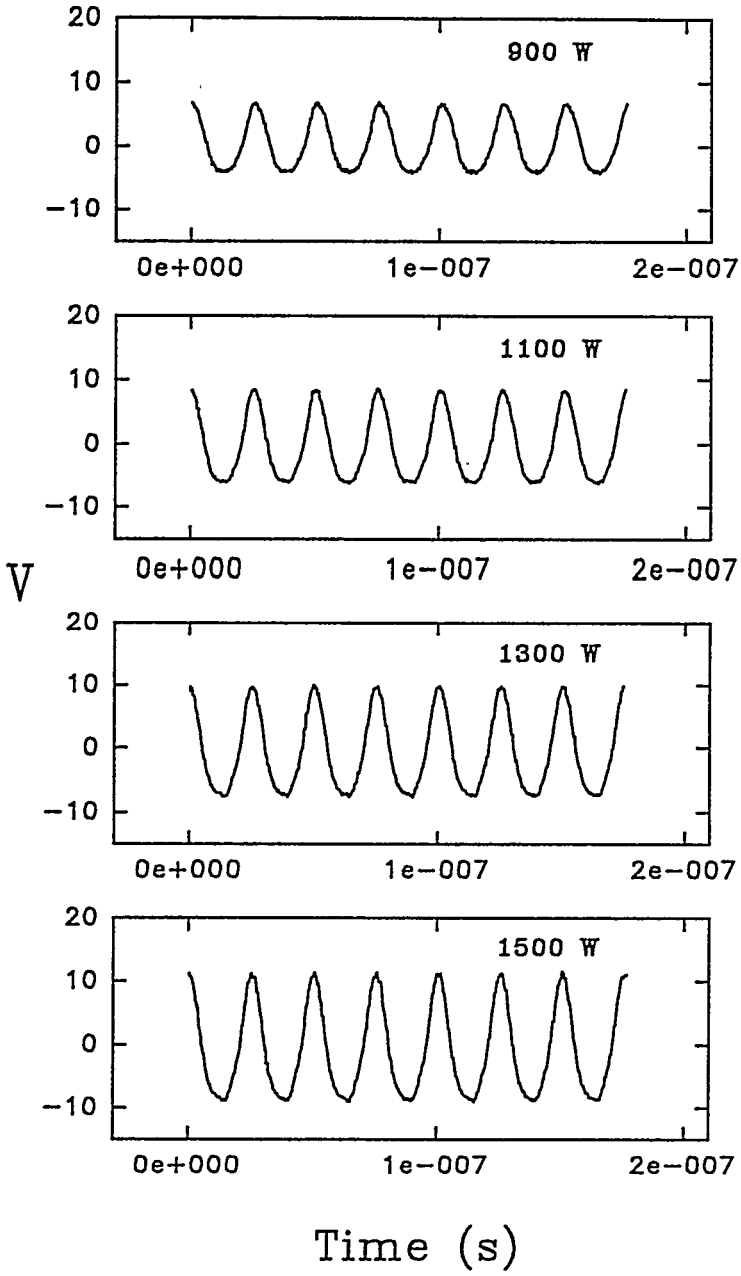

Fig. 6. Measured RF voltage waveforms at various values of forward power. The aerosol gas flow rate is 1.0 L/min.

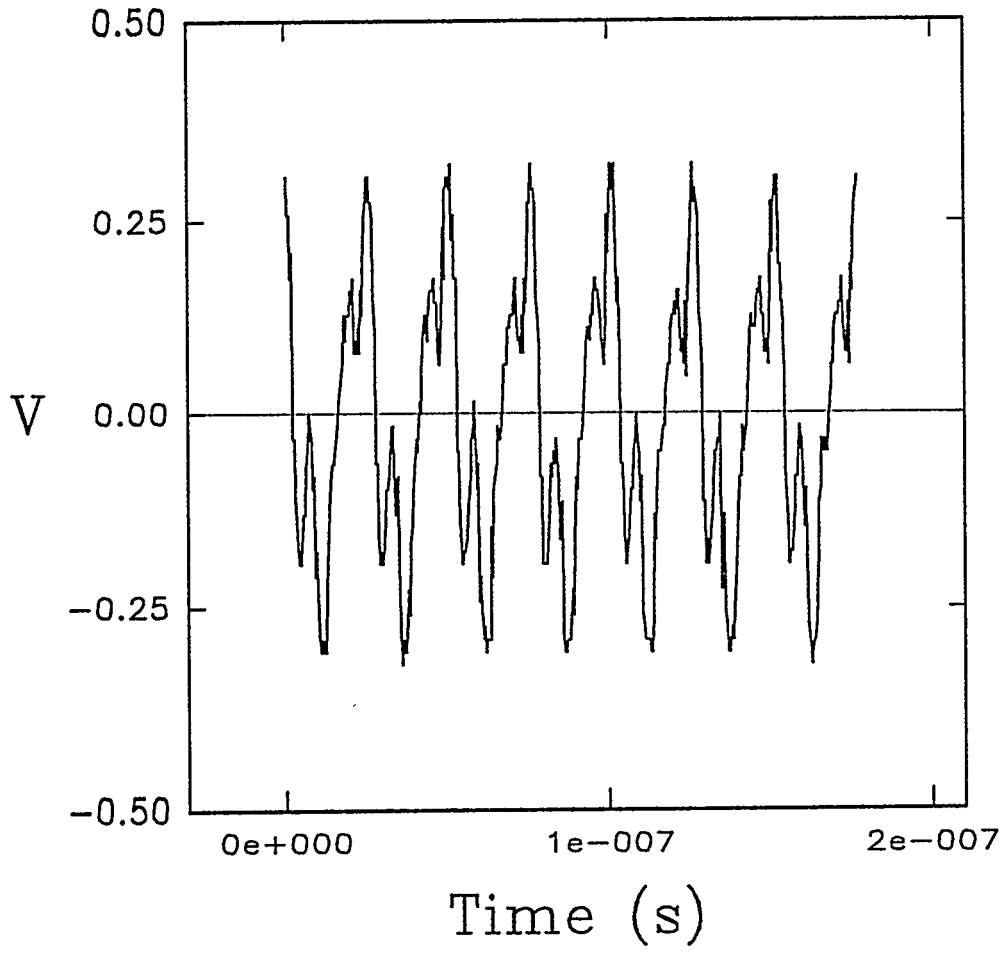

Fig. 7. Measured RF voltage waveform for "blank" situation when there is no flow of plasma through the sampling orifice.

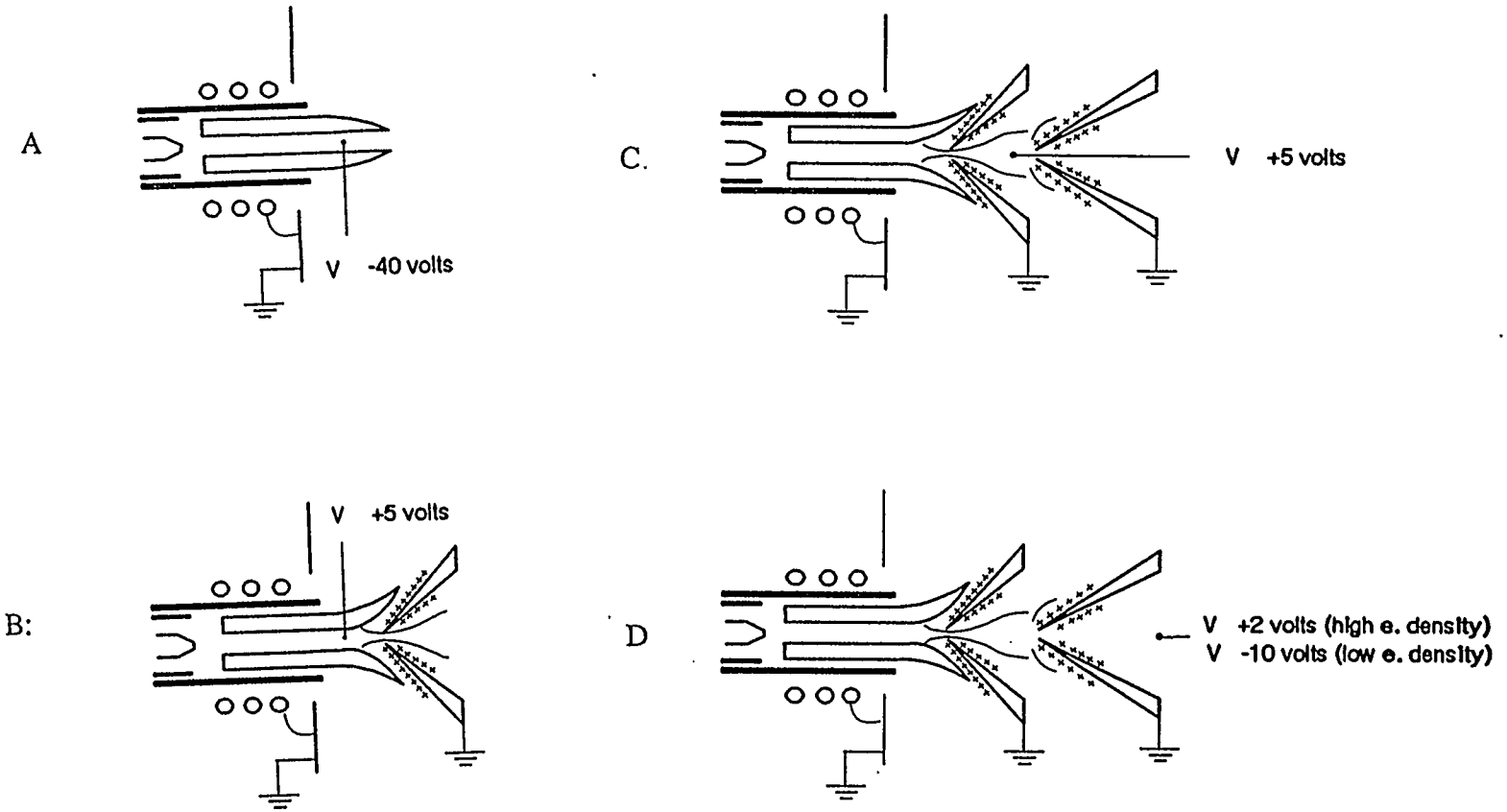

Fig. 8. Schematic diagram illustrating the behavior of probe voltage in four locations. A: probe in ICP with no sampler; B: probe in ICP that is also being extracted through sampler; C: probe inside supersonic jet; D: probe in beam leaving skimmer.

SUMMARY AND FUTURE RESEARCH

This dissertation is focused on studies of plasma extraction and beam formation processes in ICP-MS. Fundamental and practical aspects are described for extracting ions from an atmospheric pressure plasma source into an analytical mass spectrometer. Methodologies and basic concepts for interfacing the ICP ion source to the quadrupole mass spectrometer are emphasized. Some new developments and innovative designs are introduced.

The axially resolved distributions of electron density and temperature are investigated in effort to gain more physical insight of the beam processes in the interface of an ICP-MS. The beam expansion was studies by Langmuir probe measurements under different plasma conditions. A single Langmuir probe is inserted through the skimmer into the supersonic jet. Electron temperature and electron number density are measured with axial spatial resolution from 2 mm behind the sampler to 45 mm behind the skimmer. In the upstream part of the supersonic jet, n_e drop as axial position increases, as expected for a quasineutral beam. However, the measurements indicate the presence of an unexpected disturbance in front of the skimmer. Electron density behind the skimmer is much lower than would be expected if the skimmer behaved ideally. Plasma conditions that yield a high plasma potential and secondary discharge lead to further reductions in n_e behind the skimmer. The measurements generally support the concept that the extracted plasma remains

quasineutral as it passes through the sampler and skimmer in ICP-MS.

Examination of the experimental results leads to several interesting observations. The electron densities estimated at the sampler are in the range 7 x 10^{14} to 9 x 10^{15} cm^{-3}, which is reasonable. The electron densities measured at the skimmer tip are in the range 5 x 10^{12} to 9 x $10^{10}cm^{-3}$. The electron density dropped by a factor of about 10^3 along the centerline between sampler and skimmer cones in the first stage and continued to drop by a further factor of 10^4-10^5 downstream of skimmer to the ion lens. At an aerosol flow rate of 1.0 L/min for a dry plasma, electron density (n_e) is about 5 x 10^{12} cm^{-3} near the skimmer tip and drops abruptly to 5 x 10^8 cm^{-3} downstream further behind the skimmer. Electron density in the beam leaving the skimmer also depends on water loading and on the presence and mass of matrix elements.

The experimental results was compared with the ideal free-expansion of neutral gas. In the first stage, the ion beam density parallels that of a neutral beam with no skimmer interactions. Initially, the beam expansion behind the sampler cone exhibited a $1/Z^2$ intensity fall-off. As the beam approaching the skimmer, n_e stay above the predicted value. After passing the skimmer orifice the beam behavior obviously deviated from the ideal predictions in the second stage. An second beam expansion originating at the skimmer entrance was observed and the beam flow underwent with another $1/Z^2$ fall-off behind the skimmer.

The beam intensity attenuated by a factor of $\sim 10^7$ in the centerline of the

beam flow from the sampler to the ion lens. The skimming effects are proposed to be a major cause of ion loss in ICP-MS instruments. As the skimmer presented in the supersonic expansion, the plasma flow was interrupted and underwent a second beam expansion in the second vacuum stage.

The experimental observations of skimmer interference suggest that proper functioning of the skimmer is a key to success in the ICP-MS interface design. To further display such effects, more experimental investigations may be valuable such as matrix effect study and plasma beam potential measurement.

Electron temperature in the region between the sampler and skimmer was generally at a value near the source and was cooled substantially when the beam passed the skimmer. Electron temperature (T_e) is generally in the range 2000 - 11000 K and changes with probe inside an aerosol gas flow. However, T_e still remain very high in comparison with the neural beam temperature. It is reasonable to assume that ion-electron recombination in the present studies is minimal because of the high electron temperature measured in the beam expansion processes. The recombination rate coefficient is a strong inverse function of the temperature.

A T_e range of 4000 - 8000 K is reasonable in the ICP. As the plasma extracted into the interface of the mass spectrometer, the electron temperature may be changed by the sampling process. There is no consistent trend of T_e with axial position in the jet. Sometimes, T_e drops smoothly by $\sim$2000 K as the beam nears the skimmer. In other cases, there is a $\sim$1000 K increase in T_e near the skimmer, which

could be caused by the same disturbance that affects n_e, as discussed above.

Plasma conditions that cause a high plasma potential and secondary discharge elevate T_e drastically to values much higher than would be expected from the ICP alone. The secondary discharge is thought to increase the velocities and velocity spread of the electrons to artificially high values as they are extracted. Thus, T_e changes with water loading and aerosol gas flow rate in the opposite direction expected from the behavior of T_e as these parameters are changed in the ICP alone. Electron temperature is apparently much more sensitive to plasma potential than n_e, as if a mild secondary discharge can readily affect the velocities of existing free electrons but does not create many new electrons by further ionization.

Behind the skimmer ($z > 10$ mm), a surprising result is obtained. T_e drops drastically to values as low as 2000 K at $z = 20$ mm. T_e then increases again at $z > 30$ mm. One possible explanation for this trend may be diffusional cooling. In a beam containing electrons, the faster ones tend to diffuse farther from the center and are progressively depleted from the central axis as the beam moves farther away from the source. A smaller spread of velocities corresponds to a lower numerical value of T_e. Thus, removal of some of the faster electrons would diminish the measured T_e value in the center as the beam travels further downstream. However, this rationale does not account for the subsequent rise in T_e observed after $z > 25$ mm, which remains unexplained. Perhaps the rise in T_e after $z > 25$ mm represents the breakdown of quasineutrality in the extracted beam. As discussed in the next

section, the Debye length becomes large here, so perhaps external fields (such as floating potential) can accelerate and re-heat electrons when the beam gets well behind the skimmer.

The measured floating voltages are in the range of +2 to +5 volts. V_f generally decreases downstream of sampler and through the skimmer. Negative values of V_f were measured downstream of skimmer. The experimental results demonstrated the correlation of floating voltage and the RF voltage in the ICP-MS interface.

The floating voltage V_f generally decreases between the sampler and skimmer and can assume negative polarity downstream of skimmer. As the plasma flows through the sampler, the RF potential from the ICP source readily passes through the sampler into the supersonic jet. The RF voltage profiles reveal the potential in the extracted beam oscillates at the same frequency as as in the plasma source. As expected, the magnitude of the RF voltage in the extracted beam shows a net positive potential in the supersonic expansion. The observation of a reasonable RF potential behind the sampler is also further proof that the sheath around the sampler is relatively thin and the plasma flows into the ICP-MS by bulk sampling. The probe voltage measured in these experiments is probably affected by plasma "rectification effect" and the "calorelectric effect." The raise of V_f near the skimmer is consistent with the electronnumber density measurements, which may indicate a disturbance in front of the skimmer.

Some additional interesting studies are suggested by these results. Is the

disturbance in front of the skimmer a general phenomenon seen in other ICP-MS devices or is the disturbance unique to the skimmer geometry and gas flows used in this study? Optical measurements of the basic properties of this disturbance at various skimmer cone angles and skimming positions should prove interesting in this regard. If indeed the ion density behind the skimmer is several orders of magnitude below that expected for an ideal quasineutral beam, what happened to the lost ions? We have been attempting to deposit ions behind the skimmer onto spatially separated solid targets to address this issue as has Farnsworth's group (61). Can anything be done to mitigate the extensive loss of ions in the beam behind the skimmer? How are the beam properties affected by highly concentrated matrix elements and by the application of various voltages to the ion lenses? Clearly, important questions remain in our basic understanding of the ion extraction process in ICP-MS.

ADDITIONAL LITERATURE CITED

1. Fassel, V. A.; Kniseley, R. N. Anal. Chem. 1974, 46, 1110A, 1155A.
2. Fassel, V. A. 1978, Science 202, 183.
3. Houk, R. S.; Fassel, V. A.; Flesch, G. D.; Svec, H. J.; Gray A. L. and Taylor, C.E. 1980, Anal. Chem. 52, 2283.
4. Gray, A. L. Analyst 1975, 100, 289.
5. Gray, A. L. Anal. Chem. 1975, 47, 600.
6. Houk, R.S.; Fassel, V. A. and Svec, H. J. Dyn. Mass Spectrom. 1981, 6, 234-251.
7. Douglas, D. J. and French, J. B. Anal. Chem. 1981, 53, 37-41.
8. Douglas, D. J.; Quan, E. S. K. and Smith, R. G. Spectrochim. Acta 1983, 38B, 39-48.
9. Date, A. R. and Gray, A. L. Analyst 1981, 106, 1255-1267.
10. Gray, A. L. and Date, A. R. Dyn. Mass Spectrom. 1981, 6, 252-266.
11. Date, A. R. and Gray, A. L. Analyst 1983, 108, 159-165.
12. Gray, A. L. and Date, A. R. Int. J. Mass Spectrom. Ion Phys. 1983, 46, 7-10.
13. Gray, A. L. and Date, A. R. Int. J. Mass Spectrom. Ion Phys. 1983, 48, 357-360.
14. Elan ICP-MS system, Sciex, 55 Glen Cameron Rd., Thornhill, Ontario, L3T 1P2, Canada.

15. Plasma Quad ICP-MS system, V. G. Isotopes Ltd., Ion Path, Road Three, Winsford, Cheshire, CW 73BX, England.

16. Hieftje, G. M.; and Norman, L. A. Int. J. Mass Spectrom. Ion Phys. 1992, 118/119, 519-573.

17. Hieftje. G. M.; and Vickers, G. H. Anal. Chim. Acta 1989, 216, 1-24.

18. Jarvis, K. E.; Gray, A. L. and Houk, R. S. Handbook of Inductively Coupled Plasma Mass Spectrometry, 1992, Blackie, London.

19. Montaser, A. and Golightly, D. W. (Eds.), Inductively Coupled Plasma in Analytical Atomic Spectrometry, 1992, 2nd Edition, VCH, New York, Ch. 12, 13, 14.

20. Holland, G. and Eaton, A. N.(Eds.), Application of Plasma Source Mass Spectrometry, 1991, Royal Soc. Chem., Cambridge.

21. Jarvis, K. E.; Gray, A. L.; Williams, J. G.; and I. Jarvis (Eds.), Plasma Source Mass Spectrometry, 1990, Royal Soc. Chem., Cambridge.

22. Date, A. R.; and Gray A. L. (Eds.), Applications of Inductively Coupled Plasma Mass Spectrometry, 1989, Blackie, London.

23. Gray, A. L. Adv. Mass. Spectrom., 1989, 11B, 1674.

24. Houk, R. S. Anal. Chem. 1986, 58 97A.

25 Houk, R. S. and S. J. Jiang, in I. S. Krull (Ed.), Trace Metal Analysis and Speciation, Elsevier, Amsterdam, 1991, Ch. 5.

26. Shen, W. L.; Vela, N. P.; Sheppard, B. S. and J. A. Caruso, Anal. Chem.,

1991, 63, 1491.

27. Shum, S. C. K.; Pang, H. M. and Houk, R. S. Anal. Chem. 1992, 64, 2444.

28. Douglas, D. J. and French, J. B. Spectrochim. Acta. 1986, 41B, 197-204.

29. Bradshaw, N.; Hall, E. F. H.; Snaderson, N. E. J. Anal Atom. Spectrom. 1989, 4, 801-803.

30. Turner, P. J. Fourth Surry Conf. on Plasma Source Mass Spectrometry, Guildford, UK, July 1991.

31. Turner, P. J. In Applications of Plasma Source Mass Spectrometry, 1991, Holland, Eaton, A. N. Eds., Thomas Graham House. Science Park. Cambridge.

32. Hu, Ke; Clemon, P. S and Houk, R. S. J. Am Soc Mass Spectrom 1993, 4, 16-27.

33. Varian Analytical Instruments, In the 1993 Pittsburgh Conference Atlanta, Georgia, April, 1993.

34. Skata,K. 18th FACSS Conf., Anaheim, CA, October 1991, Paper No. 528.

35. Potter, D. In the 1994 Pittsburgh Conference, Chicago, IL, May, 1994.

36. Crain, J. S.; Houk, R. S. and Smith, F. G. Spectrochim. Acta. 1988, 43B, 1355-1364.

37. Tan, S. H. and Horlick, G. J. Anal Atom. Spectrom. 1987, 2, 745-763.

38. Ross, B. S. and Hieftje, G. M. Spectrochim. Acta. 1991, 9, 1263-1273.

39. Gregoire, D. C. and Horlick, G. Appl. Spectrosc. 1987, 41, 897.

40. Sheppard, B.S.; Shen, W.L. and J.A. Caruso, Anal. Chem., 1991, 63, 1491.

41. Olivares, J. A. and Houk, R. S. Anal. Chem. 1986, 58 21.

42. Vaughan, M. and Horlick, G. Appl. Spectrosc. 1986, 40, 434.

43. Ross, B. S.; Chambers, D.M. and Hieftje, G. M.; Microchim. Acta. 1990, 11, 287.

44. Gray, A. L. J. Anal Atom. Spectrom. 1986, 1, 247-249.

44. Date, A. R. and Cheung, Y. Y.; and Stuart, M. E. Spectrochim. Acta 1987, 42b, 3.

45. Gray, A. L. and Williams, J. G. J. Anal Atom. Spectrom. 1987, 2, 599.

46. Smith, F. G. Wiederin, D. R. and Houk, R. S. and Spectrochim. Acta. 1988, 43B, 1355-1364.

47. Evans, E. H. and Ebdon, L J. Anal Atom. Spectrom. 1990, 5, 425.

48. Furuta, N. and Ebdon, L J. Anal Atom. Spectrom. 1991, 6, 199.

49. Hobbs, S. E. and Olesik, Anal. Chem. 1992, 64 274-283.

50. Douglas, D. J. and Kerr. L. A. J. Anal Atom. Spectrom. 1988, 3, 749

51. Crain, J. S.; Houk, R. S. and Eckels, D. E. Anal. Chem. 1989, 6, 606-612.

52. Swift, J. D.; Schwar, M. J. R. Electrical Probes for Plasma Diagnostics 1969, Am. els.: New York.

53. Smy, P. R. Advanced in Physics 1976, 25, 517.

54. Lim, H. B.; Houk, R. S. and Crain, J. S. Spectrochim. Acta. 1989, 44B, 989-998.

55. Clements, R. M. and Smy, P. R. J. Phys. D: Appl. Phys. 1974, 7, 551.

56. Douglas, D. J. and French, J. B. Spectrochim. Acta. 1986, 41B, 197-204.

57. Gray, A. L. and Houk, R. S.; Williams, J. G. J. Anal Atom. Spectrom. 1987, 2, 283.

58. Houk, R. S.; Lim, H. B. Anal. Chem. 1986, 58 3244.

59. Chambers, D. M.; Poehlman, J.; Yang, P. and Hieftje, G. M. Spectrochim. Acta. 1991, 46B, 741-760.

60. Niu, H. S.; Hu, Ke and Houk, R. S. Spectrochim. Acta. 1991, 46B, 805.

61. Farnsworth, P.; Chen, Y.; Lee, M.; Wu, M. and J. Sin, *Pittsburgh Conf. on Anal. Chem. and Appl. Spectros.*, Chicago, IL, February-March, Paper No. 7, (1994).

ACKNOWLEDGEMENTS

I would like, first of all to express my sincere gratitude to professor R. S. Houk, whose direction, guidance, enthusiasm, and support made this work possible. I also greatly appreciate his wide latitude, encouragement and indulgence to allow me to explore many new ideas and novel technical designs beyond this dissertation, even though results were often fruitless. His friendship and support have meant and continues to mean a great deal to me.

Sincere appreciation is also extended Dr. James Fritz, Dr. Therese Cotton, Dr. James Espenson, Dr. Hsung-Cheng Hsieh, and Dr. Henry Stahr, who serve as my committee members. Their critical reading of this manuscript, interest and suggestions are greatly appreciated. Especially I thank Dr. Hiesh of the Electrical Engineering Department, and Dr. Stahr of Vet. Medical College, for the many helpful discussions and assistance for me to pursue studies in the scientific disciplines outside the field of chemistry.

I am greatly indebted to Dr. Edward Yeung for many lively discussions in a broad scope of analytical sciences and research, and Dr. Joe Coats for much help in my graduate studies. Special thanks go to Royce Winge and David Eckles of Ames Laboratory, experts of ICP-AES, for their help and cooperation in operating the ICP optical emission spectrometers and computer data acquisitions. I owe a deep appreciation to many other Ames Laboratory staff, especially machinist friends in the

Student Workshop, the Machine Shop, the Electron Engineering Service Group, the Engineering Designs, and ISU Glassblow Shop. Their skills and knowledge helped me a lot.

Many former members of Houk group I would like to acknowledge here including: Heoungbin Lim, Jeff Crain, Dan Wiederin, Fred Smith, Ke Hu, Luis Alves and Sam Shum. Great gratitude is given to the current members in the group for their friendship, assistance and cooperation: Rocky Warren, Xiaoshan Chen, Scott Clemons, Shen Luan, Lloyd Allen, Steve Johnson, Tonya Bricker, Renyi Duan, Mike Minnich, Al Gwizdala, Narong Praphairaksit, and Dr. Homing Pang. I wish the best for all of you.

Thanks go to all my friends who have made the years in graduate school bearable and enjoyable. Specially, I wish to thank Ms. Nancy Textor, and Professor Dennis Wendel for the great friendship and many wonderful social activities we enjoyed together in the past five years.

Lastly and most of all, I deeply appreciate my wife, Sue, for her love, support, patience and particularly for the sacrifices throughout the period of this endeavor. I thank my children, Michael and Kathy, for the great joy they have given me. Not to be forgotten are my parents and my elder brother, whose love and support has been limitless and invaluable. I would like to share my achievements and successes with my family, to whom I dedicate this dissertation.